

Drivers of plant nutrient acquisition and allocation strategies and their influence
on plant responses to environmental change

by

Evan A. Perkowski, B.S.

A Dissertation

In

Biological Sciences

Submitted to the Graduate Faculty
of Texas Tech University in
Partial Fulfillment of
the Requirements for
the Degree of

Doctor of Philosophy

Approved

Nicholas G. Smith, Ph.D.
Chair of Committee

Aimée T. Classen, Ph.D.

Natasja van Gestel, Ph.D.

Lindsey C. Slaughter, Ph.D.

Dylan W. Schwilk, Ph.D.

Mark Sheridan, Ph.D.
Dean of the Graduate School

May 2023

Copyright 2023, Evan A. Perkowski

Acknowledgements

Placeholder for text

Table of Contents

Acknowledgements	ii
Abstract	vii
List of Tables	viii
List of Figures	x
1. Introduction	1
2. Structural carbon costs to acquire nitrogen are determined by nitrogen and light availability in two species with different nitrogen acquisition strategies	8
2.1 Introduction	8
2.2 Methods	12
2.2.1 <i>Experiment setup</i>	12
2.2.2 <i>Plant measurements and calculations</i>	13
2.2.3 <i>Statistical analyses</i>	14
2.3 Results	16
2.3.1 <i>Carbon costs to acquire nitrogen</i>	16
2.3.2 <i>Whole plant nitrogen biomass</i>	19
2.3.3 <i>Root carbon biomass</i>	21
2.3.4 <i>Root nodule biomass</i>	23
2.4 Discussion	27
2.4.1 <i>Fertilization decreases and light availability increases carbon costs to acquire nitrogen</i>	27
2.4.2 <i>Modeling implications</i>	29
2.4.3 <i>Study limitations</i>	31
2.4.4 <i>Conclusions</i>	33
3. Soil nitrogen availability modifies leaf nitrogen economies in mature temperate deciduous forests: a direct test of photosynthetic least-cost theory	35
3.1 Introduction	35

3.2 Methods	39
3.2.1 <i>Study site description</i>	39
3.2.2 <i>Experimental design</i>	40
3.2.3 <i>Leaf gas exchange and trait measurements</i>	40
3.2.4 A_{net}/C_i curve-fitting and parameter estimation	43
3.2.5 Proportion of leaf nitrogen allocated to photosynthesis and structure	45
3.2.6 Tradeoffs between nitrogen and water use	46
3.2.7 Soil nitrogen availability and pH	47
3.2.8 Statistical analyses	49
3.3 Results	51
3.3.1 Leaf N content	51
3.3.2 Net photosynthesis and leaf biochemistry	54
3.3.3 Leaf N allocation	57
3.3.4 Tradeoffs between nitrogen and water use	60
3.4 Discussion	63
3.4.1 Soil nitrogen availability modifies tradeoffs between nitrogen and water use	64
3.4.2 Soil pH did not modify tradeoffs between nitrogen and water usage	66
3.4.3 Species identity explains a large amount of variation in leaf and whole plant traits	67
3.4.4 Implications for photosynthetic least-cost theory model development	68
3.4.5 Conclusions	70
4. The relative cost of resource use for photosynthesis drives variance in leaf nitrogen content across climate and soil resource availability gradients	71
4.1 Introduction	71
4.2 Methods	77
4.2.1 Site descriptions and sampling methodology	77

4.2.2 <i>Leaf trait measurements</i>	77
4.2.3 <i>Site climate data</i>	83
4.2.4 <i>Site edaphic characteristics</i>	83
4.2.5 <i>Plant functional group assignments</i>	85
4.2.6 <i>Data analysis</i>	86
4.3 Results	88
4.3.1 <i>Cost to acquire nitrogen relative to water</i>	88
4.3.2 <i>Leaf $C_i:C_a$</i>	92
4.3.3 <i>Leaf nitrogen content</i>	95
4.3.4 <i>Structural equation model</i>	99
4.4 Discussion	102
5. Optimal resource investment to photosynthetic capacity maximizes nutrient allocation to whole plant growth under elevated CO₂	103
5.1 Introduction	103
5.2 Methods	108
5.2.1 <i>Seed treatments and experimental design</i>	108
5.2.2 <i>Growth chamber conditions</i>	109
5.2.3 <i>Leaf gas exchange measurements</i>	111
5.2.4 <i>Leaf trait measurements</i>	112
5.2.5 <i>A/C_i curve fitting and parameter estimation</i>	114
5.2.6 Stomatal limitation	114
5.2.7 <i>Proportion of leaf nitrogen allocated to photosynthesis and structure</i>	115
5.2.8 <i>Whole plant traits</i>	117
5.2.9 <i>Statistical analyses</i>	119
5.3 Results	121
5.3.1 <i>Leaf nitrogen content, chlorophyll content, and mass per area</i>	121
5.3.2 <i>Leaf biochemistry and stomatal conductance</i>	125

5.3.3 <i>Leaf nitrogen allocation</i>	129
5.3.4 <i>Whole plant traits</i>	133
5.3.5 <i>Nitrogen fixation</i>	137
5.4 Discussion	141
5.4.1 <i>Soil nitrogen fertilization has divergent effects on leaf and whole plant acclimation responses to CO₂</i>	142
5.4.2 <i>Implications for future model development</i>	146
5.4.3 <i>Study limitations and future directions</i>	147
5.4.4 <i>Conclusions</i>	149
6. Conclusions	151
References	153

Abstract

List of Tables

2.1 Analysis of variance results exploring species-specific effects of light availability, nitrogen fertilization, and their interactions on carbon costs to acquire nitrogen (N_{cost}), whole-plant nitrogen biomass (N_{wp}), and root carbon biomass (C_{bg})	17
2.2 Analysis of variance results exploring effects of light availability, nitrogen fertilization, and their interactions on <i>G. max</i> root nodule biomass and the ratio of root nodule biomass to root biomass* . . .	24
2.3 Slopes of the regression line describing the relationship between each dependent variable and nitrogen fertilization at each light level* . .	25
3.1 Effects of soil N availability, soil pH, and species on leaf N content per unit leaf area (N_{area}), leaf N content per unit leaf mass (N_{mass}), and leaf mass per unit leaf area (M_{area})	52
3.2 Effects of soil N availability, soil pH, species, and N_{area} on leaf biochemistry	55
3.3 Effects of soil N availability, soil pH, and species on the proportion of leaf nitrogen content allocated to photosynthesis, Rubisco, bioenergetics, and structure	58
3.4 Effects of soil N availability, soil pH, species, and N_{area} on tradeoffs between nitrogen and water use	61

4.1	Site locality information, sampling year(s), 2006-2020 mean annual precipitation (MAP; mm), mean annual temperature (MAT; °C), and water holding capacity (WHC; mm)*	81
4.2	Effects of soil moisture, soil nitrogen availability, and plant functional group on β	90
4.3	Effects of soil moisture, soil nitrogen availability, and plant functional group on χ^*	93
4.4	Effects of soil nitrogen fertilization, inoculation, and CO ₂ treatments on N_{area} , N_{mass} , and M_{area}	97
4.5	Structural equation model results investigating direct effects of climatic and soil resource availability on N_{area} , N_{mass} , M_{area} , χ , and β	100
5.1	Effects of soil nitrogen fertilization, inoculation, and CO ₂ treatments on N_{area} , N_{mass} , M_{area} , and Chl_{area}	123
5.2	Effects of soil nitrogen fertilization, inoculation, and CO ₂ on leaf biochemistry	127
5.3	Effects of soil N availability, soil pH, species, and N_{area} on leaf nitrogen allocation	131
5.4	Effects of soil N availability, soil pH, species, and N_{area} on total leaf area, whole plant biomass, and carbon costs to acquire nitrogen . .	135
5.5	Effects of soil N availability, soil pH, species, and N_{area} on root nodule biomass and plant investments in symbiotic nitrogen fixation	139

List of Figures

2.1 Relationships between soil nitrogen fertilization and light availability on carbon costs to acquire nitrogen in <i>G. hirsutum</i> and <i>G. max</i>	18
2.2 Relationships between soil nitrogen fertilization and light availability on whole-plant nitrogen biomass in <i>G. hirsutum</i> and <i>G. max</i>	20
2.3 Relationships between soil nitrogen fertilization and light availability on root carbon biomass in <i>G. hirsutum</i> and <i>G. max</i>	22
2.4 Effects of shade cover and nitrogen fertilization on root nodule biomass and the ratio of root nodule biomass to root biomass in <i>G. max</i>	26
3.1 Effects of soil N availability and species on leaf N content per unit leaf area, leaf nitrogen content per unit leaf biomass, and leaf mass per leaf area	53
3.2 Effects of soil N availability, species, and leaf N content leaf biochemistry	56
3.3 Effects of soil N availability, species, and leaf N content on the fraction of leaf nitrogen allocated to photosynthesis and structure	59
3.4 Effects of soil N availability, species, and leaf N content on tradeoffs between nitrogen and water use	62
4.1 Maps that detail site locations along 2006-2020 mean annual precipitation and mean annual temperature gradients in Texas, USA.	82

4.2 Effects of soil nitrogen availability and soil moisture on the unit cost ratio β	91
4.3 Effects of 4-day mean vapor pressure deficit, 2-day soil moisture (per water holding capacity), and soil nitrogen availability on χ	94
4.4 Effects of χ , soil nitrogen availability, and soil moisture on leaf nitrogen content per unit leaf area, leaf nitrogen content per unit leaf biomass, and leaf mass per area.	98
4.5 Structural equation model results exploring direct and indirect drivers of N_{area}	101
5.1 Effects of CO_2 , fertilization, and inoculation on leaf nitrogen per unit leaf area, leaf nitrogen content, leaf mass per unit leaf area, and chlorophyll content per unit leaf area.	124
5.2 Effects of CO_2 , fertilization, and inoculation on maximum rate of Rubisco carboxylation, the maximum rate of RuBP regeneration, and the ratio of the maximum rate of RuBP regeneration to the maximum rate of Rubisco carboxylation leaf mass per unit leaf area, dark respiration, stomatal conductance, and stomatal limitation.	128
5.3 Effects of CO_2 , fertilization, and inoculation on the relative fraction of leaf nitrogen allocated to photosynthesis and the fraction of leaf nitrogen allocated to structure.	132
5.4 Effects of CO_2 , fertilization, and inoculation on total leaf area, total biomass, and structural carbon costs to acquire nitrogen.	136

5.5 Effects of CO ₂ , fertilization, and inoculation on nodule biomass, nodule: root biomass, and percent nitrogen fixed from the atmo- sphere.	140
--	-----

1 Chapter 1

2 Introduction

3 Photosynthesis represents the largest carbon flux between the atmosphere
4 and biosphere, and is regulated by complex ecosystem carbon and nutrient cy-
5 cles (Hungate et al. 2003; IPCC 2021). As a result, the inclusion of robust,
6 empirically tested representations of photosynthetic processes is critical in order
7 for terrestrial biosphere models to accurately and reliably simulate carbon and
8 nutrient fluxes between the atmosphere and terrestrial biosphere (Wieder et al.
9 2015; Smith and Dukes 2013; Prentice et al. 2015; Oreskes et al. 1994). Despite
10 evidence that the inclusion of coupled carbon and nutrient cycles can improve
11 model uncertainty, widespread divergence in predicted carbon and nutrient fluxes
12 is still apparent across model products (Arora et al. 2020; Friedlingstein et al.
13 2014; Davies-Barnard et al. 2020). Divergence in predicted carbon and nutrient
14 fluxes across terrestrial biosphere models may be due to an incomplete under-
15 standing of how plants acclimate to changing environments (Smith and Dukes
16 2013; Davies-Barnard et al. 2020), as terrestrial biosphere models are sensitive to
17 the formulation of photosynthetic processes (Ziehn et al. 2011; Bonan et al. 2011;
18 Booth et al. 2012; Smith et al. 2016; Smith et al. 2017; Rogers et al. 2017).

Many terrestrial biosphere models predict leaf-level photosynthesis through linear relationships between area-based leaf nitrogen content and the maximum rate of Ribulose-1,5-bisphosphate carboxylase/oxygenase ("Rubisco"), following from the idea that large fractions of leaf nitrogen content are allocated to the construction and maintenance of Rubisco and other photosynthetic enzymes (Evans

24 1989). The inclusion of coupled carbon and nutrient cycles in terrestrial biosphere
25 models (Shi et al. 2016; Braghieri et al. 2022) allows for the prediction of leaf ni-
26 trogen content through soil nitrogen availability, which causes models to indirectly
27 predict photosynthetic processes through shifts in soil nitrogen availability (Smith
28 et al. 2014; Lawrence et al. 2019). While these patterns are commonly observed
29 in ecosystems globally (Brix 1971; Evans 1989; Liang et al. 2020; Firn et al. 2019),
30 this formulation of photosynthetic processes does not allow for the prediction of
31 leaf and whole plant acclimation responses to changing environments (Smith and
32 Dukes 2013; Rogers et al. 2017; Harrison et al. 2021), and suggests that con-
33 stant leaf nitrogen-photosynthesis relationships are ubiquitous across ecosystems.
34 Incorporating leaf and whole plant acclimation schemes in terrestrial biosphere
35 models is important (Smith and Dukes 2013), particularly because recent work
36 indicates that variance in leaf nitrogen content and leaf photosynthesis across en-
37 vironmental gradients may be better explained as an integrated product of leaf
38 acclimation responses to changing climates and soil nitrogen availability than soil
39 nitrogen availability alone (Dong et al. 2017; Dong et al. 2020; Smith et al. 2019;
40 Querejeta et al. 2022; Dong et al. 2022; Westerband et al. 2023).

41 Photosynthetic least-cost theory (Prentice et al. 2014; Wang et al. 2017;
42 Smith et al. 2019; Scott and Smith 2022; Harrison et al. 2021) provides a con-
43 temporary framework for predicting leaf and whole plant acclimation responses
44 to environmental change. The theory, which unifies photosynthetic optimal coor-
45 dination (Chen et al. 1993; Maire et al. 2012) and least-cost (Wright et al. 2003)
46 theories, posits that plants optimize photosynthetic processes by minimizing the
47 summed cost of nitrogen and water use (referred to here and in the rest of this dis-

48 sertation as β). The minimized summed cost of nitrogen and water use is dictated
49 by the ratio of intercellular CO₂ to atmospheric CO₂ (referred to here and in the
50 rest of this dissertation as leaf C_a:C_a, or χ), which is determined by factors that
51 influence leaf nitrogen demand, such as CO₂, temperature, vapor pressure deficit,
52 and light availability (Prentice et al. 2014; Smith et al. 2019; Stocker et al. 2020;
53 Wang et al. 2017). Photosynthetic processes are optimized such that nitrogen
54 is allocated to photosynthetic enzymes in to allow net photosynthesis rates to be
55 equally co-limited by the maximum rate of Rubisco carboxylation and the max-
56 imum rate of Ribulose-1,5-bisphosphate (RuBP) regeneration (Chen et al. 1993;
57 Maire et al. 2012). The theory indicates that costs of nitrogen and water use
58 are substitutable such that, in a given environment, optimal photosynthesis rates
59 can be achieved by sacrificing inefficient use of a relatively more abundant (and
60 less costly to acquire) resource for more efficient use of a relatively less abundant
61 (and more costly to acquire) resource. These predictions imply that acclimation
62 responses to changing environments may be partially driven by trade-offs between
63 nitrogen and water use, though empirical tests of the theory are sparse.

64 Optimality models leveraging patterns expected from photosynthetic least-
65 cost theory have been developed for both C₃ (Wang et al. 2017; Smith et al. 2019;
66 Stocker et al. 2020) and more recently for C₄ species (Scott and Smith 2022). Such
67 models show broad agreement with patterns observed across environmental gradi-
68 ents (Paillassa et al. 2020; Querejeta et al. 2022; Smith et al. 2019; Westerband
69 et al. 2023), and are capable of reconciling dynamic leaf nitrogen-photosynthesis
70 relationships and acclimation responses to elevated CO₂, temperature, light avail-
71 ability, and vapor pressure deficit (Dong et al. 2017; Dong et al. 2020; Dong et al.

72 2022; Dong et al. 2022; Smith and Keenan 2020; Luo et al. 2021; Peng et al. 2021;
73 Querejeta et al. 2022; Westerband et al. 2023). Current versions of optimality
74 models that invoke patterns expected from photosynthetic least-cost theory hold
75 β constant across growing environments. As growing evidence suggests that costs
76 of nitrogen use change across resource availability and climatic gradients in species
77 with different nutrient acquisition strategies (Fisher et al. 2010; Brzostek et al.
78 2014; Allen et al. 2020; Terrer et al. 2018), one might expect that β should
79 dynamically change across environments and in species with different acquisition
80 strategies. However, manipulative experiments that test mechanisms underlying
81 nitrogen-water use trade-offs and leaf nitrogen-photosynthesis relationships pre-
82 dicted from theory across soil resource availability and climatic gradients are rare.
83 Furthermore, no study has related shifts in β to nitrogen-water use trade-offs or
84 leaf nitrogen-photosynthesis relationships. Understanding the dynamic nature of
85 β across different environmental contexts and impacts of β on patterns expected
86 from theory are critical for further optimality model development, and is the cen-
87 tral motivation for the experiments presented in this dissertation.

88 In this dissertation, I use four experiments to quantify nutrient acquisition
89 and allocation responses under different environmental conditions and in species
90 with different nutrient acquisition strategies. These experiments provide impor-
91 tant empirical data needed to evaluate patterns expected from photosynthetic
92 least-cost theory and test mechanisms that drive such patterns. In the first ex-
93 perimental chapter, I re-analyze data from a greenhouse experiment that grew
94 *Glycine max* L. (Merr) and *Gossypium hirsutum* seedlings under full-factorial
95 combinations of four light treatments and four fertilization treatments. This re-

96 analysis examined the effect of soil nitrogen availability and light availability on
97 structural carbon costs to acquire nitrogen in a species capable of forming associa-
98 tions with symbiotic nitrogen-fixing bacteria (*G. max*) and a species not capable
99 of forming such associations (*G. hirsutum*). I find strong evidence suggesting that
100 increasing light availability increases structural carbon costs to acquire nitrogen
101 and that increasing soil nitrogen fertilization decreases structural carbon costs to
102 acquire nitrogen.

103 In the second experimental chapter, I measure leaf physiological traits in
104 the upper canopy of mature trees growing in a 9-year nitrogen-by-pH field manip-
105 ulation experiment to assess whether changes in soil nitrogen availability or soil
106 pH modify nitrogen-water use trade-offs expected from photosynthetic least-cost
107 theory. I find strong nitrogen-water use trade-offs in response to increasing soil ni-
108 trogen availability, indicated by a strong negative relationship between leaf $C_i:C_a$
109 (referred to here and in the rest of this dissertation as χ) and leaf nitrogen content,
110 as well as a strong increase in leaf nitrogen content per unit leaf χ with increas-
111 ing soil nitrogen availability. Interestingly, I also find a null effect of soil pH on
112 nitrogen-water use trade-offs. These patterns provide strong support for patterns
113 expected from photosynthetic least-cost theory across soil nitrogen availability
114 gradients, and indicate that previous studies which note strong nitrogen-water
115 use trade-offs in response to soil pH may be driven by covariation between soil
116 nitrogen availability and soil pH (Paillassa et al. 2020; Westerband et al. 2023).

117 In the third experimental chapter, I leverage a broad precipitation and soil
118 nutrient availability gradient in Texan grasslands to investigate primary drivers of
119 leaf nitrogen content. In this chapter, I directly quantify β and χ using leaf $\delta^{13}\text{C}$ to

120 examine primary drivers of leaf nitrogen content and find that leaf nitrogen content
121 is driven through a negative relationship with χ . I also show that soil nitrogen
122 availability is negatively associated with β , and that β is positively associated
123 with χ . I show strong support for patterns expected from theory, showing for
124 the first time that positive effects of increasing soil nitrogen availability on leaf
125 nitrogen content are mediated by changes in β .

126 In the fourth experimental chapter, I use reach-in growth chambers to
127 quantify leaf and whole plant acclimation responses to CO₂ across a soil nitro-
128 gen fertilization gradient, while also manipulating nutrient acquisition strategy
129 by controlling whether seedlings were able to form associations with symbiotic
130 nitrogen-fixing bacteria. Specifically, I measure leaf physiological and whole plant
131 growth responses of 7-week *G. max* seedlings grown under one of two CO₂ treat-
132 ments, one of nine fertilization treatments, and one of two inoculation treatments
133 in a full factorial design. I find a down-regulation in leaf nitrogen content and
134 leaf photosynthesis under elevated CO₂, a pattern that is not modified across
135 the fertilization gradient or between inoculation treatments. However, I also find
136 strong stimulation in total leaf area and whole plant growth under elevated CO₂
137 that are enhanced with increasing fertilization. There was no observable effect of
138 inoculation in modifying whole plant growth responses to CO₂, which I speculate
139 is the result of a down-regulation in plant investments to nitrogen fixation with
140 increasing fertilization. Results from this experiment provide strong evidence sug-
141 gesting that leaf acclimation responses to CO₂ were controlled by optimal resource
142 investment to photosynthetic capacity, following patterns expected from photo-
143 synthetic least-cost theory, and suggest divergent roles of soil nitrogen fertilization

144 in modifying leaf and whole plant acclimation responses to CO₂.

145 Throughout the four experimental chapters, I find strong and consistent
146 patterns supportive of patterns expected from photosynthetic least-cost theory.
147 Specifically, I find strong nitrogen-water use trade-offs in response to changing
148 climates and soil resources, that shifts in soil nitrogen availability have strong
149 negative impacts on costs of nitrogen acquisition, and therefore tend to increase
150 β , and that constant leaf nitrogen-photosynthesis relationships only occur in sys-
151 tems where nitrogen is limiting. In a final conclusion chapter, I summarize ma-
152 jor findings from each of the four experimental chapters and synthesize common
153 mechanisms that drive leaf and whole plant responses to changing environmen-
154 tal conditions. I conclude this dissertation with brief dialogue on lessons learned
155 throughout experimental chapters, and propose future experiments that will tar-
156 get additional uncertainties in photosynthetic least-cost theory responses across
157 environmental gradients.

158

Chapter 2

159

Structural carbon costs to acquire nitrogen are determined by
160 nitrogen and light availability in two species with different nitrogen
161 acquisition strategies

162 2.1 Introduction

163

Carbon and nitrogen cycles are tightly coupled in terrestrial ecosystems.

164

This tight coupling influences photosynthesis (Walker et al. 2014; Rogers et al.

165

2017), net primary productivity (LeBauer and Treseder 2008; Thomas et al. 2013),

166

decomposition (Cornwell et al. 2008; Bonan et al. 2013; Sulman et al. 2019), and

167

plant resource competition (Gill and Finzi 2016; Xu-Ri and Prentice 2017). Ter-

168

restrial biosphere models are beginning to include connected carbon and nitrogen

169

cycles to improve the realism of their simulations (Fisher et al. 2010; Brzostek

170

et al. 2014; Wieder et al. 2015; Shi et al. 2016; Zhu et al. 2019). Simula-

171

tions from these models indicate that coupling carbon and nitrogen cycles can

172

drastically influence future biosphere-atmosphere feedbacks under global change,

173

such as elevated carbon dioxide or nitrogen deposition (Thornton et al. 2007;

174

Goll et al. 2012; Wieder et al. 2015; Wieder et al. 2019). Nonetheless, there

175

are still limitations in our quantitative understanding of connected carbon and

176

nitrogen dynamics (Thomas et al. 2015; Meyerholt et al. 2016; Rogers et al.

177

2017; Exbrayat et al. 2018; Shi et al. 2019), forcing models to make potentially

178

unreliable assumptions.

179

Plant nitrogen acquisition is a process in terrestrial ecosystems by which

180

carbon and nitrogen are tightly coupled (Vitousek and Howarth 1991; Delaire

181

et al. 2005; Brzostek et al. 2014). Plants must allocate photosynthetically de-

182 rived carbon belowground to produce and maintain root systems or exchange with
183 symbiotic soil microbes in order to acquire nitrogen (Högberg et al. 2008; Hög-
184 berg et al. 2010). Thus, plants have an inherent carbon cost associated with
185 acquiring nitrogen, which can include both direct energetic costs associated with
186 nitrogen acquisition and indirect costs associated with building structures that
187 support nitrogen acquisition (Gutschick 1981; Rastetter et al. 2001; Vitousek
188 et al. 2002; Menge et al. 2008). Model simulations (Fisher et al. 2010; Brzostek
189 et al. 2014; Shi et al. 2016; Allen et al. 2020) and meta-analyses (Terrer et al.
190 2018) suggest that these carbon costs vary between species, particularly those
191 with different nitrogen acquisition strategies. For example, simulations using iter-
192 ations of the Fixation and Uptake of Nitrogen (FUN) model indicate that species
193 that acquire nitrogen from non-symbiotic active uptake pathways (e.g. mass flow)
194 generally have larger carbon costs to acquire nitrogen than species that acquire
195 nitrogen through symbiotic associations with nitrogen-fixing bacteria (Brzostek
196 et al. 2014; Allen et al. 2020).

197 Carbon costs to acquire nitrogen likely vary in response to changes in soil
198 nitrogen availability. For example, if the primary mode of nitrogen acquisition
199 is through non-symbiotic active uptake, then nitrogen availability could decrease
200 carbon costs to acquire nitrogen as a result of increased per-root nitrogen up-
201 take (Franklin et al. 2009; Wang et al. 2018). However, if the primary mode of
202 nitrogen acquisition is through symbiotic active uptake, then nitrogen availabil-
203 ity may incur additional carbon costs to acquire nitrogen if it causes microbial
204 symbionts to shift toward parasitism along the parasitism–mutualism continuum
205 (Johnson et al. 1997; Hoek et al. 2016; Friel and Friesen 2019) or if it reduces

206 the nitrogen acquisition capacity of a microbial symbiont (van Diepen et al. 2007;
207 Soudzilovskaia et al. 2015; Muñoz et al. 2016). Species may respond to shifts in
208 soil nitrogen availability by switching their primary mode of nitrogen acquisition
209 to a strategy with lower carbon costs to acquire nitrogen in order to maximize
210 the magnitude of nitrogen acquired from a belowground carbon investment and
211 outcompete other individuals for soil resources (Rastetter et al. 2001; Menge et al.
212 2008).

213 Environmental conditions that affect demand to acquire nitrogen to sup-
214 port new and existing tissues could also be a source of variance in plant carbon
215 costs to acquire nitrogen. For example, an increase in plant nitrogen demand could
216 increase carbon costs to acquire nitrogen if this increases the carbon that must be
217 allocated belowground to acquire a proportional amount of nitrogen (Kulmatiski
218 et al. 2017; Noyce et al. 2019). This could be driven by a temporary state of
219 diminishing return associated with investing carbon toward building and main-
220 taining structures that are necessary to support enhanced nitrogen uptake, such
221 as fine roots (Matamala and Schlesinger 2000; Norby et al. 2004; Arndal et al.
222 2018), mycorrhizal hyphae (Saleh et al. 2020), or root nodules (Parvin et al. 2020).
223 Alternatively, if the environmental factor that increases plant nitrogen demand
224 causes nitrogen to become more limiting in the system (e.g. atmospheric CO₂;
225 Luo et al. (2004), LeBauer and Treseder (2008), Vitousek et al. (2010), Liang
226 et al. (2016)), species might switch their primary mode of nitrogen acquisition to
227 a strategy with lower relative carbon costs to acquire nitrogen in order to gain a
228 competitive advantage over species with either different or more limited modes of
229 nitrogen acquisition (Ainsworth and Long 2005; Taylor and Menge 2018).

230 Using a plant economics approach, I examined the influence of plant ni-
231 trogen demand and soil nitrogen availability on plant carbon costs to acquire
232 nitrogen. This was done by growing a species capable of forming associations
233 with nitrogen-fixing bacteria (*Glycine max* L. (Merr)) and a species not capable
234 of forming these associations (*Gossypium hirsutum* L.) under four levels of light
235 availability (plant nitrogen demand proxy) and four levels of soil nitrogen fertil-
236 ization (soil nitrogen availability proxy) in a full-factorial, controlled greenhouse
237 experiment. I used this experimental set-up to test the following hypotheses:

- 238 1. An increase in plant nitrogen demand due to increasing light availability will
239 increase carbon costs to acquire nitrogen through a proportionally larger
240 increase in belowground carbon than whole-plant nitrogen acquisition. This
241 will be the result of an increased investment of carbon toward belowground
242 structures that support enhanced nitrogen uptake, but at a lower nitrogen
243 return.
- 244 2. An increase in soil nitrogen availability will decrease carbon costs to acquire
245 nitrogen as a result of increased per root nitrogen uptake in *G. hirsutum*.
246 However, soil nitrogen availability will not affect carbon costs to acquire
247 nitrogen in *G. max* because of the already high return of nitrogen supplied
248 through nitrogen fixation.

249 2.2 Methods

250 2.2.1 *Experiment setup*

251 *Gossypium hirsutum* and *G. max* were planted in individual 3 liter pots
252 (NS-300; Nursery Supplies, Orange, CA, USA) containing a 3:1 mix of unfertil-
253 ized potting mix (Sungro Sunshine Mix #2, Agawam, MA, USA) to native soil
254 extracted from an agricultural field most recently planted with *G. max* at the
255 USDA-ARS Laboratory in Lubbock, TX, USA (33.59°N, -101.90°W). The field
256 soil was classified as Amarillo fine sandy loam (75% sand, 10% silt, 15% clay).
257 Upon planting, all *G. max* pots were inoculated with *Bradyrhizobium japonicum*
258 (Verdesian N-Dure™ Soybean, Cary, NC, USA) to stimulate root nodulation. In-
259 dividuals of both species were grown under similar, unshaded, ambient greenhouse
260 conditions for 2 weeks to germinate and begin vegetative growth. Three blocks
261 were set up in the greenhouse, each containing four light treatments created us-
262 ing shade cloth that reduced incoming radiation by either 0 (full sun), 30, 50,
263 or 80%. Two weeks post-germination, individuals were randomly placed in the
264 four light treatments in each block. Individuals received one of four nitrogen fer-
265 tilization doses as 100ml of a modified Hoagland solution (Hoagland and Arnon
266 1950) equivalent to either 0, 70, 210, or 630 ppm N twice per week within each
267 light treatment. Nitrogen fertilization doses were received as topical agents to
268 the soil surface. Each Hoagland solution was modified to keep concentrations of
269 other macro- and micronutrients equivalent (Supplementary Table S1). Plants
270 were routinely well watered to eliminate water stress.

271 2.2.2 *Plant measurements and calculations*

272 Each individual was harvested after 5 weeks of treatment, and biomass
273 was separated by organ type (leaves, stems, and roots). Nodules on *G. max*
274 roots were also harvested. Except for the 0% shade cover and 630 ppm N treat-
275 ment combination, all treatment combinations in both species had lower average
276 dry biomass:pot volume ratios than the 1:1 ratio recommended by Poorter et al.
277 (2012) to minimize the likelihood of pot volume-induced growth limitation (Sup-
278 plementary Tables S2, S3; Supplementary Fig. S1). All harvested material was
279 dried, weighed, and ground by organ type. Carbon and nitrogen content (g g^{-1})
280 was determined by subsampling from ground and homogenized biomass of each
281 organ type using an elemental analyzer (Costech 4010; Costech, Inc., Valencia,
282 CA, USA). We scaled these values to total leaf, stem, and root carbon and ni-
283 trogen biomass (g) by multiplying dry biomass of each organ type by carbon or
284 nitrogen content of each corresponding organ type. Whole-plant nitrogen biomass
285 (g) was calculated as the sum of total leaf (g), stem (g), and root (g) nitrogen
286 biomass. Root nodule carbon biomass was not included in the calculation of root
287 carbon biomass; however, relative plant investment toward root or root nodule
288 standing stock was estimated as the ratio of root biomass to root nodule biomass
289 (g g^{-1}), following similar metrics to those adopted by Dovrat et al. (2018) and
290 Dovrat et al. (2020).

291 Carbon costs to acquire nitrogen (N_{cost} ; gC gN^{-1}) were estimated as the
292 ratio of total root carbon biomass (C_{bg} ; gC) to whole-plant nitrogen biomass
293 (N_{wp} ; gN). This calculation quantifies the relationship between carbon spent on
294 nitrogen acquisition and whole-plant nitrogen acquisition by using root carbon

295 biomass as a proxy for estimating the magnitude of carbon allocated toward ni-
296 trogen acquisition. This calculation therefore assumes that the magnitude of root
297 carbon standing stock is proportional to carbon transferred to root nodules or my-
298 corrhizae, or lost through root exudation or turnover. The assumption has been
299 supported in species that associate with ectomycorrhizal fungi (Hobbie 2006; Hob-
300 bie and Hobbie 2008), but is less clear in species that acquire nitrogen through
301 non-symbiotic active uptake or symbiotic nitrogen fixation. It is also unclear
302 whether relationships between root carbon standing stock and carbon transfer to
303 root nodules are similar in magnitude to carbon lost through exudation or when
304 allocated toward other active uptake pathways. Thus, because of the way mea-
305 surements were calculated, proximal values of carbon costs to acquire nitrogen are
306 underestimates.

307 2.2.3 *Statistical analyses*

308 I explored the effects of light and nitrogen availability on carbon costs to ac-
309 quire nitrogen using separate linear mixed-effects models for each species. Models
310 included shade cover, nitrogen fertilization, and interactions between shade cover
311 and nitrogen fertilization as continuous fixed effects, and also included block as a
312 random intercept term. Three separate models for each species were built with
313 this independent variable structure for three different dependent variables: (i)
314 carbon costs to acquire nitrogen (gC gN^{-1}); (ii) whole plant nitrogen biomass (de-
315 nominator of carbon cost to acquire nitrogen; gN); and (iii) belowground carbon
316 biomass (numerator of carbon cost to acquire nitrogen; gC). I constructed two
317 additional models for *G. max* with the same model structure described above to

318 investigate the effects of light availability and nitrogen fertilization on root nodule
319 biomass (g) and the ratio of root nodule biomass to root biomass (unitless).

320 I used Shapiro–Wilk tests of normality to determine whether species spe-
321 cific linear mixed-effects model residuals followed a normal distribution. None of
322 our models satisfied residual normality assumptions when models were fit using
323 untransformed data (Shapiro–Wilk: $p < 0.05$ in all cases). I attempted to satisfy
324 residual normality assumptions by first fitting models using dependent variables
325 that were natural-log transformed. If residual normality assumptions were still
326 not met (Shapiro–Wilk: $p < 0.05$), then models were fit using dependent variables
327 that were square root transformed. All residual normality assumptions were satis-
328 fied when models were fit with either a natural-log or square root transformation
329 (Shapiro–Wilk: $p > 0.05$ in all cases). Specifically, I natural-log transformed *G.*
330 *hirsutum* carbon costs to acquire nitrogen and *G. hirsutum* whole-plant nitrogen
331 biomass. I also square root transformed *G. max* carbon costs to acquire nitrogen,
332 *G. max* whole-plant nitrogen biomass, root carbon biomass in both species, *G.*
333 *max* root nodule biomass, and the *G. max* ratio of root nodule biomass to root
334 biomass. I used the ‘lmer’ function in the ‘lme4’ R package (Bates et al. 2015) to
335 fit each model and the ‘Anova’ function in the ‘car’ R package (Fox and Weisberg
336 2019) to calculate Wald’s χ^2 to determine the significance ($\alpha = 0.05$) of each fixed
337 effect coefficient. Finally, I used the ‘emmeans’ R package (Lenth 2019) to conduct
338 post-hoc comparisons of our treatment combinations using Tukey’s tests. Degrees
339 of freedom for all Tukey’s tests were approximated using the Kenward–Roger ap-
340 proach (Kenward and Roger 1997). All analyses and plots were conducted in R
341 version 4.0.1 (R Core Team 2021).

342 2.3 Results

343 2.3.1 *Carbon costs to acquire nitrogen*

344 Carbon costs to acquire nitrogen in *G. hirsutum* increased with increasing
345 light availability ($p < 0.001$; Table 2.1; Fig. 2.1) and decreased with increasing
346 nitrogen fertilization ($p < 0.001$; Table 2.1; Fig. 2.1). There was no interaction
347 between light availability and nitrogen fertilization ($p = 0.486$, Table 2.1; Fig.
348 2.1).

349 Carbon costs to acquire nitrogen in *G. max* also increased with increasing
350 light availability ($p < 0.001$, Table 2.1; Fig. 2.1) and decreased with increasing
351 nitrogen fertilization ($p < 0.001$; Table 2.1; Fig. 2.1). There was no interaction
352 between light availability and nitrogen fertilization ($p = 0.261$, Table 2.1; Fig.
353 2.1).

Table 2.1. Analysis of variance results exploring species-specific effects of light availability, nitrogen fertilization, and their interactions on carbon costs to acquire nitrogen (N_{cost}), whole-plant nitrogen biomass (N_{wp}), and root carbon biomass (C_{bg})

	df	N_{cost}			N_{wp}			C_{bg}		
		Coefficient	χ^2	p	Coefficient	χ^2	p	Coefficient	χ^2	p
<i>G. hirsutum</i>										
Intercept		1.594	-	-	-3.232	-	-	0.432	-	-
Light (L)	1	-1.09E-02	56.494	<0.001	-6.41E-03	91.275	<0.001	-2.62E-03	169.608	<0.001
Nitrogen (N)	1	-1.34E-03	54.925	<0.001	1.83E-03	118.784	<0.001	1.15E-04	2.901	0.089
L*N	1	3.88E-06	0.485	0.486	-1.34E-05	10.721	0.001	-1.67E-06	3.140	0.076
<i>G. max</i>										
Intercept		1.877	-	-	0.239	-	-	0.438	-	-
Light (L)	1	-7.67E-03	174.156	<0.001	-6.72E-04	39.799	<0.001	-2.55E-03	194.548	<0.001
Nitrogen (N)	1	-2.35E-04	21.948	<0.001	1.55E-04	70.771	<0.001	2.52E-04	19.458	<0.001
L*N	1	-2.89E-06	1.262	0.261	-6.32E-07	1.435	0.231	-3.16E-06	10.803	0.001

354 *Significance determined using Wald's χ^2 tests ($P = 0.05$). P -values < 0.05 are in bold and p -values between 0.05 and
 355 0.1 are italicized. Negative coefficients for light treatments indicate a positive effect of increasing light availability
 356 on all response variables, as light availability is treated as percent shade cover in all linear mixed-effects models.

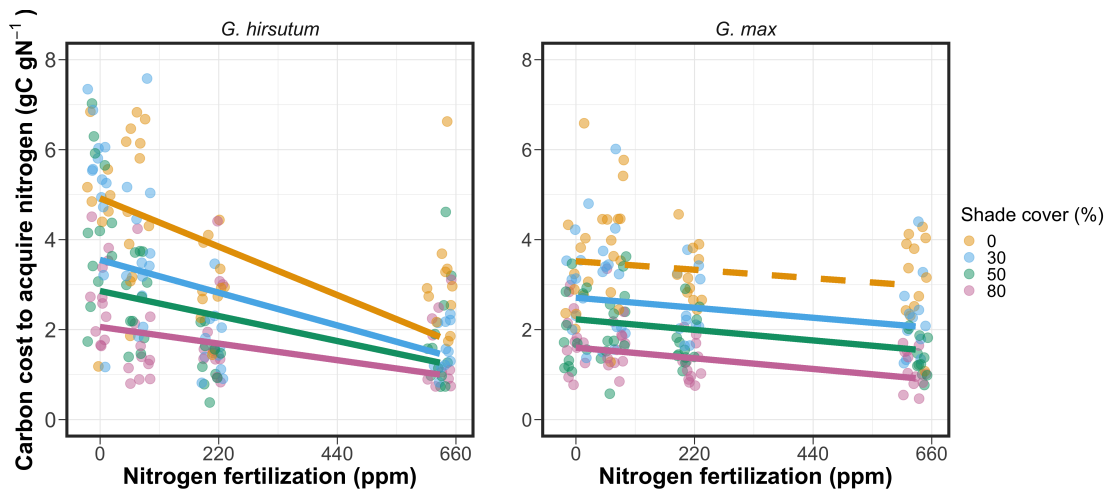


Figure 2.1. Relationships between soil nutrient fertilization and light availability on carbon costs to acquire nitrogen in *G. hirsutum* and *G. max*. Nitrogen fertilization treatments are represented on the x-axis. Shade cover treatments are represented through colored points and trendlines. Trendlines were created by back-transforming marginal mean slopes and intercepts from species-specific linear mixed-effects models. These values were calculated using the ‘emtrends’ and ‘emmmeans’ functions in the ‘emmeans’ R package (Lenth, 2019). Points are jittered for visibility. Yellow points and trendlines represent the 0% shade cover treatment, blue points and trendlines represent the 30% shade cover treatment, green points and trendlines represent the 50% shade cover treatment, and purple points and trendlines represent the 80% shade cover treatment. Solid trendlines indicate slopes that are significantly different from zero (Tukey: $p < 0.05$), while dashed trendlines indicate slopes that are not statistically different from zero.

357 2.3.2 *Whole plant nitrogen biomass*

358 Whole-plant nitrogen biomass in *G. hirsutum* was driven by an interaction
359 between light availability and nitrogen fertilization ($p = 0.001$; Table 2.1; Fig.
360 2.2). This interaction indicated a greater stimulation of whole-plant nitrogen
361 biomass by nitrogen fertilization as light levels increased (Table 2.1; Fig. 2.2).

362 Whole-plant nitrogen biomass in *G. max* increased with increasing light
363 availability ($p < 0.001$) and nitrogen fertilization ($p < 0.001$), with no interaction
364 between light availability and nitrogen fertilization ($p = 0.231$; Table 2.1; Fig.
365 2.2).

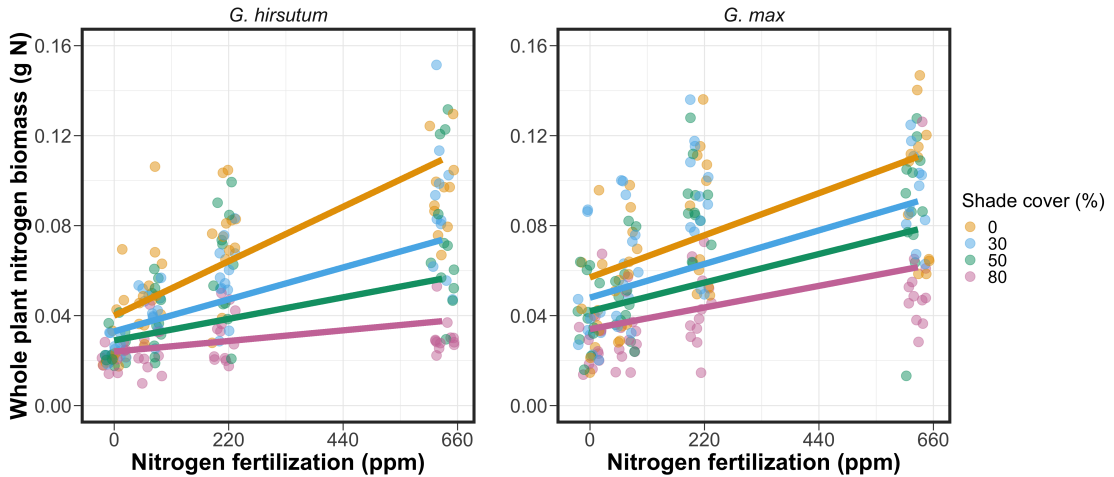


Figure 2.2. Relationships between soil nutrient fertilization and light availability on whole-plant nitrogen biomass in *G. hirsutum* and *G. max*. Whole-plant nitrogen biomass is the denominator of the carbon cost to acquire nitrogen calculation. Nitrogen fertilization treatments are represented on the x-axis. Shade cover treatments are represented through colored points and trendlines. Trendlines were created by back-transforming marginal mean slopes and intercepts from species-specific linear mixed-effects models. These values were calculated using the ‘emtrends’ and ‘emmmeans’ functions in the ‘emmeans’ R package (Lenth 2019). Points are jittered for visibility. Yellow points and trendlines represent the 0% shade cover treatment, blue points and trendlines represent the 30% shade cover treatment, green points and trendlines represent the 50% shade cover treatment, and purple points and trendlines represent the 80% shade cover treatment. Solid trendlines indicate slopes that are significantly different from zero (Tukey: $P < 0.05$), while dashed trendlines indicate slopes that are not statistically different from zero.

366 2.3.3 *Root carbon biomass*

367 Root carbon biomass in *G. hirsutum* significantly increased with increasing
368 light availability ($p < 0.001$; Table 2.1; Fig. 2.3) and marginally increased with
369 nitrogen fertilization ($p = 0.089$; Table 2.1; Fig. 2.3). There was also a marginal
370 interaction between light availability and nitrogen fertilization ($p = 0.076$; Table
371 2.1), driven by an increase in the positive response of root carbon biomass to
372 increasing nitrogen fertilization as light availability increased. This resulted in
373 significantly positive trends between root carbon biomass and nitrogen fertilization
374 in the two highest light treatments (Tukey: $p < 0.05$ in both cases; Table 2.3;
375 Fig. 2.3) and no effect of nitrogen fertilization in the two lowest light treatments
376 (Tukey: $p > 0.05$ in both cases; Table 2.3; Fig. 2.3).

377 There was an interaction between light availability and nitrogen fertiliza-
378 tion on root carbon biomass in *G. max* ($p = 0.001$; Table 2.1; Fig. 2.3). Post-hoc
379 analyses indicated that the positive effects of nitrogen fertilization on *G. max* root
380 carbon biomass increased with increasing light availability (Table 2.3; Fig. 2.3).
381 There were also positive individual effects of increasing nitrogen fertilization ($p <$
382 0.001) and light availability ($p < 0.001$) on *G. max* root carbon biomass (Table
383 2.1; Fig. 2.3).

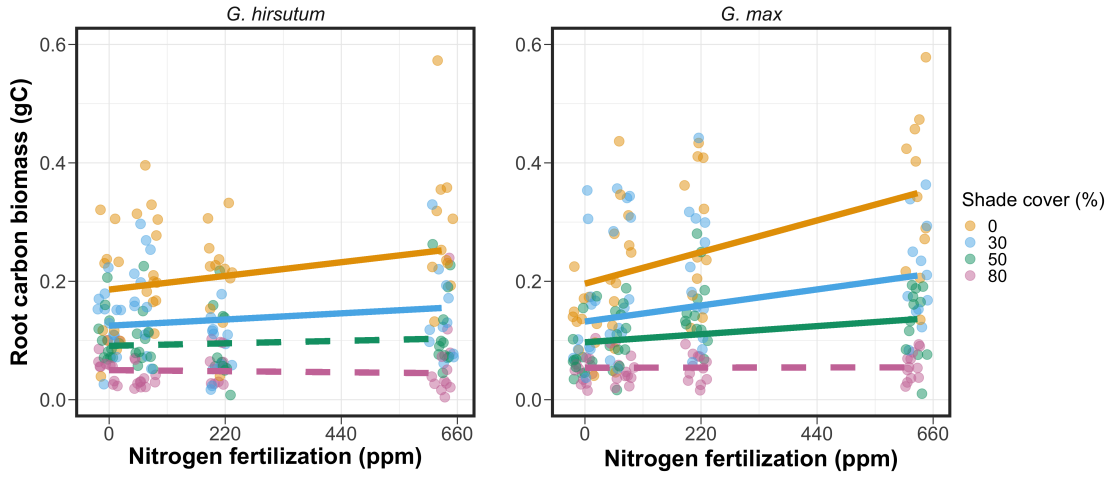


Figure 2.3. Relationships between soil nutrient fertilization and light availability on root carbon biomass in *G. hirsutum* and *G. max*. Root carbon biomass is the numerator of the carbon cost to acquire nitrogen calculation. Nitrogen fertilization treatments are represented on the x-axis. Shade cover treatments are represented through colored points and trendlines. Trendlines were created by back-transforming marginal mean slopes and intercepts from species-specific linear mixed-effects models. These values were calculated using the ‘emtrends’ and ‘emmmeans’ functions in the ‘emmeans’ R package (Lenth 2019). Points are jittered for visibility. Yellow points and trendlines represent the 0% shade cover treatment, blue points and trendlines represent the 30% shade cover treatment, green points and trendlines represent the 50% shade cover treatment, and purple points and trendlines represent the 80% shade cover treatment. Solid trendlines indicate slopes that are significantly different from zero (Tukey: $p < 0.05$), while dashed trendlines indicate slopes that are not statistically different from zero.

384 2.3.4 *Root nodule biomass*

385 Root nodule biomass in *G. max* increased with increasing light availability
386 ($p < 0.001$; Table 2.2; Fig. 2.4A) and decreased with increasing nitrogen fertiliza-
387 tion ($p < 0.001$; Table 2.2; Fig. 2.4A). There was no interaction between nitrogen
388 fertilization and light availability ($p = 0.133$; Table 2.2; Fig. 2.4A). The ratio of
389 root nodule biomass to root biomass did not change in response to light avail-
390 ability ($p = 0.481$; Table 2.2; Fig. 2.4B) but decreased with increasing nitrogen
391 fertilization ($p < 0.001$; Table 2.2; Fig. 2.4B). There was no interaction between
392 nitrogen fertilization and light availability on the ratio of root nodule biomass to
393 root biomass ($p = 0.621$; Table 2.2; Fig. 2.4B).

Table 2.2. Analysis of variance results exploring effects of light availability, nitrogen fertilization, and their interactions on *G. max* root nodule biomass and the ratio of root nodule biomass to root biomass*

	Nodule biomass			Nodule biomass: root biomass			<i>p</i>
	df	Coefficient	χ^2	<i>p</i>	Coefficient	χ^2	
(Intercept)		0.302	-	-	0.448	-	-
Light (L)	1	-1.81E-03	72.964	<0.001	-8.76E-05	0.496	0.481
Nitrogen (N)	1	-2.83E-04	115.377	<0.001	-5.09E-04	156.476	<0.001
L*N	1	1.14E-06	2.226	0.133	-7.30E-07	0.244	0.621

394 *Significance determined using Wald's χ^2 tests ($\alpha = 0.05$). *P*-values less than 0.05 are in bold. Negative coefficients
 395 for light treatments indicate a positive effect of increasing light availability on all response variables, as light avail-
 396 ability is treated as percent shade cover in all linear mixed-effects models. Root nodule biomass and nodule biomass:
 397 root biomass models were only constructed for *G. max* because *G. hirsutum* was not inoculated with *B. japonicum*
 398 and is not capable of forming root nodules.

Table 2.3. Slopes of the regression line describing the relationship between each dependent variable and nitrogen fertilization at each light level*

Shade cover	Carbon cost to acquire nitrogen	Whole plant N biomass	Belowground C biomass	Root nodule biomass	Nodule biomass: root biomass
<i>G. hirsutum</i>					
0%	-1.34E-03^a	1.83E-03^a	1.15E-04^b	-	-
30%	-1.22E-03^a	1.43E-03^a	1.17E-04^b	-	-
50%	-1.14E-03^a	1.17E-03^a	3.12E-05 ^b	-	-
80%	-1.02E-03^a	7.66E-04^a	-1.89E-06 ^b	-	-
<i>G. max</i>					
0%	-2.35E-04 ^b	1.55E-05^b	2.51E-04^b	-2.83E-04^b	-5.09E-04^b
30%	-3.22E-04^b	1.35E-05^b	1.57E-04^b	-2.49E-04^b	-5.31E-04^b
50%	-3.80E-04^b	1.23E-05^b	9.37E-05^b	-2.26E-04^b	-5.45E-04^b
80%	-4.66E-04^b	1.04E-05^b	-9.95E-07 ^b	-1.92E-04^b	-5.67E-04^b

25

399 *Slopes represent estimated marginal mean slopes from linear mixed-effects models described in the Methods. Slopes
 400 were calculated using the ‘emmeans’ R package (Lenth 2019). Superscripts indicate slopes fit to natural-log (^a) or
 401 square root (^b) transformed data. Slopes statistically different from zero (Tukey: $p < 0.05$) are indicated in bold.
 402 Marginally significant slopes (Tukey: $0.05 < p < 0.1$) are italicized.

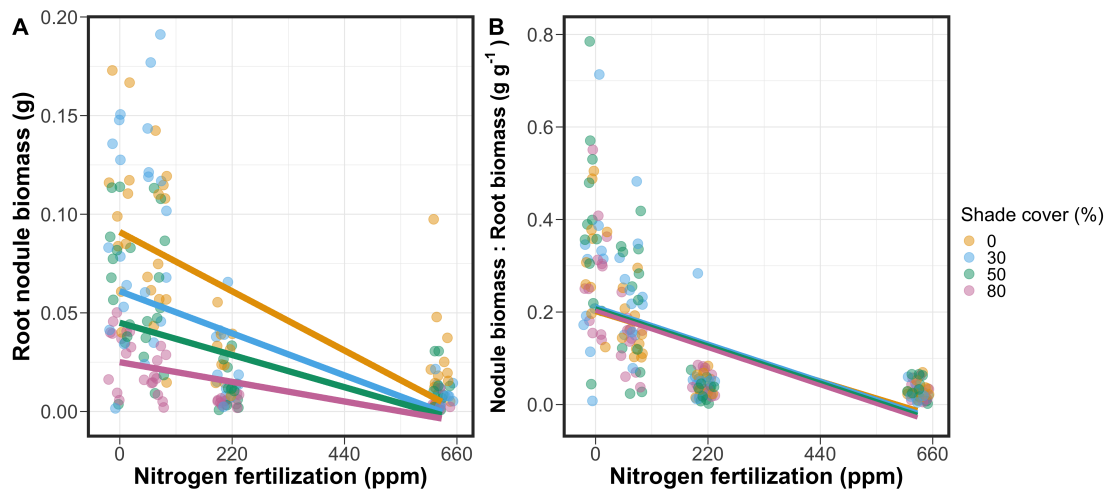


Figure 2.4. Effects of shade cover and nitrogen fertilization on root nodule biomass (A) and the ratio of root nodule biomass to root biomass (B) in *G. max*. Nitrogen fertilization treatments are represented on the x-axis. Shade cover treatments are represented through colored points and trendlines. Trendlines were created by back-transforming marginal mean slopes and intercepts from species-specific linear mixed-effects models. These values were calculated using the ‘emtrends’ and ‘emmeans’ functions in the ‘emmeans’ R package (Lenth 2019). Points are jittered for visibility. Yellow points and trendlines represent the 0% shade cover treatment, blue points and trendlines represent the 30% shade cover treatment, green points and trendlines represent the 50% shade cover treatment, and purple points and trendlines represent the 80% shade cover treatment. Solid trendlines indicate slopes that are significantly different from zero (Tukey: $p < 0.05$), while dashed trendlines indicate slopes that are not statistically different from zero.

403 2.4 Discussion

404 In this chapter, I determined the effects of light availability and soil ni-
405 trogen fertilization on root mass carbon costs to acquire nitrogen in *G. hirsutum*
406 and *G. max*. In support of my hypotheses, I found that carbon costs to acquire
407 nitrogen generally increased with increasing light availability and decreased with
408 increasing soil nitrogen fertilization in both species. These findings suggest that
409 carbon costs to acquire nitrogen are determined by factors that influence plant
410 nitrogen demand and soil nitrogen availability. In contrast to my second hypothe-
411 sis, root nodulation data suggested that *G. max* and *G. hirsutum* achieved similar
412 directional carbon cost responses to nitrogen fertilization despite a likely shift in
413 *G. max* allocation from nodulation to root biomass along the nitrogen fertilization
414 gradient (Fig. 2.4B).

415 2.4.1 *Fertilization decreases and light availaiblity increases carbon costs to*
416 *acquire nitrogen*

417 Both *G. max* and *G. hirsutum* experienced an increase in carbon costs to
418 acquire nitrogen due to increasing light availability. These patterns were driven by
419 a larger increase in root carbon biomass than whole-plant nitrogen biomass. In-
420 creases in root carbon biomass due to factors that increase plant nitrogen demand
421 are a commonly observed pattern, as carbon allocated belowground provides sub-
422 strate needed to produce and maintain structures that satisfy aboveground plant
423 nitrogen demand (Nadelhoffer and Raich 1992; Giardina et al. 2005; Raich et al.
424 2014). Findings suggest that plants allocate relatively more carbon for acquiring
425 nitrogen when demand increases over short temporal scales, which may cause a

426 temporary state of diminishing return due to asynchrony between belowground
427 carbon and whole-plant nitrogen responses to plant nitrogen demand (Kulmatiski
428 et al. 2017; Noyce et al. 2019). These responses might be attributed to a temporal
429 lag associated with producing structures that enhance nitrogen acquisition. For
430 example, fine roots (Matamala and Schlesinger 2000; Norby et al. 2004; Arndal
431 et al. 2018) and root nodules (Parvin et al. 2020) take time to build and first
432 require the construction of coarse roots. Thus, full nitrogen returns from these
433 investments may not occur immediately (Kayler et al. 2010; Kayler et al. 2017),
434 and may vary by species acquisition strategy. I speculate that increases in ni-
435 trogen acquisition from a given carbon investment may occur beyond the 5-week
436 scope of this experiment. A similar study conducted over a longer temporal scale
437 would address this.

438 Increasing soil nitrogen fertilization generally decreased carbon costs to
439 acquire nitrogen in both species. These patterns were driven by a larger increase
440 in whole-plant nitrogen biomass than root carbon biomass. In *G. hirsutum*, re-
441 ductions in carbon costs to acquire nitrogen may have been due to an increase in
442 per-root nitrogen uptake, allowing individuals to maximize the amount of nitro-
443 gen acquired from a belowground carbon investment. Interestingly, increased soil
444 nitrogen fertilization increased whole-plant nitrogen biomass in *G. max* despite
445 reductions in root nodule biomass that likely reduced the nitrogen-fixing capac-
446 ity of *G. max* (Andersen et al. 2005; Muñoz et al. 2016). While reductions in
447 root nodulation due to increased soil nitrogen availability are commonly observed
448 (Gibson and Harper 1985; Fujikake et al. 2003), root nodulation responses were
449 observed in tandem with increased root carbon biomass, implying that *G. max*

450 shifted relative carbon allocation from nitrogen fixation to soil nitrogen acquisition
451 (Markham and Zekveld 2007; Dovrat et al. 2020). This was likely because
452 there was a reduction in the carbon cost advantage of acquiring fixed nitrogen
453 relative to soil nitrogen, and suggests that species capable of associating with
454 symbiotic nitrogen-fixing bacteria shift their relative nitrogen acquisition path-
455 way to optimize nitrogen uptake (Rastetter et al. 2001). Future studies should
456 further investigate these patterns with a larger quantity of phylogenetically re-
457 lated species, or different varieties of a single species that differ in their ability to
458 form associations with symbiotic nitrogen-fixing bacteria to more directly test the
459 impact of nitrogen fixation on the patterns observed in this study.

460 2.4.2 *Modeling implications*

461 Carbon costs to acquire nitrogen are subsumed in the general discussion of
462 economic analogies to plant resource uptake (Bloom et al. 1985; Rastetter et al.
463 2001; Vitousek et al. 2002; Phillips et al. 2013; Terrer et al. 2018; Henneron et al.
464 2020). Despite this, terrestrial biosphere models rarely include costs of nitrogen
465 acquisition within their framework for predicting plant nitrogen uptake. There
466 is currently one plant resource uptake model, FUN, that quantitatively predicts
467 carbon costs to acquire nitrogen within a framework for predicting plant nitrogen
468 uptake for different nitrogen acquisition strategies (Fisher et al. 2010; Brzostek
469 et al. 2014). Iterations of FUN are currently coupled to two terrestrial biosphere
470 models: the Community Land Model 5.0 and the Joint UK Land Environment
471 Simulator (Shi et al. 2016; Lawrence et al. 2019; Clark et al. 2011). Recent work
472 suggests that coupling FUN to CLM 5.0 caused a large overprediction of plant

473 nitrogen uptake associated with nitrogen fixation (Davies-Barnard et al. 2020)
474 compared to other terrestrial biosphere model products. Thus, empirical data
475 from manipulative experiments that explicitly quantify carbon costs to acquire
476 nitrogen in species capable of associating with nitrogen-fixing bacteria across dif-
477 ferent environmental contexts is an important step toward identifying potential
478 biases in models such as FUN.

479 My findings broadly support the FUN formulation of carbon costs to ac-
480 quire nitrogen in response to soil nitrogen availability. FUN calculates carbon
481 costs to acquire nitrogen based on the sum of carbon costs to acquire nitrogen
482 via nitrogen fixation, mycorrhizal active uptake, non-mycorrhizal active uptake,
483 and retranslocation (Fisher et al. 2010; Brzostek et al. 2014). Carbon costs to
484 acquire nitrogen via mycorrhizal or non-mycorrhizal active uptake pathways are
485 derived as a function of nitrogen availability, root biomass, and two parameterized
486 values based on nitrogen acquisition strategy (Brzostek et al. 2014). Due to this,
487 FUN simulates a net decrease in carbon costs to acquire nitrogen with increasing
488 nitrogen availability for mycorrhizal and non-mycorrhizal active uptake pathways,
489 assuming constant root biomass. This was a pattern I observed in *G. hirsutum*
490 regardless of light availability. In contrast, FUN would not simulate a net change
491 in carbon costs to acquire nitrogen via nitrogen fixation due to nitrogen avail-
492 ability. This is because carbon costs to acquire nitrogen via nitrogen fixation are
493 derived from a well established function of soil temperature, which is independent
494 of soil nitrogen availability (Houlton et al. 2008; Fisher et al. 2010). I observed
495 a net reduction in carbon costs to acquire nitrogen in *G. max*, except when in-
496 dividuals were grown under 0% shade cover (Fig. 2.1). While a net reduction of

497 carbon costs in response to nitrogen fertilization runs counter to nitrogen fixa-
498 tion carbon costs simulated by FUN, these patterns were likely because *G. max*
499 individuals switched their primary mode of nitrogen acquisition from symbiotic
500 nitrogen fixation to a non-symbiotic active uptake pathway (Fig. 2.4B).

501 2.4.3 *Study limitations*

502 It should be noted that the metric used in this study to determine carbon
503 costs to acquire nitrogen has several limitations. Most notably, this metric uses
504 root carbon biomass as a proxy for estimating the amount of carbon spent on
505 nitrogen acquisition. While it is true that most carbon allocated belowground has
506 at least an indirect structural role in acquiring soil resources, it remains unclear
507 whether this assumption holds true for species that acquire nitrogen via symbi-
508 otic nitrogen fixation. I also cannot quantify carbon lost through root exudates
509 or root turnover, which may increase due to factors that increase plant nitrogen
510 demand (Tingey et al. 2000; Phillips et al. 2011), and can increase the magni-
511 tude of available nitrogen from soil organic matter through priming effects on soil
512 microbial communities (Uselman et al. 2000; Bengtson et al. 2012). It is also not
513 clear whether these assumptions hold under all environmental conditions, such
514 as those that shift belowground carbon allocation toward a different mode of ni-
515 trogen acquisition (Taylor and Menge 2018; Friel and Friesen 2019) or between
516 species with different acquisition strategies. In this study, increasing soil nitrogen
517 fertilization increased carbon investment to roots relative to carbon transferred
518 to root nodules (Fig. 2.4B). By assuming that carbon allocated to root carbon
519 was proportional to carbon allocated to root nodules across all treatment com-

520 binations, these observed responses to soil nitrogen fertilization were likely to be
521 overestimated in *G. max*. I encourage future research to quantify these carbon
522 fates independently.

523 Researchers conducting pot experiments must carefully choose pot volume
524 to minimize the likelihood of growth limitations induced by pot volume (Poorter
525 et al. 2012). Poorter et al. (2012) indicate that researchers are likely to avoid
526 growth limitations associated with pot volume if measurements are collected when
527 the plant biomass:pot volume ratio is less than 1 g L⁻¹. In this experiment, all
528 treatment combinations in both species had biomass:pot volume ratios less than
529 1 g L⁻¹ except for *G. max* and *G. hirsutum* that were grown under 0% shade
530 cover and had received 630 ppm N. Specifically, *G. max* and *G. hirsutum* had
531 average respective biomass:pot volume ratios of 1.24±0.07 g L⁻¹ and 1.34±0.13 g
532 L⁻¹, when grown under 0% shade cover and received 630 ppm N (Supplementary
533 Tables S2, S3; Supplementary Fig. S1). If growth in this treatment combination
534 was limited by pot volume, then individuals may have had larger carbon costs
535 to acquire nitrogen than would be expected if they were grown in larger pots.
536 This pot volume induced growth limitation could cause a reduction in per-root
537 nitrogen uptake associated with more densely packed roots, which could reduce
538 the positive effect of nitrogen fertilization on whole-plant nitrogen biomass relative
539 to root carbon biomass (Poorter et al. 2012).

540 Growth limitation associated with pot volume provides a possible explana-
541 tion for the marginally insignificant effect of increasing nitrogen fertilization on *G.*
542 *max* carbon costs to acquire nitrogen when grown under 0% shade cover (Table
543 2.3; Fig. 2.1). This is because the regression line describing the relationship be-

544 tween carbon costs to acquire nitrogen and nitrogen fertilization in *G. max* grown
545 under 0% shade cover would have flattened if growth limitation had caused larger
546 than expected carbon costs to acquire nitrogen in the 0% shade cover, 630 ppm
547 N treatment combination. This may have been exacerbated by the fact that *G.*
548 *max* likely shifted relative carbon allocation from nitrogen fixation to soil nitrogen
549 acquisition, which could have increased the negative effect of more densely packed
550 roots on nitrogen uptake. These patterns could have also occurred in *G. hirsutum*
551 grown under 0% shade cover; however, there was no change in the effect of nitro-
552 gen fertilization on *G. hirsutum* carbon costs to acquire nitrogen grown under 0%
553 shade cover relative to other shade cover treatments. Regardless, the possibility
554 of growth limitation due to pot volume suggests that effects of increasing nitro-
555 gen fertilization on carbon costs to acquire nitrogen in both species grown under
556 0% shade cover could have been underestimated. Follow-up studies using a simi-
557 lar experimental design with a larger pot volume would be necessary in order to
558 determine whether these patterns were impacted by pot volume-induced growth
559 limitation.

560 2.4.4 *Conclusions*

561 In conclusion, this chapter provides empirical evidence that carbon costs to
562 acquire nitrogen are influenced by light availability and soil nitrogen fertilization
563 in a species capable of acquiring nitrogen via symbiotic nitrogen fixation and a
564 species not capable of forming such associations. We show that carbon costs to
565 acquire nitrogen generally increase with increasing light availability and decrease
566 with increasing nitrogen fertilization. This chapter provides important empirical

567 data needed to evaluate the formulation of carbon costs to acquire nitrogen in
568 terrestrial biosphere models, particularly carbon costs to acquire nitrogen that
569 are associated with symbiotic nitrogen fixation. My findings broadly support the
570 general formulation of these carbon costs in the FUN biogeochemical model in
571 response to shifts in nitrogen availability. However, there is a need for future
572 studies to explicitly quantify carbon costs to acquire nitrogen under different en-
573 vironmental contexts, over longer temporal scales, and using larger selections of
574 phylogenetically related species. In addition, I suggest that future studies mini-
575 mize the limitations associated with the metric used here by explicitly measuring
576 belowground carbon fates independently.

577

Chapter 3

578 Soil nitrogen availability modifies leaf nitrogen economies in mature
579 temperate deciduous forests: a direct test of photosynthetic least-cost
580 theory

581 3.1 Introduction

582 Photosynthesis represents the largest carbon flux between the atmosphere
583 and land surface (IPCC 2021), and plays a central role in biogeochemical cycling
584 at multiple spatial and temporal scales (Vitousek and Howarth 1991; LeBauer and
585 Treseder 2008; Kaiser et al. 2015; Wieder et al. 2015). Therefore, carbon and
586 energy fluxes simulated by terrestrial biosphere models are sensitive to the formu-
587 lation of photosynthetic processes (Ziehn et al. 2011; Bonan et al. 2011; Booth
588 et al. 2012; Smith et al. 2016; Smith et al. 2017) and must be represented using
589 robust, empirically tested processes (Prentice et al. 2015; Wieder et al. 2019).
590 Current formulations of photosynthesis vary across terrestrial biosphere models
591 (Smith and Dukes 2013; Rogers et al. 2017), which causes variation in modeled
592 ecosystem processes (Knorr 2000; Knorr and Heimann 2001; Bonan et al. 2011;
593 Friedlingstein et al. 2014) and casts uncertainty on the ability of these models to
594 accurately predict terrestrial ecosystem responses and feedbacks to global change
595 (Zaehle et al. 2005; Schaefer et al. 2012; Davies-Barnard et al. 2020).

596 Terrestrial biosphere models commonly represent C₃ photosynthesis th-
597 rough variants of the Farquhar et al. (1980) biochemical model (Smith and Dukes
598 2013; Rogers 2014; Rogers et al. 2017). This well-tested photosynthesis model
599 estimates leaf-level carbon assimilation, or photosynthetic capacity, as a function
600 of the maximum rate of Ribulose-1,5-bisphosphate carboxylase-oxygenase (Ru-

601 bisco) carboxylation (V_{cmax}) and the maximum rate of Ribulose-1,5-bisphosphate
602 (RuBP) regeneration (J_{max}) (Farquhar et al. 1980). Many terrestrial biosphere
603 models predict these model inputs based on plant functional group specific linear
604 relationships between leaf nutrient content and V_{cmax} (Smith and Dukes 2013;
605 Rogers 2014; Rogers et al. 2017) under the tenet that a large fraction of leaf
606 nutrients, and nitrogen (N) in particular, are partitioned toward building and
607 maintaining enzymes that support photosynthetic capacity, such as Rubisco (Brix
608 1971; Gulmon and Chu 1981; Evans 1989; Kattge et al. 2009; Walker et al. 2014).
609 Terrestrial biosphere models also predict leaf nutrient content from soil nutrient
610 availability based on the assumption that increasing soil nutrients generally in-
611 creases leaf nutrients (Firn et al. 2019; Li et al. 2020; Liang et al. 2020) which, in
612 the case of N, generally corresponds with an increase in photosynthetic processes
613 (Li et al. 2020; Liang et al. 2020).

614 Recent work calls the generality of relationships between soil nutrient avail-
615 ability, leaf nutrient content, and photosynthetic capacity into question, suggest-
616 ing instead that leaf nutrients and photosynthetic capacity are better predicted as
617 an integrated product of aboveground climate, leaf traits, and soil nutrient avail-
618 ability, rather than soil nutrient availability alone (Dong et al. 2017; Dong et al.
619 2020; Dong et al. 2022; Firn et al. 2019; Smith et al. 2019; Peng et al. 2021).
620 It has been reasoned that this result is because plants allocate added nutrients to
621 growth and storage rather than alterations in leaf chemistry (Smith et al. 2019),
622 perhaps as a result of nutrient limitation of primary productivity (LeBauer and
623 Treseder 2008; Fay et al. 2015). Additionally, recent work suggests that relation-
624 ships between leaf nutrient content and photosynthesis vary across environments,

625 and that the proportion of leaf nutrient content allocated to photosynthetic tis-
626 sue varies over space and time with plant acclimation and adaptation responses
627 to light availability, vapor pressure deficit, soil pH, soil nutrient availability, and
628 environmental factors that influence leaf mass per area (Pons and Pearcy 1994;
629 Niinemets and Tenhunen 1997; Evans and Poorter 2001; Hikosaka and Shigeno
630 2009; Ghimire et al. 2017; Onoda et al. 2017; Luo et al. 2021). The use of linear
631 relationships between leaf nutrient content and Vcmax to predict photosynthetic
632 capacity, as commonly used in terrestrial biosphere models (Rogers 2014), is not
633 capable of detecting such responses.

634 Photosynthetic least-cost theory provides an alternative framework for un-
635 derstanding relationships between soil nutrient availability, leaf nutrient content,
636 and photosynthetic capacity (Harrison et al. 2021). Leveraging a two-input mi-
637 croeconomics approach (Wright et al. 2003), the theory posits that plants accli-
638 mate to a given environment by optimizing leaf photosynthesis rates at the lowest
639 summed cost of using nutrients and water (Prentice et al. 2014; Wang et al. 2017;
640 Smith et al. 2019; Paillassa et al. 2020). Across resource availability gradients,
641 the theory predicts that optimal photosynthetic rates can be achieved by trading
642 less efficient use of a resource that is less costly to acquire (or more abundant)
643 for more efficient use of a resource more costly to acquire (or less abundant). For
644 example, an increase in soil nutrient availability should reduce the cost of acquir-
645 ing and using nutrients (Bae et al. 2015; Eastman et al. 2021; Perkowski et al.
646 2021), which could increase leaf nutrient investments in photosynthetic proteins to
647 allow similar photosynthetic rates to be achieved with higher nutrient use (lower
648 nutrient use efficiency) but lower water use (greater water use efficiency). The

649 theory suggests similar tradeoffs in response to increasing soil pH (Paillassa et al.
650 2020), specifically, that increasing soil pH should reduce the cost of acquiring soil
651 nutrients due to an increase in plant-available nutrient concentration (Paillassa
652 et al. 2020; Dong et al. 2022). The theory is also capable of reconciling dynamic
653 leaf nutrient-photosynthesis relationships at global scales (Luo et al. 2021).

654 Patterns expected from photosynthetic least-cost theory have recently re-
655 ceived empirical support both in global environmental gradient (Smith et al.
656 2019; Paillassa et al. 2020; Luo et al. 2021; Querejeta et al. 2022; Wester-
657 band et al. 2023) and local manipulative invasion (Bialic-Murphy et al. 2021)
658 studies. However, nutrient addition experiments that directly examine nutrient-
659 water use tradeoffs expected from the theory are rare (Guerrieri et al. 2011), and
660 only global gradient studies testing the theory have considered soil pH in their
661 analyses. As a result, there is a need to use nutrient addition and soil pH manu-
662 lation experiments to test mechanisms driving responses predicted by the theory.
663 Such experiments would also be useful to detect whether patterns expected from
664 theory translate to finer spatial scales.

665 In this study, we measured leaf responses to soil N availability in five decid-
666 uous tree species growing in the upper canopy of mature closed canopy temperate
667 forests in the northeastern United States. Soil N availability and pH were manipu-
668 lated through an N-by-pH field manipulation experiment with treatments applied
669 since 2011, eight years prior to measurement. Two different soil N treatments
670 were applied to increase N availability with opposing effects on soil pH. An addi-
671 tional N-free acidifying treatment was expected to decrease soil pH. I hypothesized
672 that increased soil N availability would enable plants to increase nutrient uptake

673 and create more photosynthetic enzymes per leaf, allowing similar photosynthetic
674 rates achieved with lower leaf C_i:C_a and increased leaf N content allocated to
675 photosynthetic leaf tissue. I expected that this response would be driven by a
676 reduction in the cost of acquiring N, which would cause trees to sacrifice efficient
677 N use to enable more efficient use of other limiting resources (i.e., water). Finally,
678 I hypothesized similar leaf responses to increasing soil pH.

679 3.2 Methods

680 3.2.1 *Study site description*

681 We conducted this study in summer 2019 at three stands located within
682 a 20-km radius of Ithaca, NY, USA (42.444 °N, 76.502 °W). All stands contain
683 mature, closed-canopy forests dominated by deciduous tree species. Stands con-
684 tained abundant sugar maple (*Acer saccharum* Marshall), American beech (*Fagus*
685 *grandifolia* Ehrh.), and white ash (*Fraxinus americana* L.), accounting for 43%,
686 15%, and 17% of the total aboveground biomass across the three stands, respec-
687 tively, with less frequent red maple (*Acer rubrum* L.; 9% of total aboveground
688 biomass) and red oak occurrences (*Quercus rubra* L.; 10% of total aboveground
689 biomass). Soils at each site were broadly classified as a channery silt loam Incep-
690 tisols using the USDA NRCS Web Soil Survey data product (Soil Survey Staff
691 2022). Between 2006 and 2020, study sites averaged 972 mm of precipitation per
692 year and had an average temperature of 7.9 °C per a weather station located near
693 the Cornell University campus (42.449 °N, 76.449 °W) part of the NOAA NCEI
694 Global Historical Climatology Network (Menne et al. 2012).

695 3.2.2 *Experimental design*

696 Four 40 m x 40 m plots were set up at each site in 2009, each with an
697 additional 10 m buffer along plot perimeters (60 m x 60 m total). The plots
698 were set up as a nitrogen-by-pH field manipulation experiment, with one each of
699 four treatments at each site. Two nitrogen treatments were applied, both at 50
700 kg N ha⁻¹ yr⁻¹, as either sodium nitrate (NaNO₃) to raise soil pH, or ammonium
701 sulfate ((NH₄)₂SO₄) to acidify; an elemental sulfur treatment was selected to acid-
702 ify without N, applied at the same rate of S addition (57 kg S ha⁻¹ yr⁻¹); and
703 control plots received no additions. All amendments were added in pelletized form
704 using hand-held fertilizer spreaders to both the main plots and buffers. Amend-
705 ments were divided into three equal doses distributed across the growing season
706 from 2011-2017 and added as a single dose from 2018 onward. During 2019, plots
707 were fertilized during the week of May 20.

708 3.2.3 *Leaf gas exchange and trait measurements*

709 We sampled one leaf each from 6 to 10 individuals per plot between June
710 25 and July 12, 2019 for gas exchange measurements (Table S1). Leaves were
711 collected from deciduous broadleaf trees represented across all sites and plots
712 and were replicated in efforts to mimic the species abundance of each plot at
713 each site. We also attempted to collect leaves from the upper canopy to reduce
714 differential shading effects on leaf physiology. Leaves were accessed by pulling
715 down small branches using an arborist's slingshot and weighted beanbag attached
716 to a throw line. Branches were immediately recut under deionized water and
717 remained submerged to reduce stomatal closure and avoid xylem embolism (as in

718 Smith & Dukes, 2018) until gas exchange data were collected.

719 Randomly selected leaves with little to no visible external damage were
720 attached to a Li-COR LI-6800 (Li-COR Bioscience, Lincoln, Nebraska, USA)
721 portable photosynthesis machine to measure net photosynthesis (A_{net} ; $\mu\text{mol m}^{-2}$
722 s^{-1}), stomatal conductance (g_{sw} ; $\text{mol m}^{-2} \text{s}^{-1}$), and intercellular CO_2 concentra-
723 tion (C_i ; $\mu\text{mol mol}^{-1}$) at different reference CO_2 concentrations (C_a ; $\mu\text{mol mol}^{-1}$)
724 concentrations (i.e., an A_{net}/C_i curve) under saturating light conditions (2,000
725 $\mu\text{mol m}^{-2} \text{s}^{-1}$). Reference CO_2 concentrations followed the sequence: 400, 300,
726 200, 100, 50, 400, 400, 600, 800, 1000, 1200, 1500, and 2000 $\mu\text{mol mol}^{-1} \text{CO}_2$. Leaf
727 temperatures were not controlled in the cuvette and ranged from 21.8 °C to 31.7
728 °C (mean±SD: 27.2 ± 2.2 °C). A linear and second order log-polynomial nonlinear
729 regression suggested no effect of temperature on stomatal conductance measured
730 at 400 $\mu\text{mol mol}^{-1} \text{CO}_2$ or net photosynthesis measured at $\mu\text{mol mol}^{-1} \text{CO}_2$ (Ta-
731 ble S2-3; Fig. S1). All A_{net}/C_i curves were generated within one hour of branch
732 severance.

733 Leaf morphological and chemical traits were collected on the same leaf used
734 to generate each A_{net}/C_i curve. Images of each leaf were taken using a flat-bed
735 scanner to determine fresh leaf area using the ‘LeafArea’ R package (Katabuchi
736 2015), which automates leaf area calculations using ImageJ software (Schneider
737 et al. 2012). Each leaf was dried at 65°C for at least 48 hours, weighed, and
738 ground using a Retsch MM200 ball mill grinder (Verder Scientific, Inc., Newtown,
739 PA, USA) until homogenized. Leaf mass per area (M_{area} , g m^{-2}) was calculated
740 as the ratio of dry leaf biomass to fresh leaf area. Using a subsample of ground and
741 homogenized leaf biomass, leaf N content (N_{mass} ; gN g^{-1}) and leaf $\delta^{13}\text{C}$ (‰, rela-

742 tive to VPDB) were measured at the Cornell Stable Isotope Lab with an elemental
743 analyzer (NC 2500, CE Instruments, Wigan, UK) interfaced to an isotope ratio
744 mass spectrometer (Delta V Isotope Ratio Mass Spectrometer, ThermoFisher Sci-
745 entific, Waltham, MA, USA). Leaf N content per unit leaf area (N_{area} ; gN m⁻²)
746 was calculated by multiplying N_{mass} by M_{area} .

747 We used leaf $\delta^{13}\text{C}$ values to estimate χ (unitless), which is an isotope-
748 derived estimate of the leaf $C_i:C_a$ ratio. While intercellular and atmospheric CO₂
749 concentrations were directly measured during each A_{net}/C_i curve, deriving χ from
750 $\delta^{13}\text{C}$ provides a more integrative estimate of the $C_i:C_a$ over an individual leaf's
751 lifespan. We derived χ following the approach of Farquhar et al. (1989) described
752 in Cernusak et al. (2013):

$$\chi = \frac{\Delta^{13}\text{C} - a}{b - a} \quad (3.1)$$

753 where $\Delta^{13}\text{C}$ represents the relative difference between leaf $\delta^{13}\text{C}$ (‰) and air $\delta^{13}\text{C}$
754 (‰), and is calculated from the following equation:

$$\Delta^{13}\text{C} = \frac{\delta^{13}\text{C}_{\text{air}} - \delta^{13}\text{C}_{\text{leaf}}}{1 + \delta^{13}\text{C}_{\text{leaf}}} \quad (3.2)$$

755 where $\delta^{13}\text{C}_{\text{air}}$ is assumed to be -8‰ (Keeling et al. 1979; Farquhar et al. 1989), a
756 represents the fractionation between ¹²C and ¹³C due to diffusion in air, assumed
757 to be 4.4‰, and b represents the fractionation caused by Rubisco carboxylation,
758 assumed to be 27‰ (Farquhar et al. 1989).

759 3.2.4 A_{net}/C_i curve-fitting and parameter estimation

760 We fit A_{net}/C_i curves of each individual using the ‘fitaci’ function in the
761 ‘plantecophys’ R package (Duursma 2015). This function estimates the maxi-
762 mum rate of Rubisco carboxylation (V_{cmax} ; $\mu\text{mol m}^{-2} \text{s}^{-1}$) and maximum rate
763 of electron transport for RuBP regeneration (J_{max} ; $\mu\text{mol m}^{-2} \text{s}^{-1}$) based on the
764 Farquhar, von Caemmerer, and Berry biochemical model of C₃ photosynthesis
765 (Farquhar et al. 1980). For each curve fit, we included triose phosphate uti-
766 lization (TPU) limitation to avoid underestimating J_{max} (Gregory et al. 2021).
767 Curves were visually examined to confirm the likely presence of TPU limitation.

768 We determined Michaelis-Menten coefficients for Rubisco affinity to CO₂
769 (K_c ; $\mu\text{mol mol}^{-1}$) and O₂ (K_o ; $\mu\text{mol mol}^{-1}$), and the CO₂ compensation point
770 (Γ^* ; $\mu\text{mol mol}^{-1}$) using leaf temperature and equations described in Medlyn et al.
771 (2002) and derived in Bernacchi et al. (2001). Specifically, K_c and K_o were
772 calculated as:

$$K_c = 404.9 * \exp^{\frac{79430(T_k - 298)}{298RT_k}} \quad (3.3)$$

773 and

$$K_o = 278.4 * \exp^{\frac{36380(T_k - 298)}{298RT_k}} \quad (3.4)$$

774 while Γ^* was calculated as:

$$\Gamma^* = 42.75 * \exp^{\frac{37830(T_k - 298)}{298RT_k}} \quad (3.5)$$

775 In all three equations, T_k is the leaf temperature (in Kelvin) during each A_{net}/C_i

776 curve and R is the universal gas constant ($8.314 \text{ J mol}^{-1} \text{ K}^{-1}$).

777 We standardized V_{cmax} and J_{max} estimates to 25°C using a modified Ar-

778 rhenius equation (Kattge and Knorr 2007):

$$k_{25} = \frac{k_{\text{obs}}}{e^{\frac{H_a(T_{\text{obs}} - T_{\text{ref}})}{T_{\text{ref}}RT_{\text{obs}}}} * \frac{1+e^{\frac{T_{\text{ref}}\Delta S - H_d}{T_{\text{obs}}}}}{1+e^{\frac{T_{\text{obs}}\Delta S - H_d}{T_{\text{obs}}}}}} \quad (3.6)$$

779 k_{25} represents the standardized V_{cmax} or J_{max} rate at 25°C , k_{obs} represents

780 the V_{cmax} or J_{max} estimate at the average leaf temperature measured inside the

781 cuvette during the A_{net}/C_i curve. H_a is the activation energy of V_{cmax} ($71,513$

782 J mol^{-1}) Kattge and Knorr (2007) or J_{max} ($49,884 \text{ J mol}^{-1}$) (Kattge and Knorr

783 2007). H_d represents the deactivation energy of both V_{cmax} and J_{max} ($200,000 \text{ J}$

784 mol^{-1}) (Medlyn et al. 2002), and R represents the universal gas constant (8.314

785 $\text{J mol}^{-1} \text{ K}^{-1}$). T_{ref} represents the standardized temperature of 298.15 K (25°C)

786 and T_{obs} represents the mean leaf temperature (in K) during each A_{net}/C_i curve.

787 ΔS is an entropy term that (Kattge and Knorr 2007) derived as a linear relation-

788 ship with average growing season temperature (T_g ; $^\circ\text{C}$), where:

$$\Delta S_{v_{\text{cmax}}} = -1.07 T_g + 668.39 \quad (3.7)$$

789 and

$$\Delta S_{j_{\text{max}}} = -0.75 T_g + 659.70 \quad (3.8)$$

790 We estimated T_g in Equations 3.7 and 3.8 based on mean daily (24-hour) air
791 temperature of the 30 days leading up to the day of each sample collection using
792 the same weather station reported in the site description. We then used V_{cmax25}
793 and J_{max25} estimates to calculate the ratio of J_{max25} to V_{cmax25} ($J_{max25}:V_{cmax25}$;
794 unitless).

795 3.2.5 *Proportion of leaf nitrogen allocated to photosynthesis and structure*

796 We used equations from Niinemets and Tenhunen (1997) to estimate the
797 proportion of leaf N content allocated to Rubisco and bioenergetics. The propor-
798 tion of leaf N allocated to Rubisco (ρ_{rub} ; gN gN $^{-1}$) was calculated as a function
799 of V_{cmax25} and N_{area} :

$$\rho_{rubisco} = \frac{V_{cmax25} N_r}{V_{cr} N_{area}} \quad (3.9)$$

800 where N_r is the amount of nitrogen in Rubisco, set to 0.16 gN (gN in Rubisco) $^{-1}$
801 and V_{cr} is the maximum rate of RuBP carboxylation per unit Rubisco protein,
802 set to 20.5 μ mol CO $_2$ (g Rubisco) $^{-1}$. The proportion of leaf nitrogen allocated to
803 bioenergetics (ρ_{bioe} ; gN gN $^{-1}$) was similarly calculated as a function of J_{max25} and
804 N_{area} :

$$\rho_{bioe} = \frac{J_{max25} N_b}{J_{mc} N_{area}} \quad (3.10)$$

805 where N_b is the amount of nitrogen in cytochrome f, set to 0.12407 gN (μ mol
806 cytochrome f) $^{-1}$ assuming a constant 1: 1: 1.2 cytochrome f: ferredoxin NADP
807 reductase: coupling factor molar ratio (Evans and Seemann 1989; Niinemets and

808 Tenhunen 1997), and J_{mc} is the capacity of electron transport per cytochrome f,
809 set to $156 \mu\text{mol electron} (\mu\text{mol cytochrome f})^{-1}\text{s}^{-1}$.

810 We estimated the proportion of leaf N content allocated to photosynthetic
811 tissue (ρ_{photo} ; gN gN^{-1}) as the sum of ρ_{rub} and ρ_{bioe} . This calculation is an un-
812 derestimate of the proportion of leaf N allocated to photosynthetic tissue because
813 it does not include N allocated to light harvesting proteins. This leaf N pool was
814 not included because we did not perform chlorophyll extractions on focal leaves.
815 However, the proportion of leaf N content allocated to light harvesting proteins
816 tends to be small relative to ρ_{rub} and ρ_{bioe} , and may scale with changes in ρ_{rub}
817 and ρ_{bioe} (Niinemets and Tenhunen 1997).

818 Finally, we estimated the proportion of leaf N content allocated to struc-
819 tural tissue (ρ_{str} ; gN gN^{-1}) using an empirical equation from Onoda et al. (2017):

$$N_{cw} = 0.000355 * M_{area}^{1.39} \quad (3.11)$$

820 where N_{cw} is the leaf N content allocated to cell walls (gN m^{-2}). ρ_{str} was estimated
821 by dividing N_{cw} by N_{area} .

822 3.2.6 *Tradeoffs between nitrogen and water use*

823 Photosynthetic nitrogen use efficiency (PNUE; $\mu\text{mol CO}_2 \text{ mol}^{-1} \text{ N s}^{-1}$)
824 was calculated by dividing A_{net} by N_{area} , first converting N_{area} to mol N m^{-2}
825 using the molar mass of N (14 g mol^{-1}). We used χ as an indicator of water
826 use efficiency, which exploratory analyses suggest had similar responses to soil N
827 availability and pH as intrinsic water use efficiency measured from gas exchange

828 (A_{net}/g_s). Tradeoffs between nitrogen and water use were determined by cal-
829 culating the ratio of N_{area} to χ ($N_{\text{area}}:\chi$; g N m⁻²) and V_{cmax25} to χ ($V_{\text{cmax25}}:\chi$;
830 $\mu\text{mol m}^{-2} \text{s}^{-1}$). This approach is similar to tradeoff calculations in which nitrogen-
831 water use tradeoffs are measured as the ratio of N_{area} or V_{cmax25} to g_s (Paillassa
832 et al. 2020; Bialic-Murphy et al. 2021). In this study, we quantify these re-
833 lationships using χ in lieu of g_s because g_s rapidly changes with environmental
834 conditions and therefore may have been altered by recent tree branch severance
835 and/or placement in the cuvette.

836 3.2.7 *Soil nitrogen availability and pH*

837 To characterize soil N availability at the time of our leaf gas exchange
838 measurements, we used mixed bed resin bags to quantify mobile ammonium-N
839 and nitrate-N concentrations in each plot. Lycra mesh bags were filled with 5 g
840 of Dowex® Marathon MR-3 hydrogen and hydroxide form resin (MilliporeSigma,
841 Burlington, MA USA) and sealed with a zip tie. Each bag was activated by
842 soaking in 0.5 M HCl for 20 minutes, then in 2 M NaCl until pH of the saline
843 solution stabilized, as described in Allison et al. (2008). Five resin bags were
844 inserted about 10 cm below the soil surface at each plot on June 25, 2019: one
845 near each of the four plot corners and one near the plot center. All resin bags
846 were collected 24 days later on July 19, 2019 and were frozen until extracted.

847 Prior to anion and cation extraction, each resin bag was rinsed with ul-
848 trapure water (MilliQ IQ 7000; Millipore Sigma, Burlington, MA) to remove any
849 surface soil residues. Anions and cations were extracted from surface-cleaned resin
850 bags by individually soaking and shaking each bag in 100 mL of a 0.1 M HCl/2.0

851 M NaCl matrix for one hour. Using a microplate reader (Biotek Synergy H1;
852 Biotek Instruments, Winooski, VT USA), nitrate-N concentrations were quanti-
853 fied spectrophotometrically at 540 nm with the end product of a single reagent
854 vanadium (III) chloride reaction (Doane and Horwáth 2003), and ammonium-N
855 concentrations quantified at 650 nm with the end product of a modified phenol-
856 hypochlorite reaction (Weatherburn 1967; Rhine et al. 1998). Both the single
857 reagent vanadium (III) chloride and modified phenol-hypochlorite methodologies
858 have been well established for determining nitrate-N and ammonium-N concen-
859 trations in resin bag extracts (Arnone 1997; Allison et al. 2008). We used a
860 series of negative and positive controls throughout each well plate to verify the
861 accuracy and precision of our measurements, assaying each resin bag extract and
862 control in triplicate. Soil N availability was estimated as the sum of the nitrate-N
863 and ammonium-N concentration in each resin bag, normalized per g of resin and
864 duration in the field ($\mu\text{g N g}^{-1} \text{ resin d}^{-1}$), then subsequently averaged across all
865 resin bags in a plot for a plot-level mean.

866 Soil pH was measured on 0-10 cm mineral soil samples collected prior to
867 fertilization in 2019. Near each of the four plot corners, three 5.5 cm diameter soil
868 cores were collected after first removing the forest floor where present. Each set
869 of three cores was placed in a plastic bag, and later composited by hand mixing
870 and sieved to 4mm. Soil pH was determined for a 1:2 soil:water slurry (10 g field-
871 moist soil to 20 mL DI water) of each sample using an Accumet AB15 pH meter
872 with flushable junction probe (Fisher Scientific; Hampton, NH, USA), and was
873 estimated at the plot level as the mean soil pH within each plot.

874 3.2.8 *Statistical analyses*

875 We built two separate series of linear mixed-effects models to explore effects
876 of soil N availability, soil pH, species, and leaf N content on leaf physiological
877 traits. In the first series of linear mixed-effects models, we explored the effect
878 of soil N availability, soil pH, and species on leaf N content, leaf photosynthesis,
879 stomatal conductance, and nitrogen-water use tradeoffs. Models included plot-
880 level soil N availability and plot-level soil pH as continuous fixed effects, species
881 as a categorical fixed effect, and site as a categorical random intercept term.
882 Interaction terms between fixed effects were not included due to the small number
883 of experimental plots. We built a series of separate models with this independent
884 variable structure to quantify individual effects of soil N availability, soil pH,
885 and species on N_{area} , M_{area} , N_{mass} , A_{net} , V_{cmax25} , J_{max25} , $J_{\text{max25}}:V_{\text{cmax25}}$, ρ_{rubisco} ,
886 $\rho_{\text{bioenergetics}}$, ρ_{photo} , $\rho_{\text{structure}}$, χ , PNUE, $N_{\text{area}}:\chi$, and $V_{\text{cmax25}}:\chi$.

887 A second series of linear mixed-effects models were built to investigate
888 relationships between leaf N content and photosynthetic parameters. Statistical
889 models included N_{area} as a single continuous fixed effect with species and site des-
890 ignated as individual random intercept terms. We used this independent variable
891 structure to quantify individual effects of leaf N content on A_{net} , V_{cmax25} , J_{max25} ,
892 $J_{\text{max25}}:V_{\text{cmax25}}$, and χ .

893 For all linear mixed-effects models, we used Shapiro-Wilk tests of normal-
894 ity to determine whether linear mixed-effects models satisfied residual normality
895 assumptions. If residual normality assumptions were not met, then models were
896 fit using dependent variables that were natural log transformed. If residual nor-
897 mality assumptions were still not met (Shapiro-Wilk: $p < 0.05$), then models were

898 fit using dependent variables that were square root transformed. All residual nor-
899 mality assumptions for both sets of models that did not originally satisfy residual
900 normality assumptions were met with either a natural log or square root data
901 transformation (Shapiro-Wilk: $p > 0.05$ in all cases).

902 In the first series of models, models for N_{area} , M_{area} , N_{mass} , V_{cmax25} , J_{max25} ,
903 χ , $N_{\text{area}}:\chi$, and $V_{\text{cmax25}}:\chi$, ρ_{rubisco} , $\rho_{\text{bioenergetics}}$, ρ_{photo} , $\rho_{\text{structure}}$ satisfied residual
904 normality assumptions without data transformations (Shapiro-Wilk: $p > 0.05$ in
905 all cases). The model for $J_{\text{max25}}:V_{\text{cmax25}}$ satisfied residual normality assumptions
906 with a natural log data transformation, while models for A_{net} and PNUE each
907 satisfied residual normality assumptions with square root data transformations.
908 In the second series of models, models for V_{cmax25} , J_{max25} , χ , and $V_{\text{cmax25}}:\chi$ satisfied
909 residual normality assumptions without data transformations (Shapiro-Wilk: p
910 > 0.05 in all cases). The model for $J_{\text{max25}}:V_{\text{cmax25}}$ required a natural log data
911 transformation and the model for A_{net} required a square root data transformation
912 (Shapiro-Wilk: $p > 0.05$ in both cases).

913 In all models, we used the ‘lmer’ function in the ‘lme4’ R package (Bates
914 et al. 2015) to fit each model and the ‘Anova’ function in the ‘car’ R package (Fox
915 and Weisberg 2019) to calculate Type II Wald’s χ^2 and determine the significance
916 level ($\alpha = 0.05$) of each fixed effect coefficient. Finally, we used the ‘emmeans’
917 R package (Lenth, 2019) to conduct post-hoc comparisons using Tukey’s tests,
918 where degrees of freedom were approximated using the Kenward-Roger approach
919 (Kenward and Roger 1997). All analyses and plots were conducted in R version
920 4.1.1 (R Core Team 2021). All figure regression lines and associated 95% confi-
921 dence interval error bars were plotted using predictions generated across the soil

922 nitrogen availability gradient using the ‘emmeans’ R package (Lenth 2019).

923 3.3 Results

924 3.3.1 *Leaf N content*

925 Increasing soil N availability generally increased N_{area} (Table 3.1; Fig.
926 3.1a). This pattern was driven by an increase in N_{mass} (Table 3.1; Fig. 3.1c)
927 and a marginal increase in M_{area} (Table 3.1; Fig. 3.1e) with increasing soil N
928 availability. There was no effect of soil pH on N_{area} , N_{mass} , or M_{area} (Table 3.1);
929 however, we did observe strong differences in N_{area} (Fig. 3.1b), N_{mass} (Fig. 3.1d),
930 and M_{area} (Fig. 3.1e) between species (Table 3.1).

Table 3.1. Effects of soil N availability, soil pH, and species on leaf N content per unit leaf area (N_{area}), leaf N content per unit leaf mass (N_{mass}), and leaf mass per unit leaf area (M_{area})

	N_{area}			N_{mass}			M_{area}			
	df	Coefficient	χ^2	p	Coefficient	χ^2	p	Coefficient	χ^2	p
Intercept	-	9.03E-01	-	-	1.68E+00	-	-	4.60E+01	-	-
Soil N	1	1.68E-02	11.990	0.001	1.25E-02	6.902	0.009	4.87E-01	4.143	0.042
Soil pH	1	9.28E-02	0.836	0.361	8.08E-02	0.663	0.415	4.05E+00	0.653	0.419
Species	4	-	72.128	<0.001	-	35.074	<0.001	-	29.869	<0.001

931 *Significance determined using Type II Wald χ^2 tests ($\alpha = 0.05$). P-values < 0.05 are in bold.

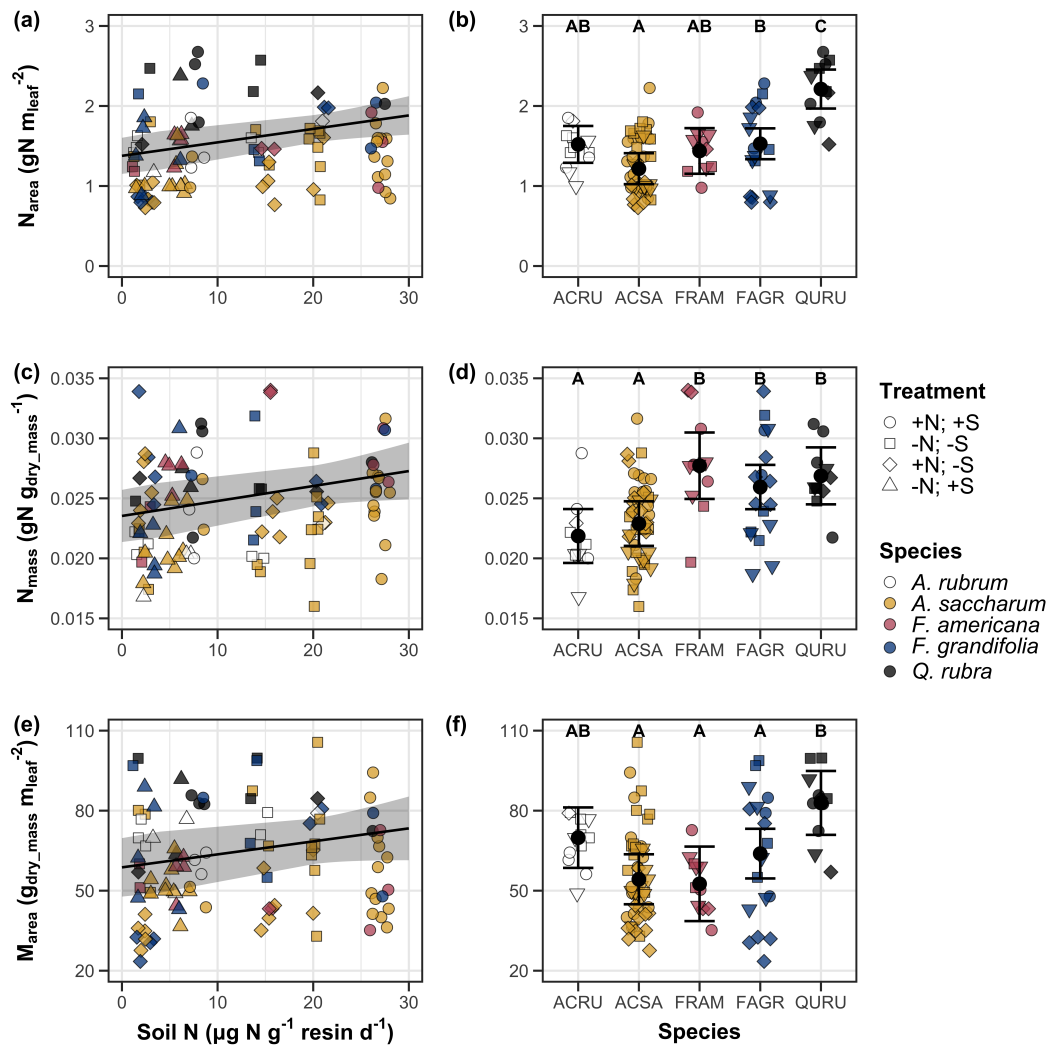


Figure 3.1. Effects of soil N availability and species on leaf N content per unit leaf area (a-b), leaf nitrogen content per unit leaf biomass (c-d), and leaf mass per leaf area (e-f). Soil N availability is represented on the x-axis in the left column of panels, while species is represented on the x-axis in the right column of panels. Tree species are represented as colored points and treatment plots are represented as shaped points, jittered for visibility. Species are abbreviated in the right column of panels through their assigned NRCS PLANTS Database symbol (USDA NRCS 2022), grouped along the x-axis per common mycorrhizal association, where the first three species commonly associate with arbuscular mycorrhizae (ACRU, ASCA, FAGR) and the second two species with ectomycorrhizae (FAGR, QURU). Trendlines are only included when the regression slope is statistically different from zero ($p < 0.05$).

932 3.3.2 *Net photosynthesis and leaf biochemistry*

933 Increasing soil N availability generally had no effect on A_{net} , V_{cmax25} , J_{max25} ,
934 or $J_{\text{max25}}:V_{\text{cmax25}}$ (Table 3.2, Figs. 3.2a, 3.2d, 3.2g). We also observed strong
935 species effects on all measured leaf photosynthetic traits (Table 3.2; Figs. 3.2b,
936 3.2e, 3.2h). Increasing soil pH had a marginal negative effect on A_{net} , but had no
937 effect on V_{cmax25} , J_{max25} , or $J_{\text{max25}}:V_{\text{cmax25}}$ (Table 3.2). There was a weak positive
938 effect of increasing N_{area} on A_{net} (Fig. 3.2c), but quite strong positive effects of
939 increasing N_{area} on V_{cmax25} and J_{max25} (Table 3.2; Fig. 3.2f and 3.2i).

Table 3.2. Effects of soil N availability, soil pH, species, and N_{area} on leaf biochemistry

	A_{net}			V_{cmax25}			J_{max25}			
	df	Coefficient	χ^2	p	Coefficient	χ^2	p	Coefficient	χ^2	p
(Intercept)	-	3.29E+00 ^b	-	-	6.38E+01	-	-	1.12E+02	-	-
Soil N	1	-1.23E-03 ^b	1.798	0.180	-3.84E-01	1.745	0.187	-6.70E-01	2.172	0.141
Soil pH	1	-3.09E-01 ^b	3.312	0.069	-4.91E+00	0.655	0.418	-8.18E+00	0.742	0.389
Species	4	-	11.838	0.019	-	31.748	<0.001	-	27.291	<0.001
(N_{area} int.)	-	6.59E-01 ^b	-	-	1.45E-01	-	-	2.86E+01	-	-
N_{area}	4	3.13E-01 ^b	4.790	0.029	2.43E+01	22.616	<0.001	4.04E+01	28.259	<0.001

	$J_{\text{max25}}:V_{\text{cmax25}}$			
	df	Coefficient	χ^2	p
(Intercept)	-	6.59E-01 ^a	-	-
Soil N	1	7.04E-04 ^a	0.088	0.767
Soil pH	1	-7.84E-03 ^a	0.025	0.874
Species	4	-	12.745	0.013
(N_{area} int.)	-	6.69E-01 ^a	-	-
N_{area}	4	-4.69E-02 ^a	1.142	0.285

940 *Significance determined using Type II Wald χ^2 tests ($\alpha = 0.05$). P-values < 0.05 are in bold, while p-values between
 941 0.05 and 0.1 are italicized. Superscript letters indicate model coefficients fit to natural-log (^a) or square-root (^b)
 942 transformed data. Relationships between N_{area} and each response variable were fit using the second series of bivariate
 943 mixed-effects models, so model coefficients and results are independent of model coefficients and results reported
 944 for relationships between soil N, soil pH, and species for each response variable. Key: A_{net} – light saturated net
 945 photosynthesis rate; V_{cmax25} – maximum rate of Rubisco carboxylation at 25°C; J_{max25} – maximum rate of electron
 946 transport for RuBP regeneration at 25°C, $J_{\text{max25}}:V_{\text{cmax25}}$ – the ratio of J_{max25} to V_{cmax25} .

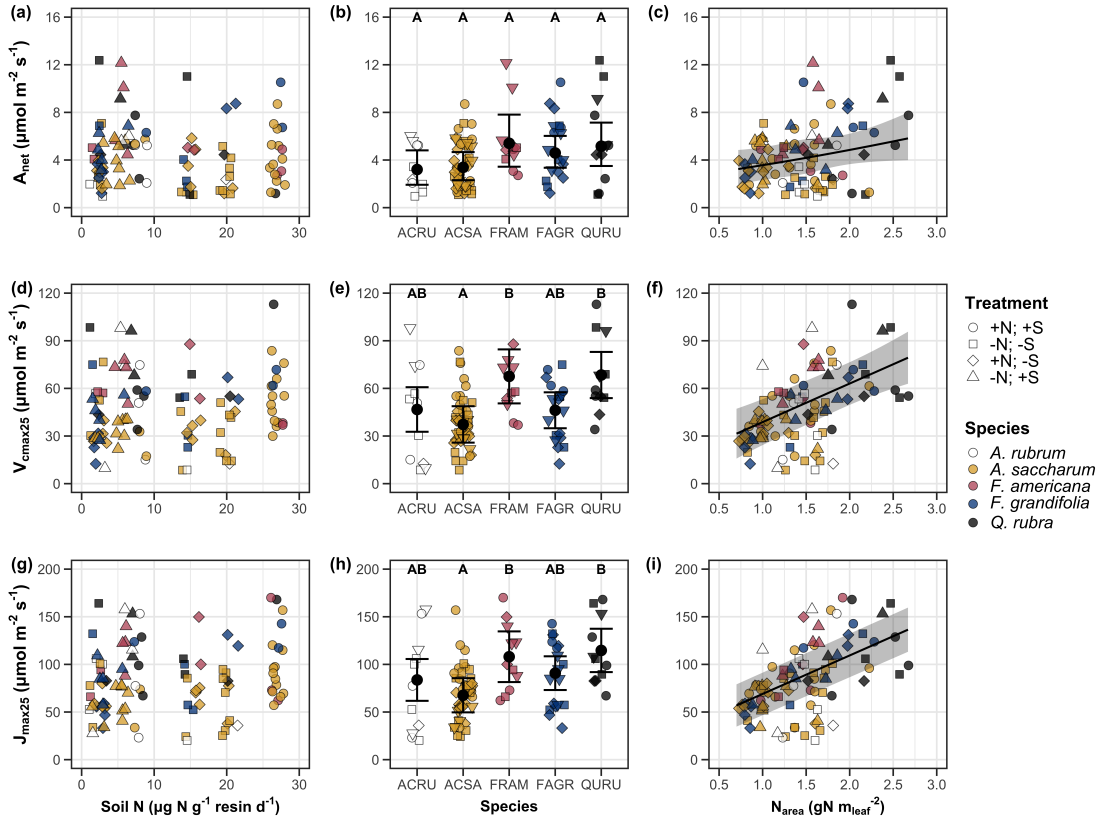


Figure 3.2. Effects of soil N availability (left column of panels), species (middle column of panels), and leaf N content per unit leaf area (right column of panels) on net photosynthesis (a-c), maximum Rubisco carboxylation rate (d-f), and maximum RuBP regeneration rate (g-i). Soil N availability is represented on the x-axis in the left column of panels, species is represented on the x-axis in the middle column of panels, and leaf N content per unit leaf area is represented continuously on the x-axis in the right column of panels. Species abbreviations and position along the x-axis in the middle column of panels, colored points, shapes, and trendlines are as explained in Figure 3.1.

947 3.3.3 *Leaf N allocation*

948 Neither soil N availability nor soil pH affected the proportion of leaf N
949 allocated to Rubisco or bioenergetics (Table 3.3; Fig. 3.3a, Fig. 3.3c), nor was
950 there any subsequent effect on the proportion of leaf N allocated to photosynthesis
951 (Table 3.3; Fig. 3.3f). We also found no effect of soil N availability or soil pH on
952 the proportion of leaf N allocated to structure (Table 3.3; Fig 3.3g). Species varied
953 in the proportion of leaf N allocated to Rubisco, photosynthesis, and structure (Fig
954 3.3b, Fig. 3.3d, Fig 3.3h), with no detectable species effect on the proportion of
955 leaf N allocated to bioenergetics (Table 3.3).

Table 3.3. Effects of soil N availability, soil pH, and species on the proportion of leaf nitrogen content allocated to photosynthesis, Rubisco, bioenergetics, and structure

	ρ_{photo}			ρ_{rub}			ρ_{bioe}			
	df	Coefficient	χ^2	p	Coefficient	χ^2	p	Coefficient	χ^2	p
Intercept	-	4.93E-01	-	-	4.17E-01	-	-	7.64E-02	-	-
Soil N	1	-1.23E-03	0.521	0.470	-1.04E-03	0.501	0.479	-1.77E-04	0.557	0.455
Soil pH	1	-4.37E-02	1.581	0.209	-3.70E-02	1.511	0.219	-6.84E-03	1.941	0.164
Species	4	-	13.106	0.011	-	14.152	0.007	-	7.300	0.121

	ρ_{str}			
	df	Coefficient	χ^2	p
Intercept	-	9.77E-02	-	-
Soil N	1	-2.29E-04	1.165	0.280
Soil pH	1	-1.87E-03	0.179	0.672
Species	4	-	16.428	0.002

58

956 *Significance determined using Type II Wald χ^2 tests ($\alpha = 0.05$). P-values < 0.05 are in bold. Key: ρ_{photo} -
 957 proportion of leaf nitrogen content allocated to photosynthesis; ρ_{rub} - proportion of leaf nitrogen content allocated
 958 to Rubisco; ρ_{bioe} - proportion of leaf nitrogen content allocated to bioenergetics; ρ_{str} - proportion of leaf nitrogen
 959 content allocated to structure.

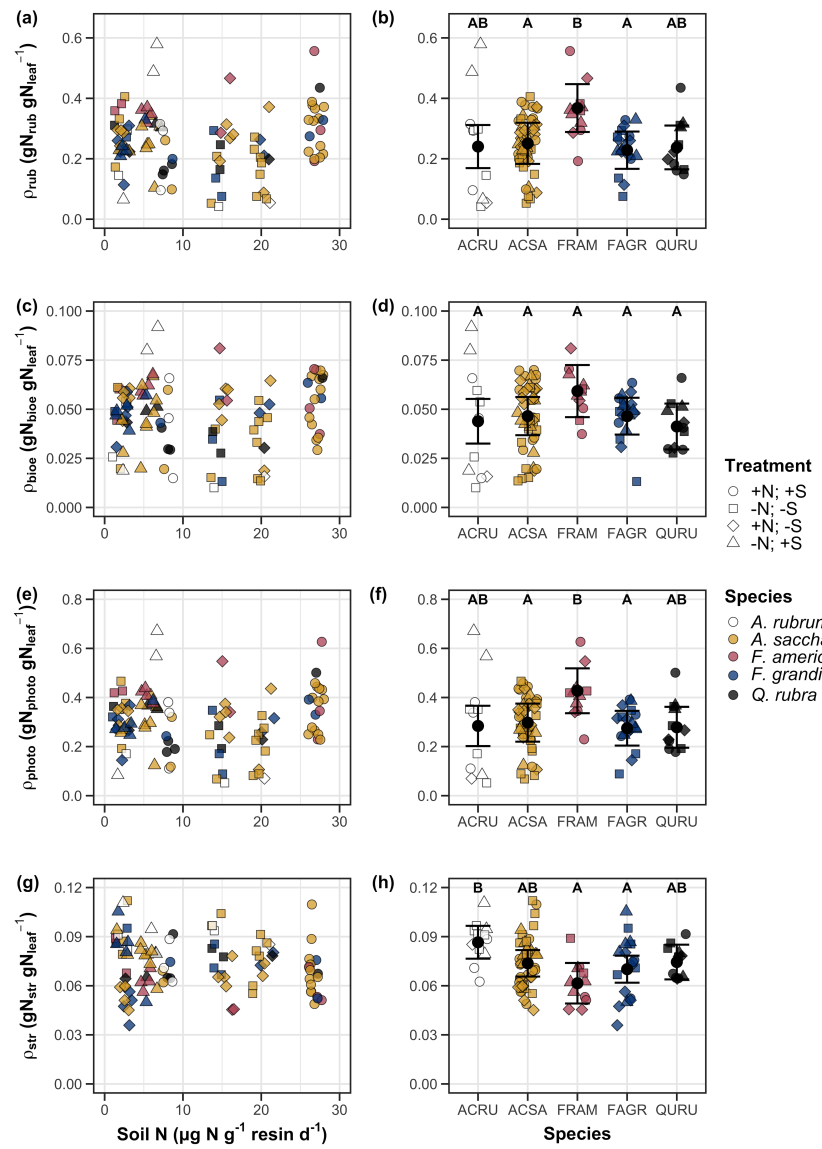


Figure 3.3. Effects of soil nitrogen availability and species on the proportion of leaf nitrogen content allocated to Rubisco (a-b), bioenergetics (c-d), photosynthesis (e-f), and structure (g-h). Soil nitrogen availability is represented on the x-axis in the left column of panels and species are represented on the x-axis in the right column of panels. Species abbreviations and position along the x-axis in the middle column of panels, colored points, shapes, trendlines, error bars, and compact lettering are as explained in Figure 3.1.

960 3.3.4 *Tradeoffs between nitrogen and water use*

961 Although soil N availability did not affect χ (Table 3.4; Fig. 3.4a), increasing
962 soil N availability decreased PNUE (Table 3.4; Fig. 3.4d) and increased the
963 ratio of $N_{\text{area}}:\chi$ (Table 3.4; Fig. 3.4f). Specifically, this response yielded a 26%
964 reduction in PNUE and 37% stimulation in $N_{\text{area}}:\chi$ across the soil nitrogen avail-
965 ability gradient. There was no apparent effect of soil N availability on $V_{\text{cmax25}}:\chi$
966 (Table 3.4; Fig. 3.4h). Increasing soil pH had a weak marginal negative effect
967 on PNUE, but did not influence χ , $N_{\text{area}}:\chi$, or $V_{\text{cmax25}}:\chi$ (Table 3.4). We also
968 observed differences in χ (Fig. 3.4b), PNUE (Fig. 3.4e), $N_{\text{area}}:\chi$ (Fig. 3.4g), and
969 $V_{\text{cmax25}}:\chi$ (Fig. 3.4i) between species (Table 3.4). Finally, increasing N_{area} had a
970 strong negative effect on χ (Table 3.4; Fig. 3.4c) and a strong positive effect on
971 $V_{\text{cmax25}}:\chi$ (Table 3.4; Fig. 3.4j).

Table 3.4. Effects of soil N availability, soil pH, species, and N_{area} on tradeoffs between nitrogen and water use

	χ	PNUE				$N_{\text{area}}:\chi$				
	df	Coefficient	χ^2	p	Coefficient	χ^2	p	Coefficient	χ^2	p
(Intercept)	-	8.12E-01	-	-	9.57E+00	-	-	9.19E-01	-	-
Soil N	1	-1.14E-03	1.698	0.193	-6.63E-02	6.396	0.011	2.60E-02	9.533	0.002
Soil pH	1	-1.91E-02	1.087	0.297	-9.25E-01	2.843	<i>0.092</i>	2.03E-01	1.321	0.250
Species	4	-	18.843	0.001	-	13.454	0.009	-	52.983	<0.001
$(N_{\text{area}} \text{ int.})$	-	8.93E-01	-	-	-	-	-	-	-	-
N_{area}	1	-1.11E-01	80.606	<0.001	-	-	-	-	-	-

	$V_{\text{cmax25}}:\chi$			
	df	Coefficient	χ^2	p
(Intercept)	-	7.20E+01	-	-
Soil N	1	3.99E-01	0.963	0.326
Soil pH	1	-3.12E+00	0.138	0.711
Species	4	-	31.450	<0.001
$(N_{\text{area}} \text{ int.})$	-	1.18E+01	-	-
N_{area}	4	3.87E+01	32.797	<0.001

*Significance determined using Type II Wald χ^2 tests ($\alpha = 0.05$). P-values < 0.05 are in bold, while p-values between 0.05 and 0.1 are italicized. Superscript letters indicate model coefficients fit to natural-log ^(a) or square-root ^(b) transformed data. Relationships between N_{area} and each response variable were fit using the second series of bivariate mixed-effects models, so model coefficients and results are independent of model coefficients and results reported for relationships between soil N, soil pH, and species for each response variable. Key: χ - isotope-derived estimate of the $C_i:C_a$; PNUE - photosynthetic N use efficiency, ratio of net photosynthesis to leaf N content per unit leaf area; $N_{\text{area}}:\chi$ - ratio of N_{area} to χ ; $V_{\text{cmax25}}:\chi$ - ratio of V_{cmax25} to χ .

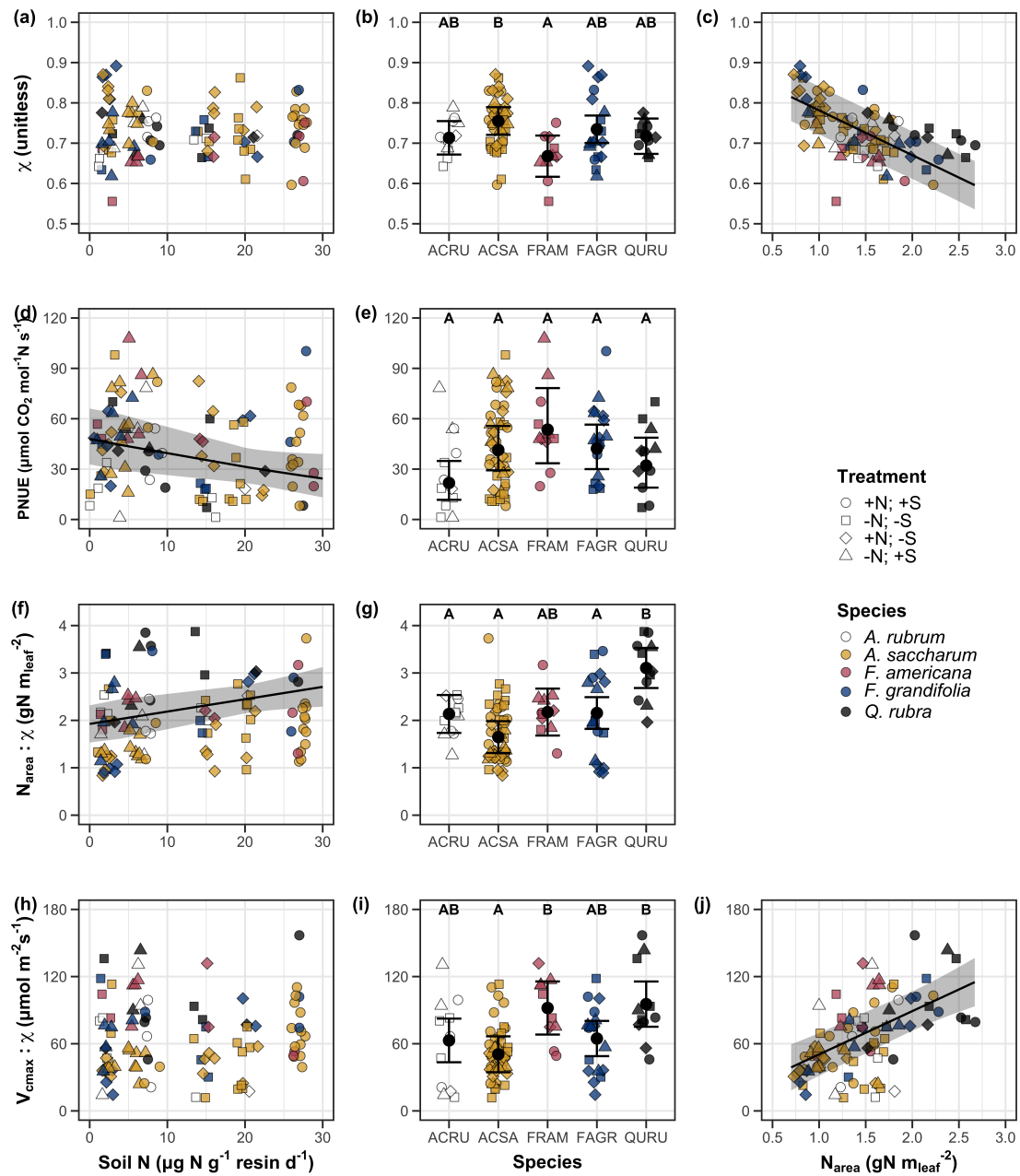


Figure 3.4. Effects of soil nitrogen availability and species on the proportion of leaf nitrogen content allocated to Rubisco (a-b), bioenergetics (c-d), photosynthesis (Rubisco + bioenergetics; e-f), and structure (g-h). Soil nitrogen availability is represented on the x-axis in the left column of panels and species are represented on the x-axis in the right column of panels. Species abbreviations and position along the x-axis in the middle column of panels, colored points, shapes, trendlines, error bars, and compact lettering are as explained in Figure 3.1.

979 3.4 Discussion

980 Photosynthetic least-cost theory provides an explanation for understand-
981 ing relationships between soil nutrient availability, leaf nutrient allocation, and
982 photosynthetic capacity. The theory suggests that plants acclimate to a given
983 environment by optimizing leaf photosynthesis rates at the lowest summed cost
984 of using nutrients and water Prentice et al. (2014), Wang et al. (2017), Smith
985 et al. (2019), Paillassa et al. (2020). The theory predicts that an increase in
986 soil nutrient availability should allow similar photosynthesis rates to be achieved
987 with increased leaf nutrient content and photosynthetic capacity (i.e., V_{cmax25} and
988 J_{max25}) at lower leaf $C_i:C_a$ (χ), resulting in an increase in water use efficiency,
989 decrease in nutrient use efficiency, and increase in both leaf nutrient content and
990 photosynthetic capacity per unit χ . The theory predicts similar leaf responses to
991 increasing soil pH under acidic conditions, presumably due to generally faster nu-
992 trient cycle dynamics and consequent reductions in the cost of acquiring nutrients
993 relative to water with increasing soil pH (Wang et al. 2017; Paillassa et al. 2020;
994 Dong et al. 2020).

995 Supporting the theory, we showed that increasing soil N availability was
996 associated with increased leaf N content (Fig 3.1a, 3.1c), a pattern that reduced
997 photosynthetic N use efficiency (Fig 3.4d) and increased leaf N content per unit
998 χ (Fig 3.4f). Increasing soil N coincided with slight, but non-significant decreases
999 in χ and increases in V_{cmax25} and J_{max25} ($p < 0.2$, Table 3.2). The positive trend
1000 between soil N availability and photosynthetic capacity was supported by the con-
1001 current strong increase in leaf N content with increasing soil N availability, which
1002 resulted in no change in the proportion of leaf N content allocated to photosynthe-

1003 sis across the soil N availability gradient. Additionally, leaf N content exhibited a
1004 strong negative correlation with χ , indicative of strong nitrogen-water use trade-
1005 offs at the leaf level. Responses tended to vary more due to soil N availability
1006 than soil pH. Overall, these findings are consistent with the nutrient-water use
1007 tradeoffs predicted from theory.

1008 3.4.1 *Soil nitrogen availability modifies tradeoffs between nitrogen and water use*

1009 In support of expected least-cost outcomes and past environmental gradient
1010 studies (Dong et al. 2017; Paillassa et al. 2020), we found that increasing soil N
1011 availability was associated with increased leaf N content. Soil N availability had
1012 smaller impacts on measures of net photosynthesis and χ , which led to reductions
1013 in PNUE and increases in leaf N content per unit χ , as expected from theory.
1014 Photosynthetic least-cost theory suggests that reductions in PNUE should be
1015 driven by an increase in the proportion of leaf N allocated to photosynthetic tissue,
1016 a pattern that should allow plants to achieve optimal photosynthetic rates with
1017 greater photosynthetic capacity to make better use of available light. Contrasting
1018 theory predictions, we found no effect of soil N availability on photosynthetic
1019 capacity. However, photosynthetic capacity did tend to increase with increasing
1020 soil N availability ($p < 0.20$; Table 3.2) resulting in no effect of soil N availability on
1021 the relative fraction of leaf N allocated to photosynthesis, Rubisco, or bioenergetics
1022 (Fig. 3.3). These lines of evidence support the idea that trees use additional N
1023 to support increased leaf N allocation toward photosynthetic tissue and enhance
1024 photosynthetic capacity (Wright et al. 2003).

1025 Soil N availability had a stronger effect on leaf N than photosynthetic ca-

1026 pacity. This pattern suggests that additional plant N uptake due to increased
1027 soil N availability was also being used to support non-photosynthetic N pools,
1028 possibly to structural tissue or stress-induced amino acid and polyamine synthe-
1029 sis (Minocha et al. 2000; Onoda et al. 2004; Bubier et al. 2011). While we
1030 found no change in the proportion of leaf N allocated to leaf structural tissue, the
1031 overall stimulation in leaf N content with increasing soil N availability suggests an
1032 increase in the net amount of N invested in leaf structural tissue along the N avail-
1033 ability gradient. Importantly, leaf N allocated to structure was calculated using
1034 an empirical relationship between M_{area} and the amount of leaf N allocated to cell
1035 walls (Onoda et al. 2017). As the generality of relationships between M_{area} and
1036 the amount of leaf N allocated to cell walls has been called into question (Harrison
1037 et al. 2009), future work should consider explicitly measuring N allocation to cell
1038 wall tissue and stress-induced amino acid synthesis to confirm these patterns.

1039 In opposition to patterns expected from least-cost theory, increasing soil
1040 N availability had no apparent effect on χ (Fig. 3.4a). Interestingly, despite
1041 the null effect of soil N availability on χ , we observed a strong negative effect of
1042 increasing N_{area} on χ (Fig. 3.4c), consistent with the nitrogen-water use tradeoffs
1043 expected from theory. The null response of χ to increasing soil N availability may
1044 have been due to a lack of water limitation in the system, given that the area
1045 received approximately 20% more precipitation (1167 mm) during the 12-month
1046 period leading up to our measurement period than normally expected (972 mm).
1047 However, droughts can and do occur in temperate forests of the northeastern
1048 United States (Sweet et al. 2017), so the observed increase in leaf N content
1049 with increasing soil N availability could be a strategy that allows trees to hedge

1050 bets against drier than normal growing seasons (Onoda et al. 2004; Onoda et al.
1051 2017; Hallik et al. 2009). As was suggested in Paillassa et al. (2020), and more
1052 recently by Querejeta et al. (2022), negative effects of soil N availability on χ may
1053 increase with increasing aridity. This strategy would be especially advantageous if
1054 it allows individuals growing in arid regions to maintain carbon assimilation rates
1055 with reduced water loss. Future work should attempt to quantify interactive roles
1056 of climate and soil nitrogen availability on nitrogen-water use tradeoffs, which
1057 could be done by leveraging coordinated and multifactor nutrient (Borer et al.
1058 2014) and water (Knapp et al. 2017) manipulation experiments across broad
1059 climatic gradients.

1060 3.4.2 *Soil pH did not modify tradeoffs between nitrogen and water usage*

1061 While the primary purpose of this study was to examine the role of soil N
1062 availability on nitrogen-water use tradeoffs, our experimental design manipulated
1063 both soil N and pH, providing an opportunity to isolate the roles of these variables.
1064 Previous correlational studies along environmental gradients identified soil pH as
1065 a particularly important factor that can modify tradeoffs between nutrient and
1066 water use (Smith et al. 2019; Paillassa et al. 2020; Westerband et al. 2023)
1067 and the proportion of leaf nitrogen allocated to photosynthesis (Luo et al. 2021).
1068 Such studies implied that these patterns may be driven by reductions in the cost of
1069 acquiring nutrients relative to water with increasing pH, which may be exacerbated
1070 in acidic soils.

1071 Consistent with theory (Wright et al. 2003; Prentice et al. 2014), our
1072 results indicate that increasing soil pH was negatively associated with PNUE.

1073 However, there was no effect of soil pH on leaf N content, χ , or leaf N content per
1074 unit χ , most likely because the experimental N additions increased soil N sup-
1075 ply while both increasing (sodium nitrate) and decreasing (ammonium sulfate)
1076 soil pH. These results suggest that soil pH did not play a major role in modify-
1077 ing expected photosynthetic least-cost theory patterns, contrasting findings from
1078 Paillassa et al. (2020) and other gradient studies that note positive effects of in-
1079 creasing soil pH on leaf N content, Rubisco carboxylation, and χ (Viet et al. 2013;
1080 Cornwell et al. 2018; Luo et al. 2021). Instead, null responses to soil pH show
1081 that leaf photosynthetic parameters depend more on soil N availability than pH
1082 per se, and that inferences from gradient studies might be confounding covariation
1083 between N availability and soil acidity.

1084 3.4.3 *Species identity explains a large amount of variation in leaf and whole*
1085 *plant traits*

1086 Species generally explained a larger amount of variation in measured leaf
1087 traits than soil N availability or soil pH. Interspecies variation is an important
1088 factor to consider when deducing mechanisms that drive photosynthetic least-
1089 cost theory, particularly for species that form distinct mycorrhizal associations or
1090 have different photosynthetic pathways, growth forms, or leaf habit (Espelta et al.
1091 2005; Adams et al. 2016; Bialic-Murphy et al. 2021; Scott and Smith 2022). The
1092 need to consider species may also be important when comparing nutrient-water
1093 use tradeoffs in early and late successional species, or in species with different
1094 resource economic strategies (Abrams and Mostoller 1995; Ellsworth and Reich
1095 1996; Wright et al. 2004; Reich 2014; Onoda et al. 2017; Ziegler et al. 2020).

1096 A strength of the study design and sampling effort is that it controls for
1097 many species differences that should modify nitrogen-water use tradeoffs expected
1098 from theory. All tree species measured in this study shared the leaf habit of decid-
1099 uous broadleaves, were growing in forests of similar successional stage, but differed
1100 in mycorrhizal association and consequent resource economic strategies. As stands
1101 tended to be dominated by trees that associate with arbuscular mycorrhizae (*Frax-*
1102 *inus* and both *Acer* species made up 70% of total aboveground biomass across
1103 stands), ecosystem biogeochemical cycle dynamics may be more closely aligned
1104 to the inorganic nutrient economy proposed in Phillips et al. (2013), which may
1105 promote stronger nitrogen-water use tradeoffs in tree species that associate with
1106 arbuscular mycorrhizae. This result was not observed here, as photosynthetic
1107 properties varied as much within as across the two mycorrhizal associations rep-
1108 resented. Given the high variability in measured photosynthetic traits within
1109 and across species, effects of mycorrhizal association likely require more intensive
1110 sampling efforts to detect than were possible here.

1111 3.4.4 *Implications for photosynthetic least-cost theory model development*

1112 In the field, soil nutrient availability is heterogeneous across time and space
1113 (Table S4). Unaccounted within-plot heterogeneity may have contributed to the
1114 low amount of variation explained by soil N availability in our statistical mod-
1115 els, as resin bags are a coarse surrogate for soil N availability. Despite this, we
1116 still observed evidence for nutrient-water use tradeoffs, suggesting that observed
1117 responses reported here may be an underestimate toward the net effect of soil
1118 N availability on these tradeoffs. While we urge caution in the interpretation of

1119 these results, they do provide a promising baseline for future studies investigating
1120 patterns expected from photosynthetic least-cost theory at finer spatiotemporal
1121 resolutions.

1122 The general stronger relationship between leaf N content and photosyn-
1123 thetic parameters versus between leaf N content and soil N availability suggests
1124 that leaf N content is more directly tied to photosynthesis than soil N availabil-
1125 ity. While this could be due to the high spatiotemporal heterogeneity of soil N
1126 availability, principles from photosynthetic least-cost theory suggest that leaf N
1127 content is the downstream product of leaf nutrient demand to build and maintain
1128 photosynthetic machinery, which is set by aboveground environmental conditions
1129 such as light availability, CO₂, temperature, or vapor pressure deficit (Smith
1130 et al. 2019; Paillassa et al. 2020; Peng et al. 2021; Westerband et al. 2023). The
1131 stronger relationship between leaf N and photosynthetic parameters paired with
1132 the strong negative relationship between leaf N and χ could indicate a relatively
1133 stronger effect of climate on leaf N-photosynthesis relationships than soil resource
1134 availability. However, the short distance between plots and across sites limited
1135 our ability to test this mechanism.

1136 Variation in soil pH affected least cost responses less than variations in
1137 soil N availability, in part because experimental treatments directly increased soil
1138 N and affected soil pH in opposite directions. While soil pH has been shown
1139 to drive nitrogen-water tradeoffs in global gradient analyses (Viet et al. 2013;
1140 Paillassa et al. 2020), these responses may be due to covariations between soil pH
1141 and nutrient cycling rather than a role of pH per se. The direct manipulations
1142 of soil pH and soil N availability in this study allowed us to partly disentangle

1143 these factors and show that variation in N availability matters more for least-cost
1144 tradeoffs than pH alone.

1145 3.4.5 *Conclusions*

1146 Increasing soil N availability generally increased leaf N content (both area-
1147 and mass-based), but did not significantly influence χ . This shift in leaf N led
1148 to a reduction in PNUE, and an increase in leaf N per unit χ with increasing
1149 soil N availability. Despite null effects of soil N availability on χ , we observed a
1150 strong negative relationship between leaf N content and χ . These results provide
1151 empirical support for the nutrient-water use tradeoffs expected from photosyn-
1152 thetic least-cost theory in response to soil nutrient availability, but suggest that
1153 all tenets of the theory may not hold in every environment. These results exper-
1154 imentially test previous work suggesting that leaf water-nitrogen economies vary
1155 across gradients of soil nutrient availability and pH, and show that variations in
1156 nutrient availability matter more for determining variation in leaf photosynthetic
1157 traits than soil pH.

1158

Chapter 4

1159 The relative cost of resource use for photosynthesis drives variance in
1160 leaf nitrogen content across climate and soil resource availability
1161 gradients

1162 4.1 Introduction

1163 Terrestrial biosphere models, which comprise the land surface component of
1164 Earth system models, are sensitive to the formulation of photosynthetic processes
1165 (Knorr 2000; Ziehn et al. 2011; Booth et al. 2012). This is because photosynthe-
1166 sis is the largest carbon flux between the atmosphere and terrestrial biosphere,
1167 and is constrained by ecosystem carbon and nutrient cycles (Hungate et al. 2003;
1168 LeBauer and Treseder 2008; IPCC 2021; Fay et al. 2015). Many terrestrial bio-
1169 sphere models formulate photosynthesis by parameterizing photosynthetic capac-
1170 ity within plant functional groups through empirical linear relationships between
1171 area-based leaf nitrogen content (N_{area}) and the maximum carboxylation rate
1172 of Ribulose-1,5-bisphosphate carboxylase/oxygenase (Kattge et al. 2009; Rogers
1173 2014; Rogers et al. 2017). Models are also beginning to include connected carbon-
1174 nitrogen cycles (Wieder et al. 2015; Shi et al. 2016; Davies-Barnard et al. 2020;
1175 Braghieri et al. 2022), which allows leaf photosynthesis to be predicted directly
1176 through changes in N_{area} and indirectly through changes in soil nitrogen avail-
1177 ability (e.g., LPJ-GUESS, Smith et al., 2014; CLM5.0, Lawrence et al., 2019).
1178 Despite recent model developments, open questions remain regarding the gen-
1179 erality of ecological relationships between soil nitrogen availability, leaf nitrogen
1180 content, and leaf photosynthesis across edaphic and climatic gradients.
1181 Empirical support for positive relationships between soil nitrogen avail-

ability and N_{area} is abundant (Firn et al. 2019; Liang et al. 2020), and is a result often attributed to the high nitrogen cost of building and maintaining Rubisco (Evans 1989; Evans and Seemann 1989; Onoda et al. 2004; Onoda et al. 2017; Dong et al. 2020). Such patterns imply that positive relationships between soil nitrogen availability and N_{area} should cause an increase in leaf photosynthesis and photosynthetic capacity by increasing the maximum rate of Rubisco carboxylation through increased investments to Rubisco construction and maintenance. This integrated N_{area} -photosynthesis response to soil nitrogen availability has been observed both in manipulative experiments and across environmental gradients (Field and Mooney 1986; Evans 1989; Walker et al. 2014; Li et al. 2020), and is thought to be driven by ecosystem nitrogen limitation, which limits its primary productivity globally (LeBauer and Treseder 2008; Fay et al. 2015). However, this response is not consistently observed, as recent studies note variable N_{area} -photosynthesis relationships across soil nitrogen availability gradients (Liang et al. 2020; Luo et al. 2021) and that aboveground growing conditions (e.g., light availability, temperature, vapor pressure deficit) or species identity traits (e.g., photosynthetic pathway, nitrogen acquisition strategy) may be more important for explaining variance in N_{area} and photosynthetic capacity across time and space (Adams et al. 2016; Dong et al. 2017; Dong et al. 2020; Dong et al. 2022; Smith et al. 2019; Peng et al. 2021; Westerband et al. 2023).

One hypothesized mechanism to explain variance in N_{area} across environmental gradients has been proposed via photosynthetic least-cost theory (Wright et al. 2003; Prentice et al. 2014; Paillassa et al. 2020; Harrison et al. 2021). The theory predicts that plants acclimate to environments by optimizing photo-

1206 synthetic assimilation rates at the lowest summed cost of nitrogen and water use
1207 (Wright et al. 2003; Prentice et al. 2014). In a given environment, the theory
1208 proposes that nitrogen and water use can be substituted for each other to main-
1209 tain the lowest summed cost to satisfy leaf resource demand, such that optimal
1210 photosynthetic rates are achieved with less efficient use of the more abundant
1211 and less costly resource to acquire in exchange for more efficient use of the less
1212 abundant and more costly resource to acquire.

1213 Photosynthetic least-cost theory predicts that, all else equal, an increase
1214 in soil nitrogen availability should decrease the cost of acquiring and using nitro-
1215 gen relative to water (β), resulting in optimal photosynthetic rates achieved with
1216 greater N_{area} at lower stomatal conductance and lower leaf $C_i:C_a$ (χ) (Wright et al.
1217 2003; Prentice et al. 2014). Alternatively, an increase in soil moisture should re-
1218 duce costs of water acquisition and use, increasing β , stomatal conductance, and
1219 χ , resulting in optimal photosynthetic rates achieved with decreased N_{area} . The
1220 theory also predicts variability in stomatal conductance and N_{area} in response to
1221 climatic factors, suggesting that the optimal response to increased vapor pressure
1222 deficit (VPD) should be a reduction in stomatal conductance and χ that is coun-
1223 terbalanced by an increase in N_{area} to support the higher photosynthetic capacity
1224 needed to maintain high assimilation at lower conductance (Grossiord et al. 2020;
1225 Dong et al. 2020; Westerband et al. 2023).

1226 Leaf nitrogen allocation responses to changing climates or soil resource
1227 availability may also depend on their mode of nutrient acquisition or photo-
1228 synthetic pathway. For example, species that form associations with symbiotic
1229 nitrogen-fixing bacteria (referred as “N-fixing species” from this point forward)

1230 should, in theory, have access to a less finite nitrogen supply, which may result in
1231 lower β values than species not capable of forming such associations (referred as
1232 “non-fixing species” from this point forward). This result was previously shown
1233 in a greenhouse experiment, where a leguminous species generally had lower costs
1234 of nitrogen acquisition compared to a non-leguminous species, although these dif-
1235 ferences were generally stronger under increased nitrogen limitation (Fig. 2.1)
1236 (Perkowski et al. 2021). Lower β values could be a possible explanation for
1237 why N-fixing species commonly have higher leaf nitrogen content than non-fixing
1238 species (Adams et al. 2016; Dong et al. 2017).

1239 Similarly, leaf nitrogen allocation patterns across environmental gradients
1240 may be dependent on photosynthetic pathway. General lower χ values in C₄
1241 species suggests that C₄ species should have lower β values than C₃ species, a
1242 pattern that could be the result of increased costs associated with water acquisition
1243 and use or reduced costs associated with nutrient acquisition and use relative to
1244 C₃ species. No study to date has directly quantified χ in C₄ species aside from the
1245 dataset used to initially parameterize an optimality model for C₄ species (Scott
1246 and Smith 2022).

1247 While photosynthetic least-cost theory provides a unified hypothesis for
1248 understanding effects of climate and soil resource availability on N_{area} , empiri-
1249 cal tests of the theory are sparse. Increasing soil nitrogen availability has been
1250 previously shown to decrease the cost of acquiring nutrients (Bae et al. 2015; Lu
1251 et al. 2022; Eastman et al. 2021), which can induce predictable nutrient-water use
1252 tradeoffs expected from the theory across broad environmental gradients (Paillassa
1253 et al. 2020; Querejeta et al. 2022; Westerband et al. 2023) and in manipulation

1254 experiments (Bialic-Murphy et al. 2021). Additionally, increasing VPD has been
1255 shown to have a positive effect on N_{area} (Dong et al. 2017; Dong et al. 2020; Firn
1256 et al. 2019). However, studies have been restricted to exploring these patterns
1257 with C₃ species and, while previous studies have shown that variance in N_{area}
1258 across environmental gradients is driven by strong negative relationships with χ
1259 (Fig 3.4c)(Dong et al. 2017; Paillassa et al. 2020; Westerband et al. 2023),
1260 no study to date has explicitly investigated effects of soil resource availability or
1261 plant functional group on N_{area} using β as a direct predictor of χ . Additionally, as
1262 N_{area} can be broken down into structural (leaf mass per area; M_{area} ; g m⁻²) and
1263 metabolic (mass-based leaf nitrogen content; N_{mass} ; gN g⁻¹) components (Dong et
1264 al. 2017), no study has investigated which component of N_{area} drives the hypothe-
1265 sized response of N_{area} to χ , which would be useful for detecting whether changes
1266 in N_{area} due to χ are driven by changes in leaf morphology or stoichiometry.

1267 Here, I measured N_{area} , N_{mass} , M_{area} , leaf δ¹³C-derived estimates of χ , and
1268 leaf δ¹³C-derived estimates of β in 520 individuals spanning 57 species scattered
1269 across 24 grassland sites in Texas, USA (Table S1). Texas contains a diverse
1270 climatic gradient, indicated by 2006-2020 mean annual precipitation totals ranging
1271 from 204 to 1803 mm and 2006-2020 mean annual temperature ranging from
1272 11.8° to 24.6°C. Variability in soil nitrogen availability and soil moisture was
1273 expected across sites, owing to differences in soil texture and aboveground climate
1274 that would drive differential rates of water retention and nitrogen transformations
1275 to plant-available substrate. I leveraged the expected climatic and soil resource
1276 variability across sites to test the following hypotheses:

1277 1. Soil nitrogen availability will decrease β through a reduction in costs of

1278 nitrogen acquisition and use, while soil moisture will increase β through a
1279 reduction in costs of water acquisition and use. We expected that N-fixing
1280 species would have lower β values due to their ability to minimize costs
1281 of nitrogen acquisition under low nitrogen availability and that C₄ species
1282 would have lower β values due to increased costs of water acquisition and
1283 use or reduced costs of nitrogen acquisition and use.

1284 2. χ will be positively related to β , a pattern that will result in a negative
1285 indirect effect of increasing soil nitrogen availability, positive indirect effect
1286 of increasing soil moisture on χ , and lower χ in both N-fixing species and
1287 C₄ species. We also expected that χ would be negatively related to VPD,
1288 as increasing atmospheric dryness should cause plants to close stomata to
1289 minimize water loss.

1290 3. N_{area} will be negatively related to χ . This response will result in an indi-
1291 rect positive effect of increasing soil nitrogen availability, a negative effect of
1292 increasing soil moisture on N_{area} , and generally larger N_{area} values in both N-
1293 fixing species. We expected these patterns to be mediated through a positive
1294 relationship between β and χ . While theory predicts that negative relation-
1295 ships between N_{area} and χ should yield generally larger N_{area} in C₄ species,
1296 we expected that C₄ species would have lower N_{area} due to generally greater
1297 nitrogen use efficiency in C₄ species than C₃ species. Additionally, VPD
1298 was expected to increase N_{area} , a pattern that would be directly mediated
1299 through the reduction in χ with increasing VPD.

1300 4.2 Methods

1301 4.2.1 *Site descriptions and sampling methodology*

1302 I collected leaf and soil samples from 24 open grassland sites across cen-
1303 tral and eastern Texas in summer 2020 and summer 2021 (Fig. 4.1). Twelve
1304 sites were visited between June and July 2020 and 14 sites (11 unique from 2020)
1305 were visited between May and June 2021 (Table 1). I explicitly chose sites that
1306 maximized variability in precipitation and edaphic variability between sites while
1307 minimizing temperature variability across the environmental gradient (Table 1).
1308 No site with personally communicated or anecdotal evidence of grazing or distur-
1309 bance (e.g., mowing, feral hog activity, etc.) were used. I collected leaf material
1310 from three individuals each of the five most abundant species at random locations
1311 at each site, only selecting species that were broadly classified as graminoid or
1312 forb/herb growth habits per the USDA PLANTS database (USDA NRCS 2022).
1313 All collected leaves were fully expanded with no visible herbivory or other external
1314 damage and also free from shading by nearby shrubs or trees. Five soil samples
1315 were collected from 0-15cm below the soil surface at each site near the leaf collec-
1316 tion sample locations. Soil samples were later mixed together by hand to create
1317 one composite soil sample per site.

1318 4.2.2 *Leaf trait measurements*

1319 Images of each leaf were taken immediately following each site visit using
1320 a flat-bed scanner. Fresh leaf area was determined from each image using the
1321 'LeafArea' R package (Katabuchi 2015), which automates leaf area calculations
1322 using ImageJ software (Schneider et al. 2012). Each leaf was dried at 65°C for at

1323 least 48 hours to a constant mass, weighed, and manually ground in a mortar and
1324 pestle until homogenized. Leaf mass per area (M_{area} ; g m⁻²) was calculated as the
1325 ratio of dry leaf biomass to fresh leaf area. Subsamples of dried and homogenized
1326 leaf tissue were used to measure leaf nitrogen content (N_{mass} ; gN g⁻¹) through el-
1327 emental combustion analysis (Costech-4010, Costech Instruments, Valencia, CA).
1328 Leaf nitrogen content per unit leaf area (N_{area} ; gN m⁻²) was then calculated as
1329 the product of N_{mass} and M_{area} .

1330 Subsamples of dried and homogenized leaf tissue were sent to the University
1331 of California-Davis Stable Isotope Facility to determine leaf $\delta^{13}\text{C}$. Leaf $\delta^{13}\text{C}$ values
1332 were determined using an elemental analyzer (PDZ Europa ANCA-GSL; Sercon
1333 Ltd., Chestshire, UK) interfaced to an isotope ratio mass spectrometer (PDZ
1334 Europa 20-20 Isotope Ratio Mass Spectrometer, Sercon Ltd., Chestshire, UK).
1335 I used leaf $\delta^{13}\text{C}$ values (‰; relative to Vienna Pee Dee Belemnite international
1336 reference standard) to estimate the ratio of intercellular (C_i) to extracellular (C_a)
1337 CO₂ ratio (leaf $C_i:C_a$, χ ; unitless) following the approach of Farquhar et al. (1989)
1338 described in Cernusak et al. (2013). Specifically, I derived χ as:

$$\chi = \frac{C_i}{C_a} = \frac{\Delta^{13}\text{C} - a}{b - a} \quad (4.1)$$

1339 where $\Delta^{13}\text{C}$ represents the relative difference between leaf $\delta^{13}\text{C}$ (‰) and air $\delta^{13}\text{C}$
1340 (‰), and is calculated as:

$$\Delta^{13}\text{C} = \frac{\delta^{13}\text{C}_{\text{air}} - \delta^{13}\text{C}_{\text{leaf}}}{1 + \delta^{13}\text{C}_{\text{leaf}}} \quad (4.2)$$

1341 $\delta^{13}\text{C}_{\text{air}}$, traditionally assumed to be -8‰ (Keeling et al. 1979; Farquhar et al.

1342 1989), was calculated as a function of calendar year t using an empirical equation
1343 derived in Feng (1999):

$$\delta^{13}C_{air} = -6.429 - 0.006e^{0.0217(t-1740)} \quad (4.3)$$

1344 This calculation resulted in $\delta^{13}C_{air}$ values for 2020 and 2021 as -9.04 and -9.09,
1345 respectively. a represents the fractionation between ^{12}C and ^{13}C due to diffusion
1346 in air, assumed to be 4.4‰, and b represents the fractionation caused by Rubisco
1347 carboxylation, assumed to be 27‰ (Farquhar et al. 1989). For C_4 species, b in
1348 Eqn. 4.1 was set to 6.3‰, and was derived from:

$$b = c + (d \cdot \phi) \quad (4.4)$$

1349 Where c was set to -5.7‰ and d was set to 30‰ (Farquhar et al. 1989). ϕ , which
1350 is the bundle sheath leakiness term, was set to 0.4. All χ values less than 0.2 and
1351 greater than 1.0 were assumed to be incorrect and removed.

1352 I derived the unit cost of resource use (β) using leaf χ and site climate data
1353 with equations first described in Prentice et al. (2014) and simplified in Lavergne
1354 et al. (2020):

$$\beta = 1.6\eta^*D \frac{\chi - (\frac{\Gamma^*}{C_a})^2}{(1 - \chi)^2(K_m + \Gamma^*)} \quad (4.5)$$

1355 where η^* is the viscosity of water relative to 25°C, calculated using elevation and
1356 mean air temperature of the seven days leading up to each site visit following
1357 equations in Huber et al. (2009). D represents vapor pressure deficit (Pa), set

1358 to the mean vapor pressure deficit of the seven days leading up to each site visit,
1359 C_a represents atmospheric CO₂ concentration, arbitrarily set to 420 $\mu\text{mol mol}^{-1}$
1360 CO². K_m (Pa) is the Michaelis-Menten coefficient for Rubisco affinity to CO₂ and
1361 O₂, calculated as:

$$K_m = K_c \cdot \left(1 + \frac{O_i}{K_o}\right) \quad (4.6)$$

1362 where K_c (Pa) and K_o (Pa) are the Michaelis-Menten coefficients for Rubisco
1363 affinity to CO₂ and O₂, respectively, and O_i is the intercellular O₂ concentration.
1364 Γ^* (Pa) is the CO₂ compensation point in the absence of dark respiration. K_c , K_o ,
1365 and Γ^* were determined using equations described in Medlyn et al. (2002) and
1366 derived in Bernacchi et al. (2001), invoking an elevation correction for atmospheric
1367 pressure as explained in Stocker et al. (2020).

Table 4.1. Site locality information, sampling year(s), 2006-2020 mean annual precipitation (MAP; mm), mean annual temperature (MAT; °C), and water holding capacity (WHC; mm)*

Site	Latitude	Longitude	Sampling year	MAP	MAT	WHC
Edwards_2019_17	29.95	-100.36	2020	563.5	19.0	224.7
Uvalde_2020_02	29.59	-100.09	2020, 2021	648.5	19.5	224.7
Menard_2020_01	30.91	-99.59	2020	641.9	18.3	220.2
Kerr_2020_03	30.06	-99.34	2021	672.4	18.3	237.5
Bandera_2020_03	29.85	-99.30	2021	789.4	18.8	235.1
Sansaba_2020_01	31.29	-98.62	2020	733.0	18.8	234.3
Comal_2020_21	29.79	-98.43	2020	878.5	19.9	220.7
Blanco_2019_16	29.99	-98.43	2020	833.0	19.2	222.2
Bexar_2019_13	29.24	-98.43	2020	759.3	21.5	206.0
Burnet_2020_14	30.84	-98.34	2021	763.3	19.5	217.8
Comal_2020_19	30.01	-98.32	2021	845.0	19.3	220.4
Hays_2020_54	29.96	-98.17	2021	861.3	20.0	225.6
Burnet_2020_12	30.82	-98.06	2021	815.1	19.4	245.3
Williamson_2019_09	30.71	-97.86	2020	867.7	19.7	270.2
Williamson_2019_10	30.54	-97.77	2020	819.5	19.9	239.8
Bell_2021_08	31.06	-97.55	2021	937.3	19.6	232.3
Fayette_2021_12	29.86	-97.21	2021	985.7	20.4	165.6
Fayette_2019_04	30.09	-96.78	2020	1017.4	20.6	226.9
Fayette_2020_09	29.86	-96.71	2021	1002.7	20.8	187.6
Washington_2020_08	30.28	-96.41	2021	1077.4	20.4	203.9
Austin_2020_03	29.78	-96.24	2021	1108.7	20.6	253.0
Brazos_2020_16	30.93	-96.23	2021	1078.0	20.1	202.2
Brazos_2020_18	30.52	-96.21	2020, 2021	1099.4	20.4	233.5
Harris_2020_03	29.88	-95.31	2020, 2021	1492.0	21.6	265.6

1368 *Rows are arranged by longitude to visualize precipitation variability across sites

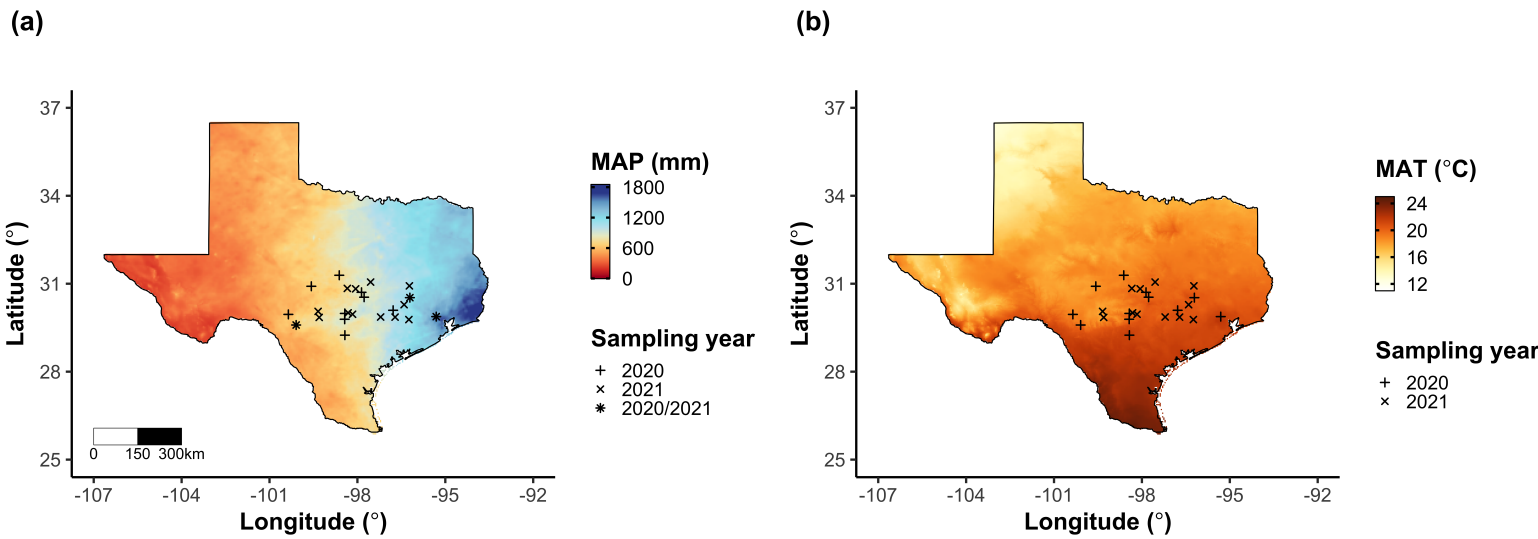


Figure 4.1. Maps that detail site locations along 2006-2020 mean annual precipitation (a) and mean annual temperature (b) gradients in Texas, USA. Precipitation and temperature data were plotted at a 4-km grid resolution and are masked to include only grid cells that occur in the Texas state boundary in the United States. In both panels, open circles refer to sites visited in 2020, open triangles to sites visited in 2021, and closed circles to sites visited in 2020 and 2021. The scale bar in panel A also applies to panel B.

1369 4.2.3 *Site climate data*

1370 I used the Parameter-elevation Regressions on Independent Slopes Model
1371 (PRISM) (Daly et al. 2008)climate product to access gridded daily temperature
1372 and precipitation data for the coterminous United States at a 4-km grid resolution
1373 between January 1, 2006 and July 31, 2021 (PRISM Climate Group, Oregon State
1374 University, <https://prism.oregonstate.edu>, data created 4 Feb 2014, accessed 24
1375 Mar 2022). Daily mean air temperature, mean VPD, and total precipitation
1376 data were extracted from the grid cell that contained the latitude and longitude
1377 of each property using the ‘extract’ function in the ‘terra’ R package (Hijmans
1378 2022). PRISM data were used in lieu of local weather station data because several
1379 rural sites did not have a local weather station present within a 20-km radius of
1380 the site. Daily site climate data were used to estimate mean annual precipitation
1381 and mean annual temperature for each site between 2006 and 2020 (Table 1). I
1382 calculated total precipitation and mean daily VPD for the prior 1, 2, 3, 4, 5, 6, 7,
1383 8, 9, 10, 15, 20, 25, 30, 60, and 90 days leading up to each site visit.

1384 4.2.4 *Site edaphic characteristics*

1385 Subsamples of composited soil samples were sent to the Texas A & M
1386 Soil, Water and Forage Laboratory to quantify soil nitrate concentration (NO₃-N;
1387 ppm). Soil NO₃-N was determined by extracting composite soil samples in 1 M
1388 KCl, measuring absorbance values of extracts at 520 nm using the end product of
1389 a NO₃-N to NO₂-N cadmium reduction reaction (Kachurina et al. 2000). Soil tex-
1390 ture data from 0-15cm below the soil surface were accessed using the SoilGrids2.0
1391 data product (Poggio et al. 2021) through the ‘fetchSoilGrids’ function in the

1392 ‘soilDB’ R package (Beaudette et al. 2022). I used SoilGrids2.0 to access soil
1393 texture data in lieu of analyses using the collected composite soil sample due to
1394 a lack of soil material from some sites after sending samples for soil NO₃-N.

1395 Soil moisture was not measured in the field, but was estimated using
1396 the ‘Simple Process-Led Algorithms for Simulating Habitats’ model (‘SPLASH’)
1397 (Davis et al. 2017). This model, derived from the STASH model (Cramer and
1398 Prentice 1988), spins up a bucket model using Priestley-Taylor equations (Priest-
1399 ley and Taylor 1972) to calculate daily soil moisture (W_n ; mm) as a function
1400 of the previous day’s soil moisture (W_{n-1} ; mm), daily precipitation (P_n ; mm),
1401 condensation (C_n ; mm), actual evapotranspiration (E_n^a ; mm), and runoff (RO;
1402 mm):

$$W_n = W_{n-1} + P_n + C_n - E_n^a - RO \quad (4.7)$$

1403 Models were spun up by equilibrating the previous day’s soil moisture using
1404 successive model iterations with daily mean air temperature, daily precipitation
1405 total, the number of daily sunlight hours, and latitude as model inputs (Davis et al.
1406 2017). Daily sunlight hours were estimated for each day at each site using the
1407 ‘getSunlightTimes’ function in the ‘suncalc’ R package, which estimated sunrise
1408 and sunset times of each property using date and site coordinates (Thieurmel and
1409 Elmarhraoui 2019). Water holding capacity (mm), or bucket size, was estimated
1410 as a function of soil texture using pedotransfer equations explained in Saxton and
1411 Rawls (2006), as done in Stocker et al. (2020) and Bloomfield et al. (2023). A
1412 summary of these equations is included in the Supplemental Information.

1413 Daily soil moisture outputs from the SPLASH model for each site were
1414 used to calculate mean daily soil moisture for the prior 1, 2, 3, 4, 5, 6, 7, 8, 9,
1415 10, 15, 20, 25, 30, 60, and 90 days leading up to each site visit. Mean daily
1416 soil moisture values were then expressed as a fraction of water holding capacity
1417 to normalize across sites with different bucket depths, as done in Stocker et al.
1418 (2018).

1419 4.2.5 *Plant functional group assignments*

1420 Plant functional group was assigned to each species and used as the pri-
1421 mary descriptor of species identity. Specifically, I assigned plant functional groups
1422 based on photosynthetic pathway (C_3 , C_4) and ability to form associations with
1423 symbiotic nitrogen-fixing bacteria. The ability to form associations with symbi-
1424 otic nitrogen-fixing bacteria was assigned based on whether species were in the
1425 *Fabaceae* family, and photosynthetic pathway of each species was determined from
1426 past literature and confirmed through leaf $\delta^{13}C$ values. We chose these plant func-
1427 tional groups based on *a priori* hypotheses regarding the functional role of nitrogen
1428 fixation and photosynthetic pathway on the sensitivity of plant nitrogen uptake
1429 and leaf nitrogen allocation to soil nutrient availability and aboveground growing
1430 conditions. These plant functional group classifications resulted in three distinct
1431 plant functional groups within our dataset: C_3 legumes ($n = 53$), C_3 non-legumes
1432 ($n = 350$), and C_4 non-legumes ($n = 117$).

1433 4.2.6 *Data analysis*

1434 All analyses and plotting were conducted in R version 4.1.1 (R Core Team
1435 2021). I constructed a series of separate linear mixed-effects models to investigate
1436 environmental drivers of β , χ , N_{area} , N_{mass} , and M_{area} , followed by a path analysis
1437 using a piecewise structural equation model to investigate direct and indirect
1438 effects of climate and soil resource availability on N_{area} .

1439 To explore environmental drivers of β , I built a linear mixed-effects model
1440 that included soil moisture, soil nitrogen availability, and plant functional group
1441 as fixed effect coefficients. Species were designated as a random intercept term.
1442 Interaction coefficients between all possible combinations of the three fixed effect
1443 coefficients were also included. β was natural log transformed to linearize data.
1444 I used an information-theoretic model selection approach to determine whether
1445 90-, 60-, 30-, 20-, 15-, 10-, 9-, 8-, 7-, 6-, 5-, 4-, 3-, 2-, or 1-day mean daily soil
1446 moisture conferred the best model fit for β . To do this, I constructed 16 separate
1447 linear mixed-effects models where log-transformed β was included as the response
1448 variable and each soil moisture time step was separately included as a single
1449 continuous fixed effect. Species were included as a random intercept term for all
1450 models. I used corrected Akaike Information Criterion (AICc) to select the soil
1451 moisture timescale that conferred the best model fit, indicated by the model with
1452 the lowest AICc score (Table S2; Fig. S2).

1453 To explore environmental drivers of χ , I constructed a second linear mixed
1454 effects model that included VPD, soil moisture, soil nitrogen availability, and plant
1455 functional group as fixed effect coefficients. Two-way interactions between plant
1456 functional group and VPD, soil nitrogen availability, or soil moisture were also

1457 included as fixed effect coefficients, in addition to a three-way interaction between
1458 soil moisture, soil nitrogen availability, and plant functional group. Species were
1459 included as a random intercept term. I used an information-theoretic model se-
1460 lection approach to determine whether 90-, 60-, 30-, 20-, 15-, 10-, 9-, 8-, 7-, 6-,
1461 5-, 4-, 3-, 2-, or 1-day mean daily VPD conferred the best model fit for χ using
1462 the same approach explained above for the soil moisture effect on β . The soil
1463 moisture timescale was set to the same timescale that conferred the best fit for β .

1464 To explore environmental drivers of N_{area} , N_{mass} , and M_{area} , I constructed
1465 three separate linear mixed effects model that each included χ , soil nitrogen avail-
1466 ability, soil moisture, and plant functional group as fixed effect coefficients. Two-
1467 way interactions between plant functional group and β , χ , soil nitrogen availability,
1468 or soil moisture were included as additional fixed effect coefficients, in addition to
1469 a three-way interaction between soil nitrogen availability, soil moisture, and plant
1470 functional group. Species were included as a random intercept term, with the soil
1471 moisture timescale set to the same timescale that conferred the best fit for β .

1472 In all linear mixed-effects models explained above, including those to select
1473 relevant timescales, I used the 'lmer' function in the 'lme4' R package (Bates et al.
1474 2015) to fit each model and the 'Anova' function in the 'car' R package (Fox and
1475 Weisberg 2019) to calculate Type II Wald's χ^2 and determine the significance
1476 level ($\alpha = 0.05$) of each fixed effect coefficient. I used the 'emmeans' R package
1477 (Lenth 2019) to conduct post-hoc comparisons using Tukey's tests, where degrees
1478 of freedom were approximated using the Kenward-Roger approach (Kenward and
1479 Roger 1997). Trendlines and error ribbons for all plots were drawn using a series
1480 of 'emmeans' outputs across the range in plotted x-axis values.

Finally, I conducted a path analysis using a piecewise structural equation model to examine direct and indirect pathways that determined variance in N_{area} . Seven separate linear mixed effects models were loaded into the piecewise structural equation model. Models were constructed per our *a priori* hypotheses following patterns expected from photosynthetic least-cost theory. The first model regressed N_{area} against χ , N_{mass} , and M_{area} . The second model regressed M_{area} against χ . The third model regressed N_{mass} against χ and M_{area} (Dong et al. 2017; Dong et al. 2020). The fourth model regressed χ against β and VPD. The fifth model regressed β against soil nitrogen availability, soil moisture, ability to associate with symbiotic nitrogen-fixing bacteria, and photosynthetic pathway. The sixth model regressed soil nitrogen availability against soil moisture, while the seventh model regressed VPD against soil moisture (Novick et al. 2016; Sulman et al. 2016). All models included the relevant timescale selected in the individual linear mixed effect models explained above (2-day soil moisture, 4-day vapor pressure deficit). Models also included species as a random intercept term, were built using the ‘lme’ function in the ‘nlme’ R package (Pinheiro and Bates 2022), and subsequently loaded into the piecewise structural equation model using the ‘psem’ function in the ‘piecewiseSEM’ R package (Lefcheck 2016).

1499 4.3 Results

1500 4.3.1 Cost to acquire nitrogen relative to water

Model selection indicated that 2-day soil moisture was the timescale that conferred the best model fit for β ($\text{AICc} = 1227.83$; Table S2; Fig. S1). Increasing soil nitrogen availability generally decreased β ($p < 0.001$; Table 4.2), a pattern

1504 driven by a negative effect of increasing soil nitrogen availability on β in C₃ non-
1505 legumes (Tukey: $p < 0.001$) and C₃ legumes (Tukey: $p = 0.004$; Fig. 4.2a). C₄
1506 nonlegumes also demonstrated a negative trend in the effect of increasing soil ni-
1507 trogen availability on β , but this pattern was not significantly different from zero
1508 (Tukey: $p = 0.307$; Fig. 4.2a). There was no apparent effect of soil moisture on
1509 β ($p = 0.264$; Table 4.2; Fig. 4.2b). A functional group effect ($p < 0.001$; Table
1510 4.2) indicated that C₄ nonlegumes generally had lower β values than both C₃
1511 legumes and C₃ non-legumes when averaged across soil moisture and soil nitrogen
1512 availability values (Tukey: $p < 0.001$ in both cases), while average β values in C₃
1513 legumes did not differ from C₃ nonlegumes (Tukey: $p = 0.691$).

Table 4.2. Effects of soil moisture, soil nitrogen availability, and plant functional group on β

	df	Coefficient	χ^2	p
Intercept	-	3.20E+00	-	-
Soil moisture (SM_2)	1	2.19E-01	1.244	0.265
Soil N (N)	1	-1.70E-02	26.823	<0.001
PFT	2	-	199.617	<0.001
SM_2*N	1	1.77E-03	0.438	0.508
SM_2*PFT	2	-	2.038	0.361
$N*PFT$	2	-	7.668	0.022
$SM_2*N*PFT$	2	-	0.127	0.939

1514 *Significance determined using Type II Wald χ^2 tests ($\alpha = 0.05$). P-values < 0.05

1515 are in bold. Model coefficients are expressed on the natural-log scale and are only

1516 included for continuous fixed effects. Key: df = degrees of freedom, χ^2 = Wald

1517 Type II chi-square test statistic

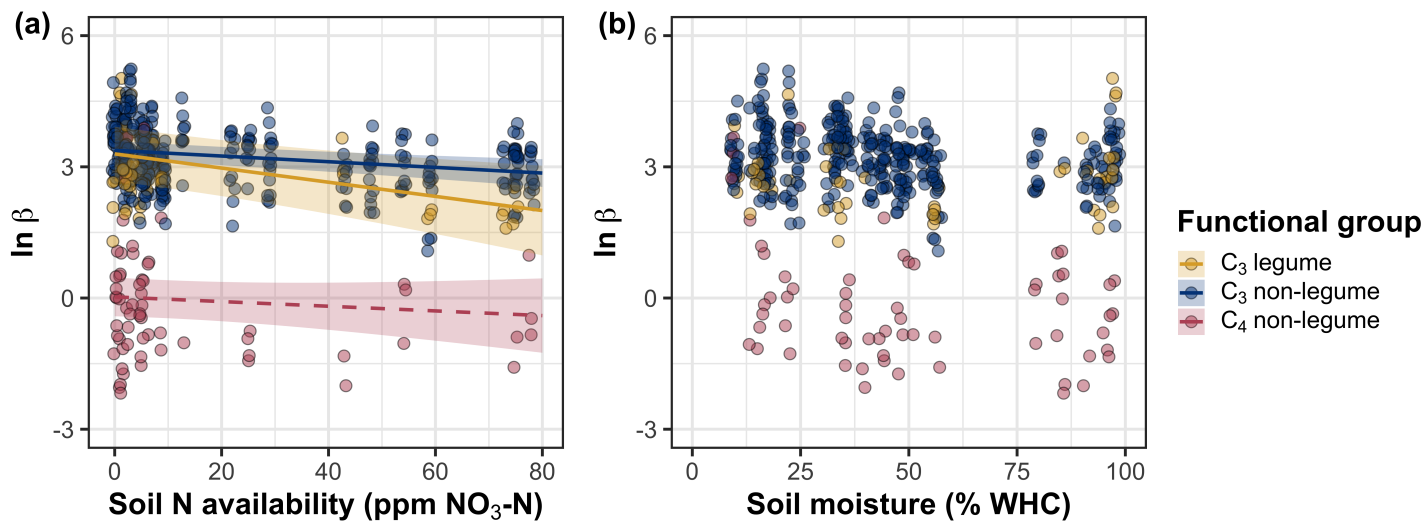


Figure 4.2. Effects of soil nitrogen availability (a) and soil moisture (b) on the unit cost ratio β . In (b), soil moisture is represented as a percent of site water holding capacity. Yellow shading and trendlines indicate C₃ legumes, blue shading and trendlines indicate C₃ non-legumes, and red shading and trendlines indicate C₄ non-legumes. Points are jittered for visibility. Variably colored trendlines are only included if there is an interaction between the x-axis and plant functional group, where solid trendlines indicate slopes that are different from zero ($p < 0.05$) and dashed trendlines indicate slopes that are not different from zero ($p > 0.05$). Error ribbons represent the upper and lower 95% confidence intervals of each fitted trendline.

1518 4.3.2 Leaf $C_i:C_a$

1519 Model selection indicated that 4-day daily VPD was the timescale that
1520 conferred the best model fit for χ (AICc = -883.97; Table S1; Fig. S2).

1521 Variance in χ was driven by a series of two-way interactions between func-
1522 tional group and VPD ($p = 0.006$; Table 3), soil moisture ($p = 0.033$, Table 3.3),
1523 and soil nitrogen availability ($p = 0.022$; Table 3). The interaction between 4-day
1524 VPD and functional group revealed that the general negative effect of increasing
1525 VPD ($p < 0.001$; Table 3) was driven by a negative effect of increasing VPD
1526 on χ in C₃ nonlegumes (Tukey: $p < 0.001$) and marginal negative effect in C₃
1527 legumes (Tukey: $p = 0.074$) paired with a positive trending, but insignificant
1528 effect of increasing VPD in C₄ nonlegumes (Tukey: $p = 0.130$; Fig. 3a). The
1529 interaction between 2-day soil moisture and functional group indicated that the
1530 general negative effect of increasing soil moisture on χ was driven by a positive
1531 effect of increasing soil moisture on χ in C₄ nonlegumes (Tukey: $p = 0.009$) de-
1532 spite a positive trending but insignificant effect of increasing soil moisture on χ
1533 in C₃ legumes (Tukey: $p = 0.116$) and a null effect of soil moisture on χ in C₃
1534 nonlegumes (Tukey: $p = 0.693$; Fig. 3c). The interaction between soil nitrogen
1535 availability and plant functional group revealed a weak negative effect of increas-
1536 ing soil nitrogen availability on χ in C₃ legumes (Tukey: $p = 0.045$), with no
1537 apparent effect in C₃ nonlegumes (Tukey: $p = 0.706$) or C₄ nonlegumes (Tukey:
1538 $p = 0.757$). Finally, an individual effect of functional group ($p < 0.001$; Table 3)
1539 revealed that C₄ nonlegumes generally had lower χ than C₃ legumes and C₃ non-
1540 legumes (Tukey: $p < 0.001$ in both cases), with no apparent difference between
1541 C₃ legumes and C₃ nonlegumes (Tukey: $p = 0.831$).

Table 4.3. Effects of soil moisture, soil nitrogen availability, and plant functional group on χ^*

	df	Coefficient	χ^2	p
Intercept	-	9.33E-01	-	-
Vapor pressure deficit (VPD_4)	1	-1.78E-01	20.792	<0.001
Soil moisture (SM_2)	1	4.53E-02	1.972	0.160
Soil N (N)	1	-1.30E-03	0.168	0.682
PFT	2	-	172.624	<0.001
SM_2^*N	1	7.40E-04	0.849	0.357
VPD_4^*PFT	2	-	10.241	0.006
SM_2^*PFT	2	-	6.806	0.033
N^*PFT	2	-	7.602	0.022
$SM_2^*N^*PFT$	2	-	0.732	0.694

1542 *Significance determined using Type II Wald χ^2 tests ($\alpha = 0.05$). *P*-values less

1543 than 0.05 are in bold and *p*-values where $0.05 < p < 0.1$ are italicized. χ was

1544 not transformed prior to model fitting, so model coefficients are reported on the

1545 response scale. Model coefficients are only included for continuous fixed effects.

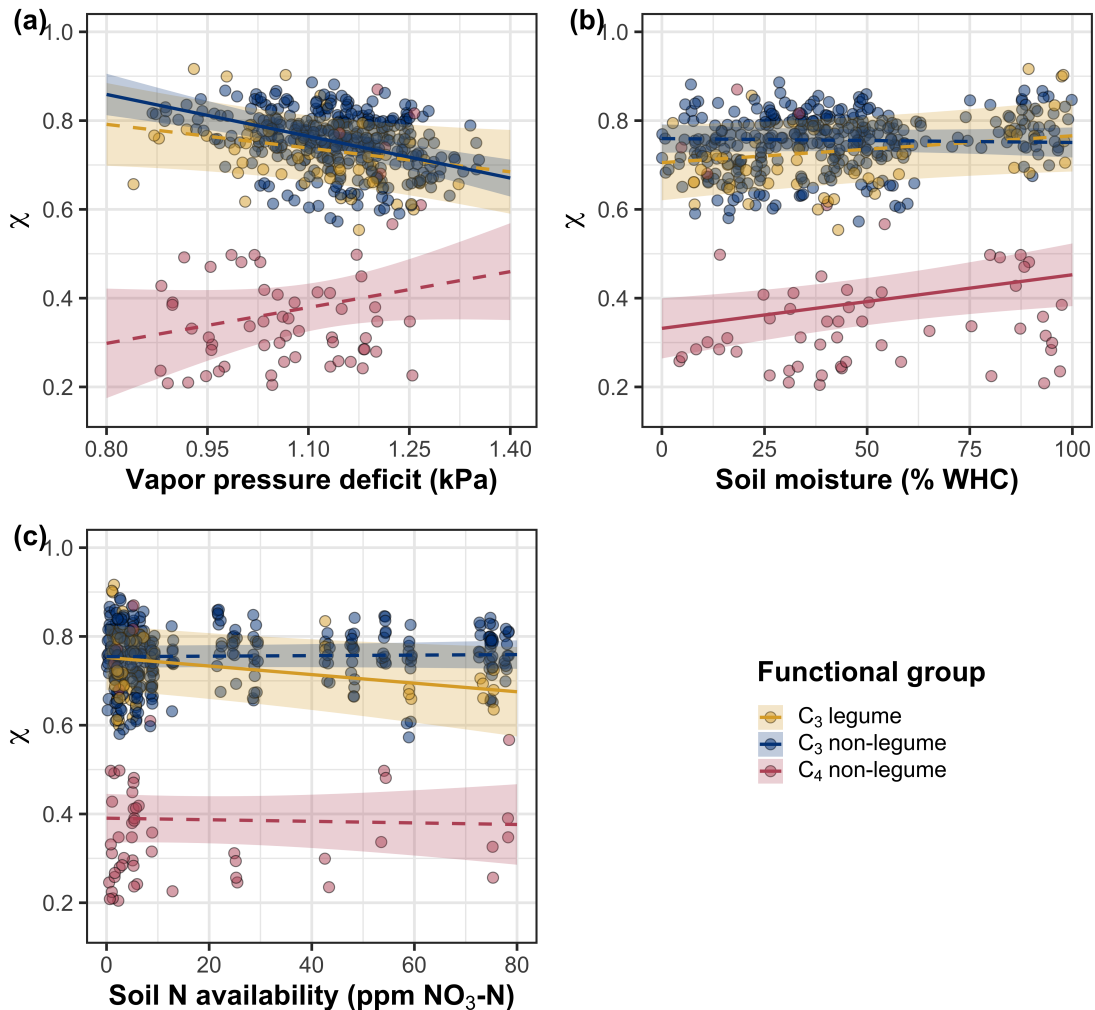


Figure 4.3. Effects of 4-day mean vapor pressure deficit (a), 2-day soil moisture (per water holding capacity; b), and soil nitrogen availability (c) on χ . Shading and trendlines are as explained in Figure 2. Points are jittered for visibility. Variably colored trendlines are only included if there is an interaction between the x-axis and plant functional group, where solid trendlines indicate slopes that are different from zero ($p < 0.05$) and dashed trendlines indicate slopes that are not different from zero ($p < 0.05$). Error ribbons represent the upper and lower 95% confidence intervals of each fitted trendline.

1546 4.3.3 *Leaf nitrogen content*

1547 An interaction between χ and plant functional group ($p < 0.001$; Table
1548 4) revealed that the general negative effect of increasing χ on N_{area} ($p < 0.001$;
1549 Table 4) was driven by a negative effect of increasing χ on N_{area} in C₃ nonlegumes
1550 (Tukey: $p < 0.001$) and C₃ legumes (Tukey: $p = 0.002$) despite a null effect of χ
1551 on N_{area} in C₄ nonlegumes (Tukey: $p = 0.795$; Fig. 4a). An interaction between
1552 soil nitrogen availability and soil moisture ($p = 0.028$; Table 4) indicated that the
1553 marginal positive effect of increasing soil nitrogen availability on N_{area} ($p = 0.091$;
1554 Table 4) decreased with increasing soil moisture, despite no apparent individual
1555 effect of soil moisture on N_{area} ($p = 0.692$; Table 4). Finally, a plant functional
1556 group effect ($p < 0.001$; Table 4) indicated that C₄ nonlegumes had lower N_{area}
1557 values on average compared to C₃ legumes (Tukey: $p < 0.001$) and C₃ nonlegumes
1558 (Tukey: $p = 0.001$), while C₃ legumes had lower average N_{area} values compared
1559 to C₃ nonlegumes (Tukey: $p = 0.012$).

1560 A marginal interaction between χ and plant functional group ($p = 0.088$;
1561 Table 4) revealed that, despite no apparent general effect of χ on N_{mass} ($p = 0.273$;
1562 Table 4), increasing χ decreased N_{mass} in C₃ nonlegumes (Tukey: $p = 0.021$), but
1563 this effect was not apparent in C₄ nonlegumes (Tukey: $p = 0.693$) or C₃ legumes
1564 (Tukey: $p = 0.477$). An interaction between soil nitrogen availability and soil
1565 moisture ($p < 0.001$; Table 4) indicated that the general positive effect of increas-
1566 ing soil nitrogen availability on N_{mass} ($p < 0.001$; Table 4) generally decreased
1567 with increasing soil moisture, despite an apparent general positive effect of in-
1568 creasing soil moisture on N_{mass} ($p < 0.001$; Table 4). This interaction indicated
1569 that the positive effect of increasing soil nitrogen availability on N_{mass} was only

1570 apparent when soil moisture was less than 70% the maximum water holding ca-
1571 pacity (Tukey: $p < 0.05$ in all cases) despite a positive effect of increasing soil
1572 moisture on N_{mass} ($p < 0.001$; Table 4). Finally, a plant functional group effect
1573 ($p < 0.001$; Table 4) indicated that C₄ nonlegumes had lower N_{mass} values on
1574 average compared to C₃ legumes (Tukey: $p = 0.002$) and C₃ nonlegumes (Tukey:
1575 $p = 0.019$), while N_{mass} did not differ between C₃ legumes and C₃ nonlegumes
1576 (Tukey: $p = 0.149$).

1577 An interaction between χ and functional group ($p = 0.005$; Table 4) indi-
1578 cated that the general negative effect of increasing χ on M_{area} ($p < 0.001$; Table
1579 4; Fig. 4c) was driven by a negative effect of increasing χ on M_{area} in C₃ legumes
1580 and C₃ nonlegumes (Tukey: $p < 0.001$ in both cases) despite a nonsignificant
1581 effect of increasing χ on M_{area} in C₄ nonlegumes (Tukey: $p = 0.724$). An in-
1582 teraction between soil nitrogen and soil moisture ($p < 0.001$; Table 4) indicated
1583 that the general negative effect of increasing soil nitrogen availability on M_{area} (p
1584 < 0.001 ; Table 4) decreased with increasing soil moisture, despite an apparent
1585 general negative effect of increasing soil moisture on M_{area} ($p = 0.002$; Table 4).
1586 Specifically, the negative effect of increasing soil nitrogen availability on M_{area} was
1587 only apparent when soil moisture was less than 65% the maximum water holding
1588 capacity (Tukey: $p < 0.05$ in all cases). An additional interaction between soil
1589 nitrogen availability and functional group ($p = 0.034$; Table 4) indicated that the
1590 general negative effect of increasing soil nitrogen availability on M_{area} was driven
1591 by decreases in C₃ nonlegumes (Tukey: $p < 0.001$) and C₄ nonlegumes (Tukey:
1592 $p = 0.003$), with no apparent effect of soil nitrogen availability on M_{area} in C₃
1593 legumes (Tukey: $p = 0.997$).

Table 4.4. Effects of soil nitrogen fertilization, inoculation, and CO₂ treatments on N_{area} , N_{mass} , and M_{area}

	df	N_{area}			N_{mass}			M_{area}		
		Coefficient	χ^2	p	Coefficient	χ^2	p	Coefficient	χ^2	p
(Intercept)	-	2.78E+00	-	-	4.42E-01	-	-	6.97E+00	-	-
χ	1	-2.53E+00	15.771	<0.001	4.56E-01	1.201	0.273	-3.10E+00	20.620	<0.001
Soil N (N)	1	1.08E-02	2.855	<i>0.091</i>	1.37E-02	54.531	<0.001	-2.87E-03	29.759	<0.001
Soil moisture (SM ₂)	1	3.61E-01	0.157	0.692	5.04E-01	16.255	<0.001	-1.26E-01	9.282	0.002
PFT	1	-	60.641	<0.001	-	21.539	<0.001	-	11.520	0.003
SM ₂ *N	1	-1.09E-02	4.779	0.029	-1.76E-02	41.784	<0.001	6.35E-03	14.111	<0.001
χ^*PFT	1	-	15.188	<0.001	-	4.864	<i>0.088</i>	-	17.032	0.025
N*PFT	1	-	2.289	<i>0.318</i>	-	0.914	0.633	-	6.760	0.034
SM ₂ *PFT	1	-	0.978	0.613	-	0.128	0.938	-	2.121	0.346
SM ₂ *N*PFT	1	-	1.289	0.525	-	2.180	0.336	-	0.629	0.730

⁹
1594 *Significance determined using Type II Wald χ^2 tests ($\alpha = 0.05$). P -values less than 0.05 are in bold and p -values
1595 where $0.05 < p < 0.1$ are italicized. Coefficients are reported on the natural-log scale and are only included for
1596 continuous fixed effects.

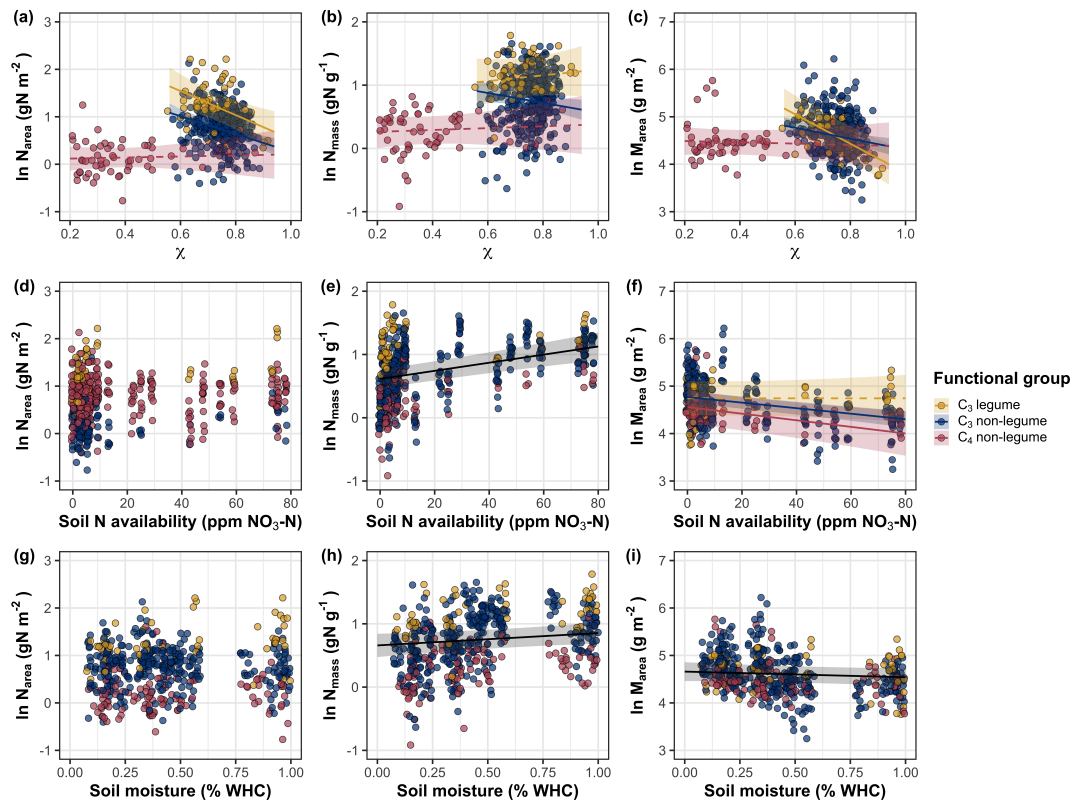


Figure 4.4. Effects of χ (a-c), soil nitrogen availability (d-f), and soil moisture (g-i) on leaf nitrogen content per unit leaf area (a, d, g), leaf nitrogen content per unit leaf biomass (b, e, h), and leaf mass per area (c, f, i). A solid black trendline indicates the bivariate relationship between the fixed effect the x-axis and response variable on the y-axis and is only included when there is no interaction between the x-axis and plant functional group.

1597 4.3.4 *Structural equation model*

1598 The piecewise structural equation model explained 90%, 54%, 80%, 92%,
1599 and 41% of variance in N_{area} , N_{mass} , M_{area} , χ , and β , respectively (Table 5; Fig.
1600 5). Variance in N_{area} was driven by a negative effect of increasing χ ($p < 0.001$;
1601 Table 5) paired with positive effects of increasing N_{mass} and M_{area} ($p < 0.001$ in
1602 both cases; Table 5; Fig. 5). Model results indicated that the negative effect
1603 of χ on N_{area} was driven by a strong reduction in M_{area} with increasing χ ($p <$
1604 0.001; Table 5) paired with no change in χ due to N_{mass} ($p = 0.150$; Table 5).
1605 However, there was a strong negative effect of increasing M_{area} on N_{mass} ($p <$
1606 0.001; Table 5; Fig. 5). χ generally increased with increasing β ($p < 0.001$; Table
1607 5) and decreased with increasing VPD ($p < 0.001$; Table 5; Fig. 5). Variance in β
1608 was driven by a negative effect of increasing soil nitrogen availability ($p < 0.001$;
1609 Table 5) and was generally higher in C₃ species ($p < 0.001$; Table 5; Fig. 5).
1610 However, β did not change with soil moisture ($p = 0.332$; Table 5) or with ability
1611 to acquire nitrogen via symbiotic nitrogen fixation ($p = 0.546$; Table 5). Finally,
1612 soil nitrogen availability was positively associated with increasing soil moisture (p
1613 < 0.001 ; Table 5; Fig. 5), while VPD was negatively associated with increasing
1614 soil moisture ($p < 0.001$; Table 5; Fig. 5).

Table 4.5. Structural equation model results investigating direct effects of climatic and soil resource availability on N_{area} , N_{mass} , M_{area} , χ , and β

Predictor	Coefficient	<i>p</i>
$N_{\text{area}} (R^2_c) = 0.90$		
χ	-0.140	<0.001
M_{area}	0.807	<0.001
N_{mass}	0.795	<0.001
$N_{\text{mass}} (R^2_c) = 0.54$		
χ	0.097	<0.001
$M_{\text{area}} (R^2_c) = 0.80$		
χ	-0.372	0.150
M_{area}	-0.303	<0.001
$\chi (R^2_c) = 0.92$		
β	0.261	<0.001
VPD_4	-0.122	<0.001
$\beta (R^2_c) = 0.41$		
Soil N	-0.201	<0.001
SM_2	-0.048	0.332
Photo. pathway	0.490	<0.001
N-fixing ability	-0.053	0.546
Soil N (R^2_c) = 0.39		
SM_2	0.410	<0.001

1615 *Reported coefficients are standardized across the structural equation model. *P*-
1616 values less than 0.05 are noted in bold. Positive coefficients for photosynthetic
1617 pathway indicate generally larger values in C₃ species, while positive coefficients
1618 for N-fixing ability indicate generally larger values in N-fixing species. Key:
1619 N_{area} =leaf nitrogen content per unit leaf area, M_{area} =leaf mass per unit leaf dry
1620 biomass, N_{mass} =leaf nitrogen content per unit leaf dry biomass, β =cost of acquiring
1621 nitrogen relative to water, χ =isotope-derived estimate of the leaf Ci:Ca ratio,
1622 VPD_4 = 4-day mean vapor pressure deficit, SM_2 =2-day mean soil moisture, R^2_c
1623 = conditional R² value

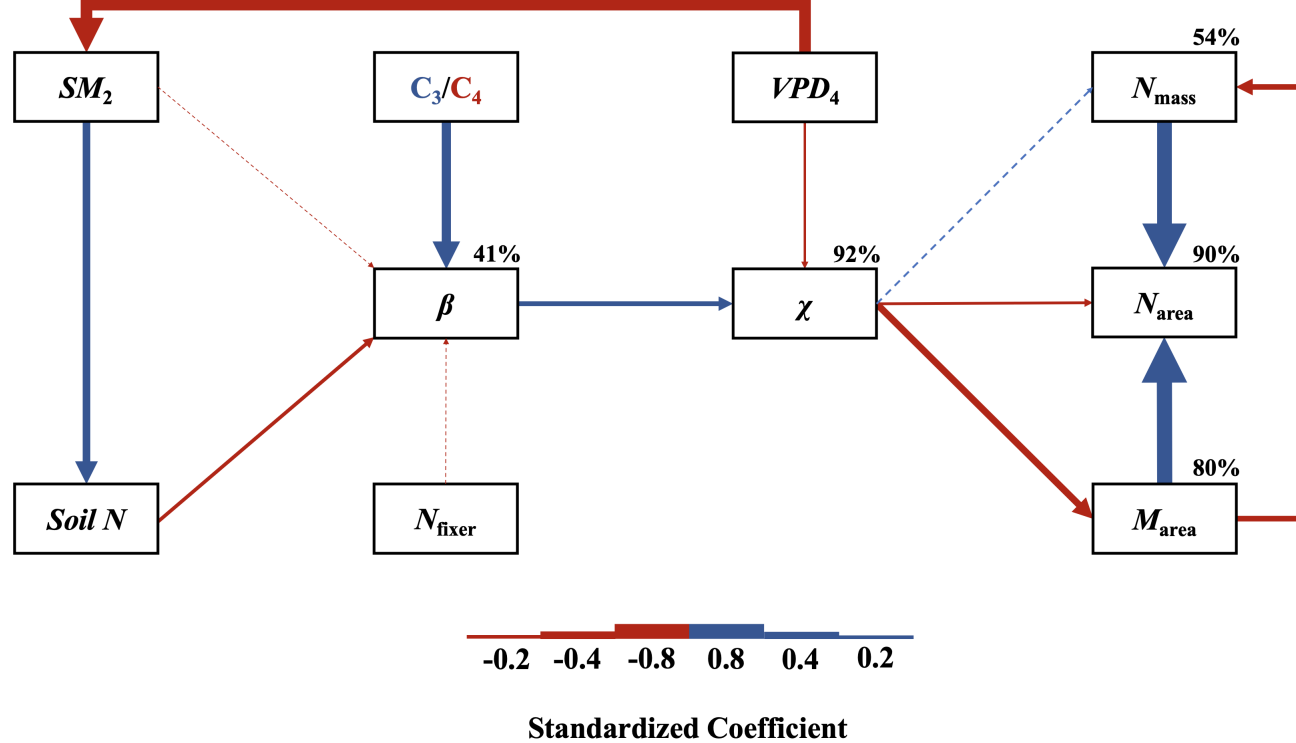


Figure 4.5. Structural equation model results exploring direct and indirect drivers of N_{area} . Boxes indicate measured edaphic factors, climatic factors, and leaf traits. Percentages above boxes indicate conditional R^2 values of each respective leaf trait. Solid arrows indicate bivariate relationships where $p < 0.05$, while dashed arrows indicate bivariate relationships where $p > 0.05$. Positive model coefficients are indicated through blue arrows, while negative model coefficients are indicated through red arrows. Arrow thickness scales with the standardized model coefficient of each bivariate relationship. A positive coefficient for photosynthetic pathway indicates generally larger values in C_3 species, while a positive coefficient for N_{fixer} indicates generally larger values in N-fixing species. Standardized model coefficients and associated p -values are reported in Table 5.

1624 4.4 Discussion

1625 In this chapter, I quantified direct and indirect effects of soil resource avail-
1626 ability, climate, β , and χ on N_{area} and components of N_{area} (N_{mass} and M_{area}) in
1627 520 individuals spanning across a soil resource availability and climate gradient
1628 in Texas, USA. We found consistent support for patterns expected from photo-
1629 synthetic least-cost theory, a result driven by a strong direct negative effect of
1630 increasing χ on N_{area} (Fig. 4.4a; Fig. 4.5) and a positive relationship between χ
1631 and β (Fig. 4.5). In further support of patterns expected from theory, increasing
1632 soil nitrogen availability had a strong negative effect on β (Fig. 4.2a), resulting in
1633 an indirect stimulation in N_{area} (Fig. 4.5) despite a marginal positive direct asso-
1634 ciation between increasing soil nitrogen availability and N_{area} ($p = 0.092$; Table
1635 4.4; Fig. 4.4d). Increasing VPD also indirectly increased N_{area} through a direct
1636 negative effect of increasing VPD on χ (Fig. 4.3a; Fig. 4.5). Interestingly, we
1637 found no effect of soil moisture on β (Fig. 1b; Fig. 4.5), though a strong posi-
1638 tive association between soil moisture and soil nitrogen availability resulted in an
1639 indirect positive effect of increasing soil moisture on N_{area} (Fig. 4.5) despite an
1640 apparent null direct effect of soil moisture on N_{area} (Fig. 4.4g). Overall, results
1641 provide strong and consistent support for patterns expected from photosynthetic
1642 least-cost theory, showing that χ is a dynamic driver of variance in N_{area} and is
1643 capable of unifying expected responses of N_{area} to shifts in soil resource availability
1644 and climate.

1645

Chapter 5

1646 Optimal resource investment to photosynthetic capacity maximizes
1647 nutrient allocation to whole plant growth under elevated CO₂

1648 5.1 Introduction

1649 Terrestrial ecosystems are regulated by complex carbon and nitrogen cy-
1650 cles. As a result, terrestrial biosphere models, which are beginning to include
1651 coupled carbon and nitrogen cycles (Shi et al. 2016; Davies-Barnard et al. 2020;
1652 Braghiere et al. 2022), must accurately represent these cycles under different
1653 environmental scenarios to reliably simulate carbon and nitrogen atmosphere-
1654 biosphere fluxes (Hungate et al. 2003; Prentice et al. 2015). While the inclusion
1655 of coupled carbon and nitrogen cycles tends to reduce model uncertainty (Arora
1656 et al. 2020), large uncertainty in role of soil nitrogen availability and nitrogen ac-
1657 quisition strategy on leaf and whole plant acclimation responses to CO₂ remains
1658 (Smith and Dukes 2013; Terrer et al. 2018; Smith and Keenan 2020). This source
1659 of uncertainty likely contributes to the widespread divergence in future carbon
1660 and nitrogen flux simulations across terrestrial biosphere models (Friedlingstein
1661 et al. 2014; Zaehle et al. 2014; Meyerholt et al. 2020).

1662 Plants grown under elevated CO₂ generally have less leaf nitrogen content
1663 than those grown under ambient CO₂, a response that often corresponds with
1664 reductions in photosynthetic capacity and stomatal conductance at the leaf-level
1665 and biomass stimulation over time at the whole plant level (Curtis 1996; Drake
1666 et al. 1997; Ainsworth et al. 2002; Makino 2003; Morgan et al. 2004; Ainsworth
1667 and Long 2005; Ainsworth and Rogers 2007; Smith and Dukes 2013; Poorter et al.
1668 2022). As net primary productivity is generally limited by nitrogen availability

1669 (Vitousek and Howarth 1991; LeBauer and Treseder 2008; Fay et al. 2015), and
1670 soil nitrogen availability is often positively correlated with leaf nitrogen content
1671 and photosynthetic capacity (Field and Mooney 1986; Evans and Seemann 1989;
1672 Evans 1989; Walker et al. 2014; Firn et al. 2019; Liang et al. 2020), some
1673 have hypothesized that leaf and whole plant acclimation responses to CO₂ are
1674 constrained by soil nitrogen availability. The progressive nitrogen limitation hy-
1675 pothesis predicts that elevated CO₂ will increase plant nitrogen demand, which
1676 will increase plant nitrogen uptake and progressively deplete soil nitrogen if soil
1677 nitrogen supply does not exceed plant nitrogen demand (Luo et al. 2004). The
1678 hypothesis predicts that this response should result in strong acute stimulations in
1679 whole plant growth and primary productivity that diminish over time as nitrogen
1680 becomes more limiting. Assuming a positive relationship between soil nitrogen
1681 availability, leaf nitrogen content, and photosynthetic capacity, this hypothesis
1682 also implies that progressive reductions in soil nitrogen availability should be the
1683 mechanism that drives the downregulation in leaf nitrogen content and photosyn-
1684 thetic capacity under elevated CO₂. This hypothesis has received some support
1685 from free air CO₂ enrichment experiments (Reich et al. 2006; Norby et al. 2010),
1686 although is not consistently observed across experiments (Finzi et al. 2006; Moore
1687 et al. 2006; Liang et al. 2016).

1688 While possible that progressive nitrogen limitation may determine leaf and
1689 whole plant acclimation responses to CO₂, growing evidence indicates that leaf ni-
1690 trogen and photosynthetic capacity are more strongly determined through above-
1691 ground growing conditions than by soil resource availability (Dong et al. 2017;
1692 Dong et al. 2020; Dong et al. 2022; Smith et al. 2019; Smith and Keenan 2020;

1693 Paillassa et al. 2020; Peng et al. 2021; Querejeta et al. 2022; Westerband et al.
1694 2023), and satellite-derived chlorophyll fluorescence data indicate that increasing
1695 atmospheric CO₂ may decrease leaf and canopy demand for nitrogen (Dong et al.
1696 2022). Together, results from these studies suggest that the downregulation in
1697 leaf nitrogen content and photosynthetic capacity due to increasing CO₂ may not
1698 be as tightly linked to progressive nitrogen limitation as previously hypothesized.

1699 A unification of optimal coordination and photosynthetic least-cost the-
1700 ories predicts that leaves acclimate to elevated CO₂ by downregulating nitrogen
1701 allocation to Ribulose-1,5-bisphosphate (RuBP) carboxylase/oxygenase (Rubisco)
1702 to optimize resource use efficiencies at the leaf level, which allows for greater re-
1703 source allocation to whole plant growth (Drake et al. 1997; Wright et al. 2003;
1704 Prentice et al. 2014; Smith et al. 2019). The theory predicts that the downregu-
1705 lation in nitrogen allocation to Rubisco results in a stronger downregulation in the
1706 maximum rate of Rubisco carboxylation (V_{cmax}) than the maximum rate of RuBP
1707 regeneration (J_{max}), which maximizes photosynthetic efficiency by allowing net
1708 photosynthesis rates to be equally co-limited by Rubisco carboxylation and RuBP
1709 regeneration (Chen et al. 1993; Maire et al. 2012). This acclimation response
1710 allows plants to make more efficient use of available light while avoiding overin-
1711 vestment in Rubisco, which has high nitrogen and energetic costs of building and
1712 maintaining (Evans 1989; Evans and Clarke 2019). Instead, additional acquired
1713 resources not needed to optimize leaf photosynthesis are allocated to the mainte-
1714 nance of structures that support whole plant growth (e.g., total leaf area, whole
1715 plant biomass, etc.) or to allocation processes not related to leaf photosynthesis
1716 or growth, such as plant defense mechanisms or leaf structural tissue. Regardless,

1717 optimized resource allocation at the leaf level should allow for greater resource
1718 allocation to whole plant growth. The theory indicates that leaf acclimation re-
1719 sponses to CO₂ should be independent of changes in soil nitrogen availability.
1720 While this leaf acclimation response maximizes nitrogen allocation to structures
1721 that support whole plant growth, the theory suggests that the positive effect of
1722 elevated CO₂ on whole plant growth may be further stimulated by soil nitrogen
1723 availability through a reduction in the cost of acquiring nitrogen (Bae et al. 2015;
1724 Perkowski et al. 2021; Lu et al. 2022).

1725 Plants acquire nitrogen by allocating photosynthetically derived carbon be-
1726 lowground in exchange for nitrogen through different nitrogen acquisition strate-
1727 gies. These nitrogen acquisition strategies can include direct uptake pathways
1728 such as mass flow or diffusion (Barber 1962), symbioses with mycorrhizal fungi or
1729 symbiotic nitrogen-fixing bacteria (Vance and Heichel 1991; Marschner and Dell
1730 1994; Smith and Read 2008; Udvardi and Poole 2013), or through the release
1731 of root exudates that prime free-living soil microbial communities (Phillips et al.
1732 2011; Wen et al. 2022). Plants cannot acquire nitrogen without first allocating
1733 carbon belowground, which implies an inherent carbon cost to the plant for acquir-
1734 ing nitrogen regardless of nitrogen acquisition strategy. Carbon costs to acquire
1735 nitrogen often vary in species with different nitrogen acquisition strategies and
1736 are dependent on external environmental factors such as atmospheric CO₂, light
1737 availability, and soil nitrogen availability (Brzostek et al. 2014; Terrer et al. 2016;
1738 Terrer et al. 2018; Allen et al. 2020; Perkowski et al. 2021; Lu et al. 2022), which
1739 suggests that acquisition strategy may be an important factor in determining ef-
1740 fects of soil nitrogen availability on leaf and whole plant acclimation responses to

1741 elevated CO₂.

1742 A recent meta-analysis using data across 20 grassland and forest CO₂ en-
1743 richment experiments suggested that species which acquire nitrogen from sym-
1744 biotic nitrogen-fixing bacteria had reduced costs of nitrogen acquisition under
1745 elevated CO₂ (Terrer et al. 2018). Findings from this meta-analysis indicated
1746 that reductions in costs of nitrogen acquisition in species that form associations
1747 with symbiotic nitrogen-fixing bacteria under elevated CO₂ may drive stronger
1748 stimulations in whole plant growth and downregulations in V_{cmax} than species that
1749 associate with arbuscular mycorrhizal fungi (Smith and Keenan 2020), which gen-
1750 erally have higher costs of nitrogen acquisition under elevated CO₂ (Terrer et al.
1751 2018). However, plant investments in symbiotic nitrogen fixation generally de-
1752 cline with increasing nitrogen availability (Dovrat et al. 2018; Perkowski et al.
1753 2021), a response that has been previously inferred to be the result of a shift in
1754 the dominant mode of nitrogen acquisition to direct uptake pathways as costs of
1755 direct uptake decrease with increasing soil nitrogen availability (Rastetter et al.
1756 2001; Perkowski et al. 2021). Thus, effects of symbiotic nitrogen fixation on plant
1757 acclimation responses to CO₂ should decline with increasing soil nitrogen avail-
1758 ability, although manipulative experiments that directly test these patterns are
1759 rare.

1760 Here, I conducted a 7-week growth chamber experiment using *Glycine max*
1761 L. (Merr.) to examine the effects of soil nitrogen fertilization and inoculation with
1762 symbiotic nitrogen-fixing bacteria on leaf and whole plant acclimation responses
1763 to elevated CO₂. Following patterns expected from theory, I hypothesized that in-
1764 dividual leaves should acclimate to elevated CO₂ by more strongly downregulating

1765 V_{cmax} relative to J_{max} , allowing leaf photosynthesis to approach optimal coordi-
1766 nation. I expected this response to correspond with a stronger downregulation in
1767 leaf nitrogen content than V_{cmax} and J_{max} , which would increase the fraction of
1768 leaf nitrogen content allocated to photosynthesis and photosynthetic nitrogen use
1769 efficiency. At the whole-plant level, I hypothesized that plants would acclimate
1770 to elevated CO₂ by stimulating whole plant growth and productivity, a response
1771 that would be driven by a strong positive response of total leaf area and above-
1772 ground biomass to elevated CO₂. I predicted that leaf acclimation responses to
1773 elevated CO₂ would be independent of soil nitrogen fertilization and inoculation
1774 with symbiotic nitrogen-fixing bacteria; however, I expected that increasing soil
1775 nitrogen fertilization would increase the positive effect of elevated CO₂ on mea-
1776 sures of whole plant growth due to a stronger reduction in the cost of acquiring
1777 nitrogen under elevated CO₂ with increasing fertilization. I also expected stronger
1778 stimulations in whole plant growth due to inoculation, but that this effect would
1779 only be apparent under low fertilization due to a reduction in root nodulation
1780 with increasing fertilization.

1781 5.2 Methods

1782 5.2.1 *Seed treatments and experimental design*

1783 *Glycine max* L. (Merr) seeds were planted in 144 6-liter surface sterilized
1784 pots (NS-600, Nursery Supplies, Orange, CA, USA) containing a steam-sterilized
1785 70:30 v:v mix of Sphagnum peat moss (Premier Horticulture, Quakertown, PA,
1786 USA) to sand (Pavestone, subsidiary of Quikrete Companies, Atlanta, GA, USA).
1787 Before planting, all *G. max* seeds were surface sterilized in 2% sodium hypochlorite

1788 for 3 minutes, followed by three separate 3-minute washes with ultrapure water
1789 (MilliQ 7000; MilliporeSigma, Burlington, MA USA). A subset of surface steril-
1790 ized seeds were inoculated with *Bradyrhizobium japonicum* (Verdesian N-Dure™
1791 Soybean, Cary, NC, USA) in a slurry following manufacturer recommendations
1792 (3.12 g inoculant and 241 g deionized water per 1 kg seed).

1793 Seventy-two pots were randomly planted with surface-sterilized seeds inoc-
1794 ulated with *B. japonicum*, while the remaining 72 pots were planted with surface-
1795 sterilized uninoculated seeds. Thirty-six pots within each inoculation treatment
1796 were randomly placed in one of two atmospheric CO₂ treatments (ambient and
1797 1000 μmol mol⁻¹ CO₂). Pots within each unique inoculation-by-CO₂ treatment
1798 combination randomly received one of nine soil nitrogen fertilization treatments
1799 equivalent to 0, 35, 70, 105, 140, 210, 280, 350, or 630 ppm N. Nitrogen fertil-
1800 ization treatments were created using a modified Hoagland solution (Hoagland
1801 and Arnon 1950) designed to keep concentrations of other macronutrients and
1802 micronutrients equivalent across treatments (Table S1). Pots received the same
1803 fertilization treatment throughout the entire duration experiment, which were ap-
1804 plied twice per week in 150 mL doses as topical agents to the soil surface through-
1805 out the duration of the experiment. This experimental design yielded a fully
1806 factorial experiment with four replicates per unique fertilization-by-inoculation-
1807 by-CO₂ combination.

1808 5.2.2 *Growth chamber conditions*

1809 Upon experiment initiation, pots were randomly placed in one of six Per-
1810 cival LED-41L2 growth chambers (Percival Scientific Inc., Perry, IA, USA) over

1811 two experimental iterations due to chamber space limitation. Two iterations were
1812 conducted such that one iteration included all elevated CO₂ pots and the second
1813 iteration included all ambient CO₂ pots. Average (\pm SD) CO₂ concentrations
1814 across chambers throughout the experiment were $439 \pm 5 \mu\text{mol mol}^{-1}$ for the
1815 ambient CO₂ treatment and $989 \pm 4 \mu\text{mol mol}^{-1}$ for the elevated CO₂ treatment.

1816 Daytime growing conditions were simulated using a 16-hour photoperiod,
1817 with incoming light radiation set to chamber maximum (mean \pm SD: 1240 ± 32
1818 $\mu\text{mol m}^{-2} \text{s}^{-1}$ across chambers), air temperature set to 25°C, and relative humid-
1819 ity set to 50%. The remaining 8 hours simulated nighttime growing conditions,
1820 with incoming light radiation set to $0 \mu\text{mol m}^{-2} \text{s}^{-1}$, chamber temperature set
1821 to 17°C, and relative humidity set to 50%. Transitions between daytime and
1822 nighttime growing conditions were simulated by ramping incoming light radiation
1823 in 45-minute increments and temperature in 90-minute increments over a 3-hour
1824 period (Table S2).

1825 Including the two, 3-hour ramping periods, pots grew under average (\pm
1826 SD) daytime light intensity of $1049 \pm 27 \mu\text{mol m}^{-2} \text{s}^{-1}$. In the elevated CO₂
1827 iteration, pots grew under $24.0 \pm 0.2^\circ\text{C}$ during the day, $16.4 \pm 0.8^\circ\text{C}$ during the
1828 night, and $51.6 \pm 0.4\%$ relative humidity. In the ambient CO₂ iteration, pots grew
1829 under $23.9 \pm 0.2^\circ\text{C}$ during the day, $16.0 \pm 1.4^\circ\text{C}$ during the night, and $50.3 \pm 0.2\%$
1830 relative humidity. We accounted for climatic differences across the six chambers
1831 by shuffling the same group of pots daily throughout the growth chambers. This
1832 process was done by iteratively moving the group of pots on the top rack of a
1833 chamber to the bottom rack of the same chamber, while simultaneously moving
1834 the group of pots on the bottom rack of a chamber to the top rack of the adjacent

1835 chamber. I moved pots within and across chambers every day throughout the
1836 course of each experiment iteration.

1837 5.2.3 *Leaf gas exchange measurements*

1838 Gas exchange measurements were collected for all individuals on the sev-
1839 enth week of development. All gas exchange measurements were collected on
1840 the center leaf of the most recent fully expanded trifoliate leaf set. Specifi-
1841 cally, I measured net photosynthesis (A_{net} ; $\mu\text{mol m}^{-2} \text{s}^{-1}$), stomatal conductance
1842 (g_{sw} ; $\text{mol m}^{-2} \text{s}^{-1}$), and intercellular CO₂ (C_i ; $\mu\text{mol mol}^{-1}$) concentrations across
1843 a range of atmospheric CO₂ concentrations (i.e., an A_{net}/C_i curve) using the
1844 Dynamic Assimilation Technique™. The Dynamic Assimilation Technique™ has
1845 been shown to correspond well with traditional steady-state CO₂ response curves
1846 in *G. max* (Saathoff and Welles 2021). A_{net}/C_i curves were generated along a
1847 reference CO₂ ramp down from 420 $\mu\text{mol mol}^{-1}$ CO₂ to 20 $\mu\text{mol mol}^{-1}$ CO₂, fol-
1848 lowed by a ramp up from 420 $\mu\text{mol mol}^{-1}$ CO₂ to 1620 $\mu\text{mol mol}^{-1}$ CO₂ after
1849 a 90-second wait period at 420 $\mu\text{mol mol}^{-1}$ CO₂. The ramp rate for each curve
1850 was set to 200 $\mu\text{mol mol}^{-1} \text{min}^{-1}$, logging every five seconds, which generated 96
1851 data points per response curve. All A_{net}/C_i curves were generated after A_{net} and
1852 g_{sw} stabilized in a LI-6800 cuvette set to a 500 mol s^{-1} , 10,000 rpm mixing fan
1853 speed, 1.5 kPa vapor pressure deficit, 25°C leaf temperature, 2000 $\mu\text{mol m}^{-2} \text{s}^{-1}$
1854 incoming light radiation, and initial reference CO₂ set to 420 $\mu\text{mol mol}^{-1}$.

1855 With the same focal leaf used to generate A_{net}/C_i curves, I measured dark
1856 respiration (R_{d25} ; $\mu\text{mol m}^{-2} \text{s}^{-1}$) following at least a 30-minute period of darkness.
1857 Measurements were collected on a 5-second log interval for 60 seconds after stabi-

1858 lizing in a LI-6800 cuvette set to a 500 mol s^{-1} , 10,000 rpm mixing fan speed, 1.5
1859 kPa vapor pressure deficit, 25°C leaf temperature, and $420 \mu\text{mol mol}^{-1}$ reference
1860 CO_2 concentration (for both CO_2 concentrations), with incoming light radiation
1861 set to $0 \mu\text{mol m}^{-2} \text{ s}^{-1}$. A single dark respiration value was determined for each
1862 focal leaf by calculating the mean dark respiration value (i.e. the absolute value
1863 of A_{net} during the logging period) across the logging interval.

1864 5.2.4 *Leaf trait measurements*

1865 The focal leaf used to generate A_{net}/C_i curves and dark respiration was
1866 harvested immediately following gas exchange measurements. Images of each focal
1867 leaf were curated using a flat-bed scanner to determine wet leaf area using the
1868 'LeafArea' R package (Katabuchi 2015), which automates leaf area calculations
1869 using ImageJ software (Schneider et al. 2012). Each leaf was dried at 65°C for
1870 at least 48 hours, and subsequently weighed and ground until homogenized. Leaf
1871 mass per area (M_{area} ; g m^{-2}) was calculated as the ratio of dry leaf biomass
1872 to fresh leaf area. Using subsamples of ground and homogenized leaf tissue, I
1873 measured leaf nitrogen content (N_{mass} ; gN g^{-1}) through elemental combustion
1874 analysis (Costech-4010, Costech, Inc., Valencia, CA, USA). Leaf nitrogen content
1875 per unit leaf area (N_{area} ; gN m^{-2}) was calculated by multiplying N_{mass} and M_{area} .

1876 I extracted chlorophyll content from a second leaf in the same trifoliolate
1877 leaf set as the focal leaf used to generate A_{net}/C_i curves. Prior to chlorophyll
1878 extraction, I used a cork borer to punch between 3 and 5 0.6 cm^2 disks from the
1879 leaf. Separate images of each punched leaf and set of leaf disks were curated using
1880 a flat-bed scanner to determine wet leaf area, again quantified using the 'LeafArea'

1881 R package (Katabuchi 2015). The punched leaf was dried and weighed after at
1882 least 65°C in the drying oven to determine M_{area} of the chlorophyll leaf.

1883 Leaf disks were shuttled into a test tube containing 10mL dimethyl sul-
1884 foxide, vortexed, and incubated at 65degreeC for 120 minutes (Barnes et al.
1885 1992). Incubated test tubes were vortexed again before loaded in 150 μL trip-
1886 licate aliquots to a 96-well plate. Dimethyl sulfoxide was also loaded in a 150
1887 μL triplicate aliquot as a blank. Absorbance measurements at 649.1 nm ($A_{649.1}$)
1888 and 665.1 nm ($A_{665.1}$) were read in each well using a plate reader (Biotek Synergy
1889 H1; Biotek Instruments, Winooski, VT USA) (Wellburn 1994), with triplicates
1890 subsequently averaged and corrected by the mean of the blank absorbance value.
1891 Blank-corrected absorbance values were used to estimate Chl_a ($\mu\text{g mL}^{-1}$) and
1892 Chl_b ($\mu\text{g mL}^{-1}$) following equations from Wellburn (1994):

$$Chl_a = 12.47A_{665.1} - 3.62A_{649.1} \quad (5.1)$$

1893 and

$$Chl_b = 25.06A_{665.1} - 6.50A_{649.1} \quad (5.2)$$

1894 Chl_a and Chl_b were converted to mmol mL^{-1} using the molar mass of chlorophyll a
1895 (893.51 g mol^{-1}) and the molar mass of chlorophyll b (907.47 g mol^{-1}), then added
1896 together to calculate total chlorophyll content in the dimethyl sulfoxide extractant
1897 (mmol mL^{-1}). Total chlorophyll content was multiplied by the volume of the
1898 dimethyl sulfoxide extractant (10 mL) and converted to area-based chlorophyll
1899 content by dividing by the total area of the leaf disks (Chl_{area} ; mmol m^{-2}). Mass-
1900 based chlorophyll content (Chl_{mass} ; mmol g^{-1}) was calculated by dividing Chl_{area}

1901 by the leaf mass per area of the punched leaf.

1902 5.2.5 A/C_i curve fitting and parameter estimation

1903 I fit A_{net}/C_i curves of each individual using the ‘fitaci’ function in the
1904 ‘plantecophys’ R package (Duursma 2015). This function estimates the maxi-
1905 mum rate of Rubisco carboxylation (V_{cmax} ; $\mu\text{mol m}^{-2} \text{s}^{-1}$) and maximum rate
1906 of electron transport for RuBP regeneration (J_{max} ; $\mu\text{mol m}^{-2} \text{s}^{-1}$) based on the
1907 Farquhar biochemical model of C₃ photosynthesis (Farquhar et al. 1980). Triose
1908 phosphate utilization (TPU) limitation was included in all curve fits, and all curve
1909 fits included measured dark respiration values. As A_{net}/C_i curves were generated
1910 using a common leaf temperature, curves were fit using Michaelis-Menten coeffi-
1911 cients for Rubisco affinity to CO₂ (K_c ; $\mu\text{mol mol}^{-1}$) and O₂ (K_o ; $\mu\text{mol mol}^{-1}$), and
1912 the CO₂ compensation point (Γ^* ; $\mu\text{mol mol}^{-1}$) reported in Bernacchi et al. (2001).
1913 Specifically, K_c was set to 404.9 $\mu\text{mol mol}^{-1}$, K_o was set to 278.4 $\mu\text{mol mol}^{-1}$, and
1914 Γ^* was set to 42.75 $\mu\text{mol mol}^{-1}$. The use of a common leaf temperature across
1915 curves and dark respiration measurements also eliminated the need to manually
1916 temperature standardize rate estimates. For clarity, I reference V_{cmax} , J_{max} , and
1917 R_d estimates throughout the rest of the paper as $V_{\text{cmax}25}$, $J_{\text{max}25}$, and R_{d25} .

1918 5.2.6 Stomatal limitation

1919 I quantified the extent by which stomatal conductance limited photosynthe-
1920 sis (l; unitless) following equations originally described in Farquhar and Sharkey
1921 (1982). Stomatal limitation was calculated as:

$$l = 1 - \frac{A_{net}}{A_{mod}} \quad (5.3)$$

1922 where A_{mod} represents the photosynthetic rate where $C_i = C_a$. A_{mod} was calcu-

1923 lated as:

$$A_{mod} = V_{cmax25} - \frac{420 - \Gamma^*}{420 + K_m} - R_{d25} \quad (5.4)$$

1924 K_m is the Michaelis-Menten coefficient for Rubisco-limited photosynthesis, calcu-

1925 lated as:

$$K_m = K_c \cdot \left(1 + \frac{O_i}{K_o}\right) \quad (5.5)$$

1926 where O_i refers to leaf intercellular O_2 concentrations, set to $210 \mu\text{mol mol}^{-1}$.

1927 5.2.7 *Proportion of leaf nitrogen allocated to photosynthesis and structure*

1928 I used equations from Niinemets and Tenhunen (1997) to estimate the

1929 proportion of leaf N content allocated to Rubisco bioenergetics, and light harvest-

1930 ing proteins. The proportion of leaf N allocated to Rubisco (ρ_{rub} ; gN gN^{-1}) was

1931 calculated as a function of V_{cmax25} and N_{area} :

$$\rho_{rubisco} = \frac{V_{cmax25} N_r}{V_{cr} N_{area}} \quad (5.6)$$

1932 where N_r is the amount of nitrogen in Rubisco, set to $0.16 \text{ gN (gN in Rubisco)}^{-1}$

1933 and V_{cr} is the maximum rate of RuBP carboxylation per unit Rubisco protein,

1934 set to $20.5 \mu\text{mol CO}_2 (\text{g Rubisco})^{-1}$. The proportion of leaf nitrogen allocated to

1935 bioenergetics (ρ_{bioe} ; gN gN^{-1}) was similarly calculated as a function of J_{max25} and

1936 N_{area} :

$$\rho_{\text{bioe}} = \frac{J_{\text{max}25} N_b}{J_{\text{mc}} N_{\text{area}}} \quad (5.7)$$

1937 where N_b is the amount of nitrogen in cytochrome f, set to 0.12407 gN (μmol cytochrome f) $^{-1}$ assuming a constant 1: 1: 1.2 cytochrome f: ferredoxin NADP reductase: coupling factor molar ratio (Evans and Seemann 1989; Niinemets and Tenhunen 1997), and J_{mc} is the capacity of electron transport per cytochrome f, set to 156 μmol electron (μmol cytochrome f) $^{-1}\text{s}^{-1}$.

1942 The proportion of leaf nitrogen allocated to light harvesting proteins was calculated as a function of Chl_{mass} and N_{mass} :

$$\rho_{\text{light}} = \frac{Chl_{\text{mass}}}{N_{\text{mass}} c_b} \quad (5.8)$$

1944 where c_b is the stoichiometry of the light-harvesting chlorophyll complexes of photosystem II, set to 2.75 mmol chlorophyll (gN in chlorophyll) $^{-1}$. We used the N_{mass} value of the focal leaf used to generate A_{net}/C_i curves instead of the leaf used to extract chlorophyll content, as the two leaves are from the same trifoliolate leaf set and are highly correlated with each other (Figure SX).

1949 The proportion of leaf nitrogen content allocated to photosynthetic tissue (ρ_{photo} ; gN gN $^{-1}$) was estimated as the sum of ρ_{rubisco} , ρ_{bioe} , and ρ_{light} .

1951 Finally, the proportion of leaf N content allocated to structural tissue (ρ_{str} ; gN gN $^{-1}$) was estimated as:

$$\rho_{\text{structure}} = \frac{N_{\text{cw}}}{N_{\text{area}}} \quad (5.9)$$

1953 where N_{cw} is the leaf N content allocated to cell walls (gN m^{-2}), calculated as a
1954 function of M_{area} using an empirical equation from Onoda et al. (2017):

$$N_{cw} = 0.000355 * M_{area}^{1.39} \quad (5.10)$$

1955 5.2.8 *Whole plant traits*

1956 Seven weeks after experiment initiation and immediately following gas ex-
1957 change measurements, I harvested all experimental individuals and separated
1958 biomass of each experimental individual into major organ types (leaves, stems,
1959 roots, and nodules when present). Fresh leaf area of all harvested leaves was mea-
1960 sured using an LI-3100C (Li-COR Biosciences, Lincoln, Nebraska, USA). Total
1961 fresh leaf area (cm^2) was calculated as the sum of all leaf areas, including the focal
1962 leaf used to collect gas exchange data and the focal leaf used to extract chlorophyll
1963 content. All harvested material was dried in an oven set to 65°C for at least 48
1964 hours, weighed, and ground to homogeneity. Leaves and nodules were manually
1965 ground either with a mortar and pestle, while stems and roots were ground using
1966 a Wiley mill (E3300 Mini Mill; Eberbach Corp., MI, USA). Total dry biomass (g)
1967 was calculated as the sum of dry leaf (including focal leaf for both the A_{net}/C_i
1968 curve and leaf used to extract chlorophyll content), stem, root, and root nodule
1969 biomass. I quantified carbon and nitrogen content of each respective organ type
1970 through elemental combustion (Costech-4010, Costech, Inc., Valencia, CA, USA)
1971 using subsamples of ground and homogenized organ tissue.

1972 Following the approach explained in the first experimental chapter, I calcu-
1973 lated structural carbon costs to acquire nitrogen as the ratio of total belowground

1974 carbon biomass to whole plant nitrogen biomass (N_{cost} ; gC gN⁻¹). Belowground
1975 carbon biomass (C_{bg} ; gC) was calculated as the sum of root carbon biomass
1976 and root nodule carbon biomass. Root carbon biomass and root nodule carbon
1977 biomass was calculated as the product of the organ biomass and the respective
1978 organ carbon content. Whole plant nitrogen biomass (N_{wp} ; gN) was similarly
1979 calculated as the sum of total leaf, stem, root, and root nodule nitrogen biomass,
1980 including the focal leaf used for A_{net}/C_i curve and chlorophyll extractions. Leaf,
1981 stem, root, and root nodule nitrogen biomass was calculated as the product of
1982 the organ biomass and the respective organ nitrogen content. This calculation
1983 only quantifies plant structural carbon costs to acquire nitrogen and does not
1984 include any additional costs of nitrogen acquisition associated with respiration,
1985 root exudation, or root turnover. An explicit explanation of the limitations for
1986 interpreting this calculation can be found in Perkowski et al. (2021) and Terrer
1987 et al. (2018).

1988 Finally, plant investments in nitrogen fixation were calculated as the ra-
1989 tio of root nodule biomass to root biomass, where increasing values indicate an
1990 increase in plant investments to nitrogen fixation (Dovrat et al. 2018; Dovrat
1991 et al. 2020; Perkowski et al. 2021). I also calculated the percent of leaf nitrogen
1992 acquired from the atmosphere (% N_{dfa}) using leaf δ¹⁵N and the following equation
1993 from Andrews et al. (2011):

$$\%N_{dfa} = \frac{\delta^{15}N_{reference} - \delta^{15}N_{sample}}{\delta^{15}N_{reference} - B} \quad (5.11)$$

1994 where δ¹⁵N_{reference} refers to a reference plant that exclusively acquires nitrogen via

1995 direct uptake, $\delta^{15}\text{N}_{\text{sample}}$ refers to an individual's leaf $\delta^{15}\text{N}$, and B refers to individuals that are entirely reliant on nitrogen fixation. Within each unique nitrogen
1996 fertilization treatment-by-CO₂ treatment combination, I calculated the mean leaf
1997 $\delta^{15}\text{N}$ for individuals growing in the non-inoculated treatment for $\delta^{15}\text{N}_{\text{reference}}$. Any
1998 individuals with visual confirmation of root nodule formation or nodule initiation
2000 were omitted from the calculation of $\delta^{15}\text{N}_{\text{reference}}$. Following recommendations
2001 from Andrews et al. (2011) I calculated B within each CO₂ treatment using
2002 the mean leaf $\delta^{15}\text{N}$ of inoculated individuals that received 0 ppm N. I did not
2003 calculate B within each unique soil nitrogen-by-CO₂ treatment combination, as
2004 previous studies suggest decreased reliance on nitrogen fixation with increasing
2005 soil nitrogen availability (Perkowski et al. 2021). This approach for estimating
2006 nitrogen fixation standardizes values such that approaching 1 indicates increasing
2007 reliance on nitrogen fixation.

2008 5.2.9 *Statistical analyses*

2009 Any uninoculated pots that had substantial root nodule formation (nodule
2010 biomass: root biomass values greater than 0.05 g g⁻¹) were removed from analyses.
2011 This was because they were assumed to have been colonized by symbiotic nitrogen-
2012 fixing bacteria from outside sources. This decision resulted in the removal of
2013 sixteen pots from our analysis: two pots in the elevated CO₂ treatment that
2014 received 35 ppm N, three pots in the elevated CO₂ treatment that received 70
2015 ppm N, one pot in the elevated CO₂ treatment that received 210 ppm N, two pots
2016 in the elevated CO₂ treatment that received 280 ppm N, two pots in the ambient
2017 CO₂ treatment that received 0 ppm N, three pots in the ambient CO₂ treatment

2018 that received 70 ppm N, two pots in the ambient CO₂ treatment that received
2019 105 ppm N, and one pot in the ambient CO₂ treatment that received 280 ppm N.

2020 I built a series of linear mixed effects models to investigate the impacts of
2021 CO₂ concentration, soil nitrogen fertilization, and inoculation with *B. japonicum*
2022 on *G. max* gas exchange, tradeoffs between nitrogen and water use, whole plant
2023 growth, and investment in nitrogen fixation. All models included CO₂ treatment
2024 as a categorical fixed effect, inoculation treatment as a categorical fixed effect,
2025 soil nitrogen fertilization as a continuous fixed effect, with interaction terms be-
2026 tween all three fixed effects. All models also accounted for climatic difference
2027 between chambers across experiment iterations by including a random intercept
2028 term that nested starting chamber rack by CO₂ treatment. Models with this
2029 independent variable structure were created for each of the following dependent
2030 variables: N_{area} , M_{area} , N_{mass} , Chl_{area} , V_{cmax25} , J_{max25} , $J_{\text{max25}}:V_{\text{cmax25}}$, R_{d25} , g_{sw} ,
2031 stomatal limitation, ρ_{rubisco} , ρ_{bioe} , ρ_{light} , ρ_{photo} , $\rho_{\text{structure}}$, N_{cost} , C_{bg} , N_{wp} , total
2032 biomass, total leaf area, nodule biomass, and the ratio of nodule biomass to root
2033 biomass.

2034 I used Shapiro-Wilk tests of normality to determine whether linear mixed
2035 effects models satisfied residual normality assumptions. If residual normality as-
2036 sumptions were not met (Shapiro-Wilk: $p < 0.05$), then models were fit using
2037 dependent variables that were natural log transformed. All residual normality
2038 assumptions that did not originally satisfy residual normality assumptions were
2039 met with either a natural log or square root data transformation (Shapiro-Wilk:
2040 $p > 0.05$ in all cases). Specifically, models for N_{area} , N_{mass} , Chl_{area} , V_{cmax25} ,
2041 J_{max25} , $J_{\text{max25}}:V_{\text{cmax25}}$, g_{sw} , stomatal limitation, ρ_{rubisco} , ρ_{bioe} , ρ_{light} , ρ_{photo} , and to-

2042 tal leaf area satisfied residual normality assumptions without data transformation.

2043 Models for M_{area} , $\rho_{\text{structure}}$, N_{cost} , C_{bg} , N_{wp} , and total biomass satisfied residual

2044 normality assumptions with a natural log data transformation, while models for

2045 nodule biomass and nodule biomass: root biomass satisfied residual normality

2046 assumptions with a square root data transformation.

2047 In all statistical models, I used the 'lmer' function in the 'lme4' R package

2048 (Bates et al. 2015) to fit each model and the 'Anova' function in the 'car' R

2049 package (Fox and Weisberg 2019) to calculate Type II Wald's χ^2 and determine

2050 the significance ($\alpha = 0.05$) of each fixed effect coefficient. I used the 'emmeans'

2051 R package (Lenth 2019) to conduct post-hoc comparisons using Tukey's tests,

2052 where degrees of freedom were approximated using the Kenward-Roger approach

2053 (Kenward and Roger 1997). All analyses and plots were conducted in R version

2054 4.2.0 (R Core Team 2021).

2055 5.3 Results

2056 5.3.1 *Leaf nitrogen content, chlorophyll content, and mass per area*

2057 Elevated CO₂ reduced N_{area} , N_{mass} , and Chl_{area} by 29%, 50%, and 31%,

2058 respectively, and stimulated M_{area} by 44% ($p < 0.001$ in all cases; Table 5.1). An

2059 interaction between fertilization and CO₂ (CO₂-by-fertilization interaction: $p_{N_{\text{area}}}$

2060 = 0.017, $p_{N_{\text{mass}}} < 0.001$, $p_{M_{\text{area}}} = 0.006$, $p_{Chl_{\text{area}}} = 0.083$; Table 5.1) indicated

2061 that the general positive effect of increasing fertilization on N_{area} , N_{mass} , and

2062 Chl_{area} ($p < 0.001$ in all cases; Table 5.1) was generally stronger under ambient

2063 CO₂ (Tukey _{N_{area}} : $p = 0.026$; Tukey _{N_{mass}} : $p < 0.001$; Tukey _{M_{area}} : $p = 0.009$;

2064 Tukey _{Chl_{area}} : $p = 0.065$; Table 5.1; Figs. 5.1a-d). This pattern resulted in a

2065 stronger reduction in N_{area} , N_{mass} , and Chl_{area} as well as a stronger stimulation
2066 in M_{area} under elevated CO₂ with increasing fertilization. An additional interac-
2067 tion between inoculation and CO₂ on N_{area} (CO₂-by-inoculation interaction: $p =$
2068 0.030; Table 5.1) indicated that the general positive effect of inoculation on N_{area}
2069 ($p < 0.001$; Table 5.1) was stronger under elevated CO₂ (45% increase; Tukey: p
2070 < 0.001) than under ambient CO₂ (18% increase; Tukey: $p < 0.001$), a result that
2071 increased the reduction in N_{area} in inoculated pots under elevated CO₂. Inocula-
2072 tion treatment did not modify the downregulation in N_{mass} (CO₂-by-inoculation
2073 interaction: $p = 0.148$; Table 5.1) and Chl_{area} ($p = 0.147$; Table 5.1) or the stimu-
2074 lation in M_{area} ($p = 0.866$; Table 5.1) under elevated CO₂. However, interactions
2075 between fertilization and inoculation on N_{area} (fertilization-by-inoculation inter-
2076 action: $p < 0.001$; Table 5.1; Fig. 5.1a), N_{mass} ($p = 0.001$; Table 5.1; Fig. 5.1b),
2077 M_{area} ($p = 0.025$; Table 5.1; Fig. 5.1c), and Chl_{area} ($p < 0.001$; Table 5.1; Fig.
2078 5.1d) indicated that the general positive effect of increasing fertilization on each
2079 trait was stronger in uninoculated pots (Tukey _{N_{area}} : $p < 0.001$; Tukey _{N_{mass}} : $p =$
2080 0.001; Tukey _{M_{area}} : $p = 0.031$; Tukey _{Chl_{area}} : $p < 0.001$).

Table 5.1. Effects of soil nitrogen fertilization, inoculation, and CO₂ treatments on N_{area} , N_{mass} , M_{area} , and Chl_{area}

	N_{area}			N_{mass}			M_{area}^a			
	df	Coefficient	χ^2	p	Coefficient	χ^2	p	Coefficient	χ^2	p
(Intercept)	-	1.10E+00	-	-	3.05E-02	-	-	3.64E+00	-	-
CO ₂	1	-5.67E-01	155.908	<0.001	-1.80E-02	272.362	<0.001	3.04E-01	151.319	<0.001
Inoculation (I)	1	6.21E-01	86.029	<0.001	7.54E-03	15.576	<0.001	1.81E-01	19.158	<0.001
Fertilization (N)	1	3.06E-03	316.408	<0.001	5.78E-05	106.659	<0.001	3.10E-04	21.440	<0.001
CO ₂ *I	1	2.63E-01	4.729	0.030	3.96E-03	2.025	0.155	-3.37E-02	0.029	0.866
CO ₂ *N	1	-3.68E-04	5.723	0.017	-2.85E-05	22.542	<0.001	2.80E-04	7.619	0.006
I*N	1	-1.36E-03	43.381	<0.001	-2.00E-05	11.137	0.001	-3.36E-04	5.022	0.025
CO ₂ *I*N	1	-3.23E-04	0.489	0.484	-2.59E-06	0.041	0.839	1.15E-04	0.208	0.649
<hr/>										
Chl_{area}										
	df	Coefficient	χ^2	p						
(Intercept)	-	2.13E-02	-	-						
CO ₂	1	-1.33E-02	69.233	<0.001						
Inoculation (I)	1	1.24E-01	136.341	<0.001						
Fertilization (N)	1	3.35E-04	163.111	<0.001						
CO ₂ *I	1	-3.18E-02	2.102	0.147						
CO ₂ *N	1	-8.79E-05	2.999	<i>0.083</i>						
I*N	1	-2.65E-04	75.769	<0.001						
CO ₂ *I*N	1	7.68E-05	2.144	0.147						

123

2081 *Significance determined using Type II Wald χ^2 tests ($\alpha = 0.05$). P -values < 0.05 are in bold, while p -values between
 2082 0.05 and 0.1 are italicized. A superscript “a” is included after trait labels to indicate if models were fit with natural
 2083 log transformed response variables. Key: df = degrees of freedom, N_{area} = leaf nitrogen content per unit leaf area,
 2084 N_{mass} = leaf nitrogen content, M_{area} = leaf mass per unit leaf area.

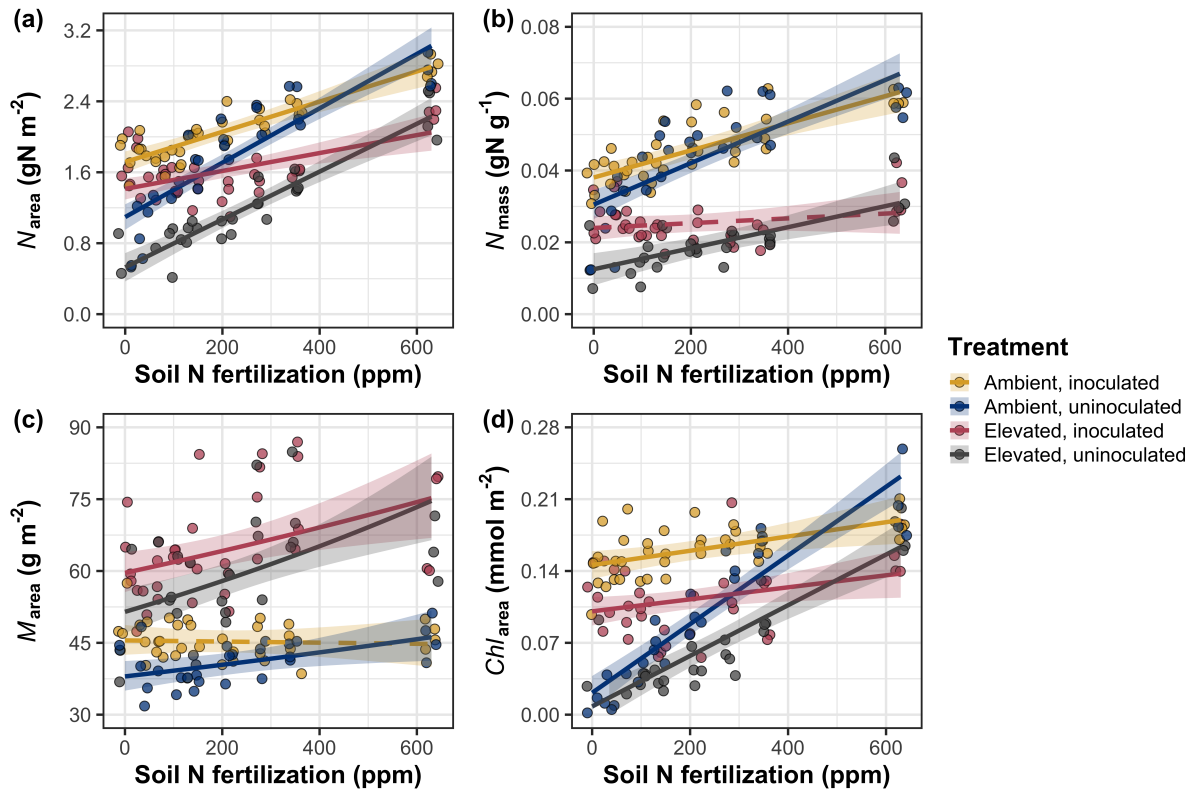


Figure 5.1. Effects of CO_2 , fertilization, and inoculation on leaf nitrogen per unit leaf area (a), leaf nitrogen content (b), leaf mass per unit leaf area (c), and chlorophyll content per unit leaf area (d). Soil nitrogen fertilization is represented on the x-axis in all panels. Yellow points and trendlines indicate inoculated individuals grown under ambient CO_2 , blue points and trendlines indicate uninoculated individuals grown under ambient CO_2 , red points and trendlines indicate inoculated individuals grown under elevated CO_2 , and grey points indicate uninoculated individuals grown under elevated CO_2 . Solid trendlines indicate regression slopes that are different from zero ($p < 0.05$), while dashed trendlines indicate slopes that are not distinguishable from zero ($p > 0.05$).

2085 5.3.2 *Leaf biochemistry and stomatal conductance*

2086 Elevated CO₂ resulted in plants with 16% lower V_{cmax25} ($p < 0.001$; Table
2087 5.2) and 10% lower J_{max25} ($p = 0.014$; Table 5.2) as compared to those grown under
2088 ambient CO₂. However, CO₂ concentration did not influence R_{d25} ($p = 0.613$;
2089 Table 5.2). A relatively stronger downregulation in V_{cmax25} than J_{max25} resulted
2090 in an 8% stimulation in $J_{max25}:V_{cmax25}$ under elevated CO₂ ($p < 0.001$; Table 5.2;
2091 Fig. 2E). The downregulatory effect of CO₂ on V_{cmax25} and J_{max25} was not modified
2092 across the fertilization gradient (CO₂-by-fertilization interaction: $p = 0.185$, $p =$
2093 0.389 for V_{cmax25} and J_{max25} , respectively; Table 5.2; Fig. 5.2a-b) or between
2094 inoculation treatments (CO₂-by-inoculation interaction: $p = 0.799$ and $p = 0.714$
2095 for V_{cmax25} and J_{max25} , respectively; Table 5.2). However, a strong interaction
2096 between fertilization and inoculation (fertilization-by-inoculation interaction: $p \leq$
2097 0.001 in all cases; Table 5.2) indicated that the general positive effect of increasing
2098 fertilization on V_{cmax25} ($p < 0.001$; Table 5.2), J_{max25} ($p < 0.001$; Table 5.2), and
2099 R_{d25} ($p = 0.015$; Table 2) was only observed in uninoculated pots (Tukey: p
2100 ≤ 0.001 in all cases), as there was no apparent effect of fertilization on V_{cmax25}
2101 (Tukey: $p = 0.456$), J_{max25} (Tukey: $p = 0.180$), or R_{d25} (Tukey: $p = 0.443$) in
2102 inoculated pots (Figs. 5.2a-d). A relatively stronger positive effect of increasing
2103 fertilization on V_{cmax25} than J_{max25} resulted in a general reduction in $J_{max25}:V_{cmax25}$
2104 with increasing fertilization ($p < 0.001$), though this pattern was only seen in
2105 uninoculated pots (Tukey: $p = 0.003$) and not inoculated plants (Tukey: $p >$
2106 0.05).

2107 Elevated CO₂ reduced stomatal conductance by 20% ($p < 0.001$; Table
2108 5.2; Fig. 5.2e) compared to ambient CO₂, but this downregulation did not influ-

ence stomatal limitation of photosynthesis ($p = 0.355$; Table 5.2; Fig. 5.2f). As with V_{cmax25} and J_{max25} , the downregulation of stomatal conductance due to elevated CO₂ was not modified across the fertilization gradient (CO₂-by-fertilization interaction: $p = 0.141$; Table 5.2) or between inoculation treatments (CO₂-by-inoculation interaction: $p = 0.179$; Table 5.2). Fertilization also did not modify the general null effect of CO₂ on stomatal limitation (CO₂-by-fertilization interaction: $p = 0.554$; Table 5.2), although an interaction between CO₂ and inoculation (CO₂-by-inoculation interaction: $p = 0.043$; Table 5.2) indicated that inoculation increased stomatal limitation under ambient CO₂ (Tukey: $p = 0.021$), but not under elevated CO₂ (Tukey: $p > 0.999$). An interaction between inoculation and fertilization on stomatal conductance (fertilization-by-inoculation interaction: $p < 0.001$; Table 5.2) indicated that increasing fertilization increased stomatal conductance in uninoculated pots (Tukey: $p = 0.003$) but decreased stomatal conductance in inoculated pots (Tukey: $p = 0.021$). The similar in magnitude, but opposite direction, trend in the effect of increasing fertilization on stomatal conductance between inoculation treatments likely drove a null general response of stomatal conductance to increasing fertilization ($p = 0.642$; Table 5.2).

Table 5.2. Effects of soil nitrogen fertilization, inoculation, and CO₂ on leaf biochemistry

	<i>V_{cmax25}</i>			<i>J_{max25}</i>			<i>R_{d25}</i>			
	df	Coefficient	χ^2	p	Coefficient	χ^2	p	Coefficient	χ^2	p
(Intercept)	-	4.36E+01	-	-	8.30E+01	-	-	1.69E+00	-	-
CO ₂	1	-7.05E+00	18.039	<0.001	-9.11E+00	6.042	0.014	4.53E-01	0.256	0.613
Inoculation (I)	1	5.87E+01	98.579	<0.001	9.62E+01	85.064	<0.001	1.04E+00	3.094	0.079
Fertilization (N)	1	1.32E-01	37.053	<0.001	2.09E-01	25.356	<0.001	2.86E-03	5.965	0.015
CO ₂ *I	1	-4.65E+00	0.065	0.799	7.84E-01	0.667	0.414	-5.71E-01	2.563	0.109
CO ₂ *N	1	-3.58E-02	1.758	0.185	-4.33E-02	0.742	0.389	-1.55E-03	2.675	0.102
I*N	1	-1.35E-01	60.394	<0.001	-2.30E-01	57.410	<0.001	-2.84E-03	12.083	0.001
CO ₂ *I*N	1	2.73E-02	0.748	0.387	3.46E-02	0.377	0.539	7.21E-04	0.244	0.622

	<i>J_{max25}:V_{cmax25}</i>			<i>g_{sw}</i>			Stomatal limitation			
	df	Coefficient	χ^2	p	Coefficient	χ^2	p	Coefficient	χ^2	p
(Intercept)	-	1.92E+00	-	-	1.95E-01	-	-	2.12E-01	-	-
CO ₂	1	5.71E-02	92.010	<0.001	-6.23E-02	9.718	0.002	3.91E-02	0.856	0.355
Inoculation (I)	1	-1.79E-01	27.768	<0.001	1.30E-01	22.351	<0.001	7.87E-02	4.582	0.032
Fertilization (N)	1	-4.61E-04	28.147	<0.001	2.50E-04	0.066	0.797	2.60E-04	32.218	<0.001
CO ₂ *I	1	8.94E-02	2.916	0.088	6.69E-02	1.810	0.179	-7.84E-02	4.093	0.043
CO ₂ *N	1	2.35E-04	3.210	0.073	-8.50E-05	2.165	0.141	-1.24E-04	0.350	0.554
I*N	1	3.27E-04	9.607	0.002	-3.09E-04	14.696	<0.001	-1.67E-04	2.547	0.110
CO ₂ *I*N	1	-1.66E-04	1.102	0.294	-8.89E-05	0.234	0.629	1.67E-04	2.231	0.135

127

2126 *Significance determined using Type II Wald χ^2 tests ($\alpha = 0.05$). *P*-values < 0.05 are in bold, while *p*-values between
 2127 0.05 and 0.1 are italicized. Key: *V_{cmax25}* = maximum rate of Rubisco carboxylation at 25°C; *J_{max25}* = maximum rate
 2128 of electron transport for RuBP regeneration at 25°C, *R_{d25}* = dark respiration at 25°C; *J_{max25}:V_{cmax25}* = the ratio of
 2129 *J_{max25}* to *V_{cmax25}*; *g_{sw}* = stomatal conductance.

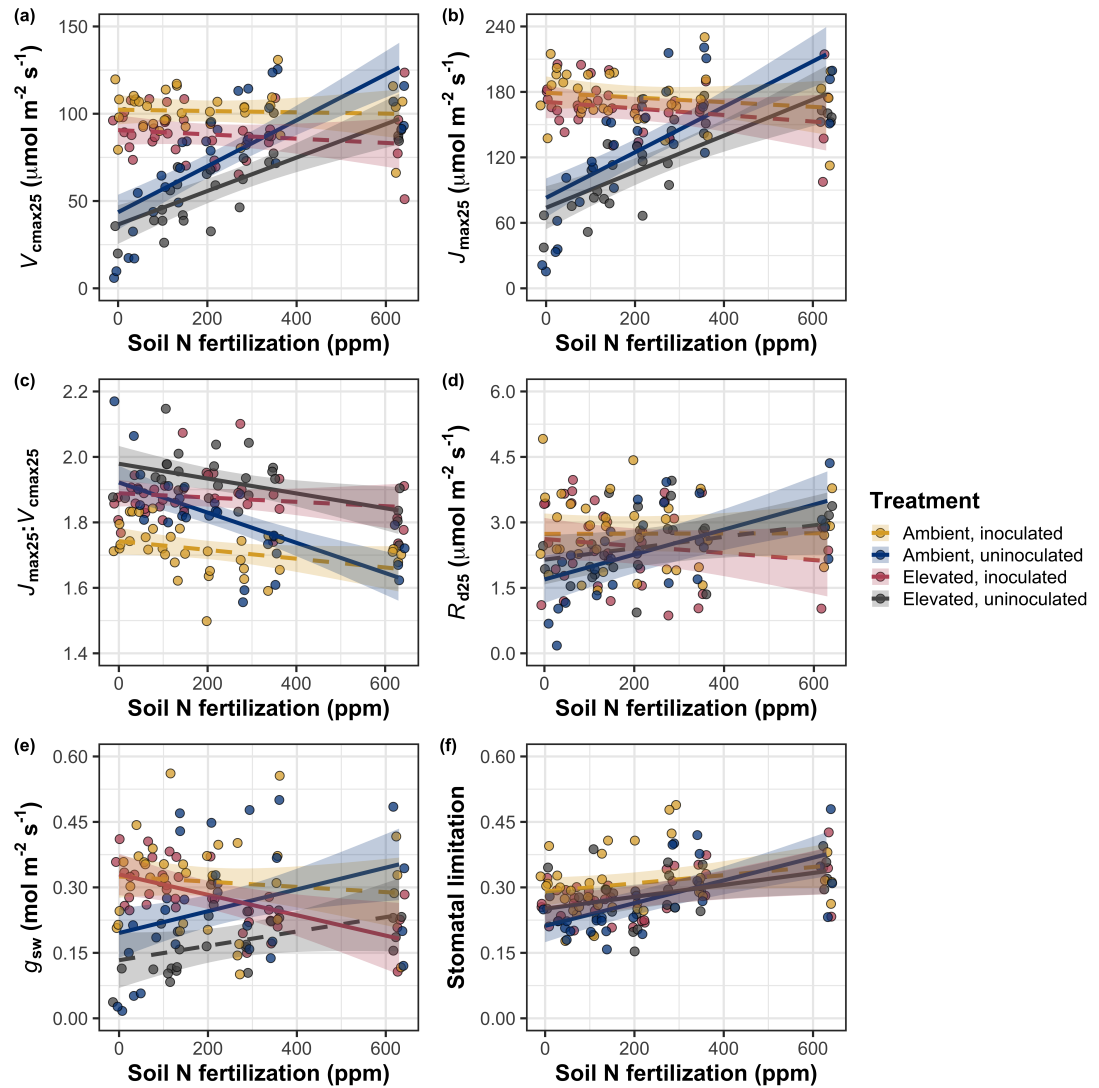


Figure 5.2. Effects of CO₂, fertilization, and inoculation on maximum rate of Rubisco carboxylation (a), the maximum rate of RuBP regeneration (b), and the ratio of the maximum rate of RuBP regeneration to the maximum rate of Rubisco carboxylation leaf mass per unit leaf area (c), dark respiration (d), stomatal conductance (e), and stomatal limitation (f). Soil nitrogen fertilization is represented on the x-axis in all panels. Colored points and trendlines are as explained in Figure 1.

2130 5.3.3 *Leaf nitrogen allocation*

2131 A relatively stronger downregulation in N_{area} than $V_{\text{cmax}25}$ or $J_{\text{max}25}$ resulted
2132 in an 20% and 29% respective stimulation in ρ_{rubisco} and ρ_{bioe} under elevated CO₂
2133 ($p < 0.001$ in both cases; Table 5.3). There was no apparent CO₂ effect on ρ_{light}
2134 ($p = 0.700$; Table 5.3), but the strong stimulation in ρ_{rubisco} and ρ_{bioe} resulted
2135 in a 21% stimulation of ρ_{photo} under elevated CO₂ ($p < 0.001$; Table 5.3; Fig.
2136 5.3a). The stimulation of ρ_{rubisco} , ρ_{bioe} , and ρ_{photo} due to elevated CO₂ was not
2137 modified across the fertilization gradient (CO₂-by-fertilization interaction: p_{rubisco}
2138 = 0.269, $p_{\text{bioe}} = 0.298$, $p_{\text{photo}} = 0.281$; Table 5.3). A marginal interaction between
2139 inoculation and CO₂ on ρ_{rubisco} and ρ_{photo} (CO₂-by-inoculation interaction: p_{rubisco}
2140 = 0.057, $p_{\text{photo}} = 0.057$; Table 5.3) indicated that the general positive effect of
2141 inoculation on ρ_{rubisco} and ρ_{photo} ($p < 0.001$ in both cases; Table 5.3) was only
2142 apparent under ambient CO₂ (Tukey: $p < 0.001$ in both cases), with no apparent
2143 effect of inoculation under elevated CO₂ (Tukey_{rubisco}: $p = 0.200$; Tukey_{photo}: p
2144 = 0.147). Inoculation did not modify the stimulation of ρ_{bioe} under elevated CO₂
2145 (CO₂-by-inoculation interaction: $p = 0.122$; Table 5.3) or the null effect of CO₂ on
2146 ρ_{bioe} (CO₂-by-inoculation interaction: $p = 0.298$; Table 5.3). Strong interactions
2147 between fertilization and inoculation on ρ_{rubisco} , ρ_{bioe} , and ρ_{photo} (fertilization-
2148 by-inoculation interaction: $p < 0.001$ in all cases; Table 5.3) indicated that the
2149 general negative effect of increasing fertilization ($p < 0.001$ in all cases; Table
2150 5.3) was only observed in inoculated pots (Tukey: $p < 0.001$ in all cases), with
2151 no apparent effect of fertilization on ρ_{rubisco} (Tukey: $p = 0.612$), ρ_{bioe} (Tukey:
2152 $p = 0.544$), or ρ_{photo} (Tukey: $p = 0.521$; Fig 5.3a) in uninoculated pots. An
2153 additional interaction between fertilization and inoculation on ρ_{light} (fertilization-

2154 by-inoculation interaction: $p < 0.001$; Table 5.3) indicated a negative effect of
2155 increasing fertilization on ρ_{light} in inoculated pots (Tukey: $p = 0.041$), but a
2156 positive effect of increasing fertilization in uninoculated pots (Tukey: $p < 0.001$).

2157 The stimulation in M_{area} resulted in an 133% stimulation of $\rho_{\text{structure}}$ under
2158 elevated CO₂ ($p < 0.001$; Table 5.3; Fig 5.3b). An interaction between fertiliza-
2159 tion and CO₂ (CO₂-by-fertilization interaction: $p = 0.039$; Table 5.3) indicated
2160 that the general negative effect of increasing fertilization ($p < 0.001$; Table 5.3) on
2161 $\rho_{\text{structure}}$ was marginally stronger under ambient CO₂ (Tukey: $p = 0.055$), resulting
2162 in a stronger stimulation in $\rho_{\text{structure}}$ under elevated CO₂ with increasing fertiliza-
2163 tion. A marginal interaction between inoculation and CO₂ (CO₂-by-inoculation
2164 interaction: $p = 0.057$; Table 5.3) indicated that the general positive effect of
2165 inoculation on $\rho_{\text{structure}}$ ($p < 0.001$; Table 5.3) was only observed under elevated
2166 CO₂ (Tukey: $p < 0.001$), with no apparent inoculation effect observed under am-
2167 bient CO₂ (Tukey: $p = 0.513$). Finally, an interaction between fertilization and
2168 inoculation (fertilization-by-inoculation interaction: $p < 0.001$; Table 5.3) indi-
2169 cated that, while increasing fertilization generally increased $\rho_{\text{structure}}$ ($p < 0.001$;
2170 Table 5.3), this response was generally stronger in uninoculated pots (Tukey: p
2171 = 0.001; Fig. 5.3b).

Table 5.3. Effects of soil N availability, soil pH, species, and N_{area} on leaf nitrogen allocation

		ρ_{rubisco}		ρ_{bioe}		ρ_{light}				
	df	Coefficient	χ^2	p	Coefficient	χ^2	p	Coefficient	χ^2	p
(Intercept)	-	2.70E-01	-	-	5.26E-02	-	-	8.48E-03	-	-
CO_2	1	1.42E-01	23.510	<0.001	3.00E-02	53.899	<0.001	2.03E-03	0.149	0.700
Inoculation (I)	1	1.83E-01	23.475	<0.001	2.80E-02	13.860	<0.001	2.04E-02	147.234	<0.001
Fertilization (N)	1	1.35E-04	16.609	<0.001	1.22E-05	26.827	<0.001	3.22E-05	19.378	<0.001
CO_2*I	1	-1.07E-01	3.629	<i>0.057</i>	-1.67E-02	2.390	0.122	-5.33E-03	0.684	0.408
CO_2*N	1	-2.16E-04	1.223	0.269	-3.59E-05	1.085	0.298	-7.01E-06	0.351	0.553
$I*N$	1	-4.26E-04	20.045	<0.001	-6.87E-05	15.458	<0.001	-4.37E-05	64.042	<0.001
CO_2*I*N	1	2.50E-04	3.327	<i>0.068</i>	4.08E-05	2.651	0.103	1.74E-05	3.735	<i>0.053</i>

		ρ_{photo}		$\rho_{\text{structure}}^a$			
	df	Coefficient	χ^2	p	Coefficient	χ^2	p
(Intercept)	-	3.32E-01	-	-	-2.93E+00	-	-
CO_2	1	1.81E-01	27.651	<0.001	8.77E-01	229.571	<0.001
Inoculation (I)	1	2.31E-01	26.238	<0.001	-2.55E-01	13.872	<0.001
Fertilization (N)	1	1.76E-04	15.899	<0.001	-1.51E-03	38.128	<0.001
CO_2*I	1	-1.36E-01	3.671	<i>0.055</i>	-2.99E-01	3.622	<i>0.057</i>
CO_2*N	1	-2.72E-04	1.163	0.281	3.14E-04	4.266	0.039
$I*N$	1	-5.37E-04	21.355	<0.001	7.00E-04	11.025	0.001
CO_2*I*N	1	3.29E-04	4.009	0.045	4.52E-04	0.669	0.413

131

2172 *Significance determined using Type II Wald χ^2 tests ($\alpha = 0.05$). P -values < 0.05 are in bold, while p -values
 2173 between 0.05 and 0.1 are italicized. A superscript “a” is included after trait labels to indicate if models were fit with
 2174 natural log transformed response variables. Key: df=degrees of freedom, ρ_{rubisco} = proportion of leaf N allocated
 2175 to photosynthesis, ρ_{bioe} = proportion of leaf N allocated to bioenergetics, ρ_{light} = proportion of leaf N allocated to
 2176 light harvesting proteins, ρ_{photo} = proportion of leaf N allocated to photosynthesis, $\rho_{\text{structure}}$ = proportion of leaf N
 2177 allocated to cell wall structural tissue

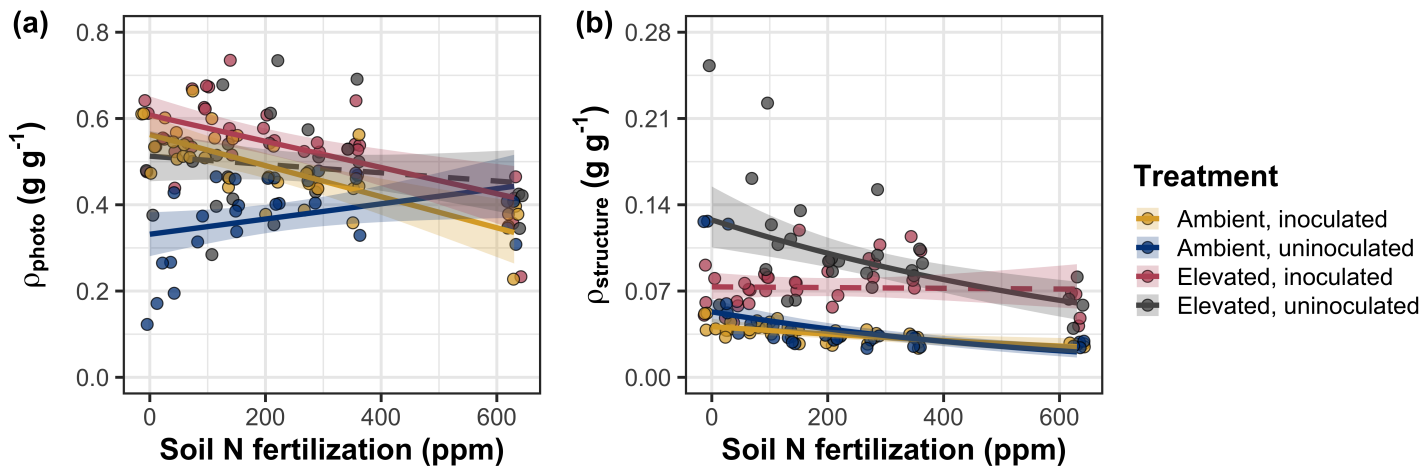


Figure 5.3. Effects of CO_2 , fertilization, and inoculation on the relative fraction of leaf nitrogen allocated to photosynthesis (a) and the fraction of leaf nitrogen allocated to structure (b). Soil nitrogen fertilization is represented on the x-axis in both panels. Colored points and trendlines are as explained in Figure 1.

2178 5.3.4 *Whole plant traits*

2179 Total leaf area was 51% greater and total biomass was 102% greater under
2180 elevated CO₂ ($p < 0.001$ in both cases; Table 5.4), a pattern that was enhanced
2181 by fertilization (CO₂-by-fertilization interaction: $p < 0.001$ in both cases; Table
2182 5.4; Figs. 5.4a-b) but was not modified across inoculation treatments (CO₂-by-
2183 inoculation interaction: $p_{total_leaf_area} = 0.151$, $p_{total_biomass} = 0.472$; Table 5.4).
2184 Specifically, the general positive effect of increasing fertilization on total leaf area
2185 and whole plant biomass ($p < 0.001$ in both cases; Table 5.4) was stronger under
2186 elevated CO₂ (Tukey: $p < 0.001$ in both cases). The general positive effect of
2187 increasing fertilization on total leaf area was modified by inoculation treatment
2188 (fertilization-by-inoculation interaction: $p < 0.001$ in both cases; Table 5.4), in-
2189 dicating a stronger positive effect of increasing fertilization in uninoculated pots
2190 (Tukey: $p_{total_leaf_area} = 0.002$, $p_{total_biomass} = 0.001$, Fig. 5.4a).

2191 A 62% stimulation in N_{cost} under elevated CO₂ was modified through a
2192 strong three-way interaction between CO₂, fertilization, and inoculation (CO₂-
2193 by-inoculation-by-fertilization interaction: $p < 0.001$; Table 5.4; Fig. 5.4). This
2194 interaction revealed a general negative effect of increasing fertilization on N_{cost}
2195 ($p < 0.001$; Table 5.4) that was observed in all treatment combinations (Tukey:
2196 $p < 0.001$ in all cases) except for inoculated pots grown under elevated CO₂
2197 (Tukey: $p = 0.779$; Fig. 5.4c). This response also resulted in generally stronger
2198 negative effects of increasing fertilization on N_{cost} in uninoculated pots grown
2199 under elevated CO₂ than uninoculated pots grown under ambient CO₂ (Tukey:
2200 $p = 0.001$) and inoculated pots grown under either ambient CO₂ (Tukey: $p <$
2201 0.001) or elevated CO₂ (Tukey: $p < 0.001$), while uninoculated pots grown under

2202 ambient CO₂ had generally stronger negative effects of increasing fertilization on
2203 N_{cost} than inoculated pots grown under elevated CO₂ (Tukey: $p = 0.002$), but
2204 not inoculated pots grown under ambient CO₂ (Tukey: $p = 0.216$; Fig. 5.4).
2205 The general reduction in N_{cost} with increasing fertilization and in uninoculated
2206 pots were driven by a stronger positive effect of increasing fertilization on N_{wp}
2207 (denominator of N_{cost}) than C_{bg} (numerator of N_{cost}), while the general stimulation
2208 in N_{cost} under elevated CO₂ was driven by a stronger positive effect of elevated
2209 CO₂ on C_{bg} than N_{wp} (Table 5.4).

Table 5.4. Effects of soil N availability, soil pH, species, and N_{area} on total leaf area, whole plant biomass, and carbon costs to acquire nitrogen

	Total leaf area			Total biomass			N_{cost}			
	df	Coefficient	χ^2	p	Coefficient	χ^2	p	Coefficient	χ^2	p
(Intercept)	-	8.78E+01	-	-	9.96E-01	-	-	8.67E+00	-	-
CO_2	1	3.36E+01	69.291	<0.001	5.07E-01	131.477	<0.001	8.75E+00	88.189	<0.001
Inoculation (I)	1	1.88E+02	35.715	<0.001	7.96E-01	34.264	<0.001	-1.68E+00	136.343	<0.001
Fertilization (N)	1	9.35E-01	274.199	<0.001	3.14E-03	269.046	<0.001	-8.50E-03	80.501	<0.001
$\text{CO}_2 * \text{I}$	1	6.44E+01	2.064	0.151	-7.69E-02	0.518	0.472	-8.38E+00	85.237	<0.001
$\text{CO}_2 * \text{N}$	1	5.05E-01	18.655	<0.001	1.61E-03	16.877	<0.001	-9.17E-03	1.050	0.306
$\text{I} * \text{N}$	1	-3.84E-01	10.804	0.001	-1.45E-03	15.779	<0.001	4.20E-03	46.489	<0.001
$\text{CO}_2 * \text{I} * \text{N}$	1	-2.97E-03	<0.001	0.990	-1.14E-04	0.023	0.880	1.32E-02	18.125	<0.001

	C_{bg}			N_{wp}			
	df	Coefficient	χ^2	p	Coefficient	χ^2	p
(Intercept)	-	-1.70E+00	-	-	1.24E-01	-	-
CO_2	1	9.21E-01	84.134	<0.001	-3.41E-03	23.890	<0.001
Inoculation (I)	1	1.18E+00	41.030	<0.001	1.68E-01	134.460	<0.001
N fertilization (N)	1	3.38E-03	152.248	<0.001	6.69E-04	529.021	<0.001
$\text{CO}_2 * \text{I}$	1	-6.18E-01	8.965	0.003	3.68E-02	1.190	0.275
$\text{CO}_2 * \text{N}$	1	-3.66E-05	1.188	0.276	1.58E-04	5.915	0.015
$\text{I} * \text{N}$	1	-2.22E-03	22.648	<0.001	-3.20E-04	55.562	<0.001
$\text{CO}_2 * \text{I} * \text{N}$	1	8.09E-04	1.109	0.292	-7.54E-05	0.620	0.431

2210 *Significance determined using Type II Wald χ^2 tests ($\alpha = 0.05$). P-values < 0.05 are in bold, while p-values between
 2211 0.05 and 0.1 are italicized. Key: df = degrees of freedom; N_{cost} = structural carbon cost to acquire nitrogen; C_{bg} =
 2212 belowground carbon biomass; N_{wp} = whole plant nitrogen biomass

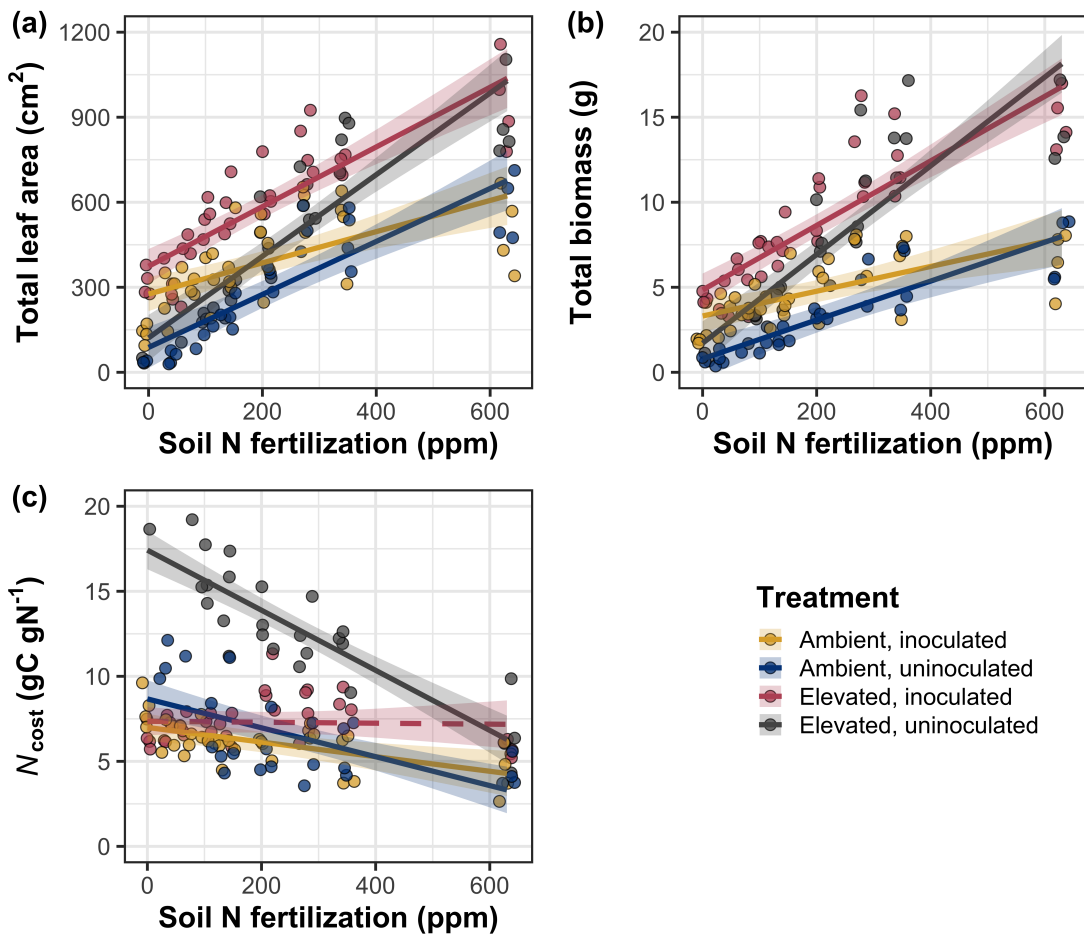


Figure 5.4. Effects of CO_2 , fertilization, and inoculation on total leaf area (a), total biomass (b), and structural carbon costs to acquire nitrogen (c). Soil nitrogen fertilization is represented continuously on the x-axis in all panels. Colored points and trendlines are as explained in Figure 1.

2213 5.3.5 *Nitrogen fixation*

2214 Nodule biomass was stimulated by 30% under elevated CO₂ ($p < 0.001$;
2215 Table 5.5), a pattern that was modified across the fertilization gradient (CO₂-
2216 by-fertilization interaction: $p = 0.479$; Table 5.5), but not between inoculation
2217 treatments (CO₂-by-inoculation interaction: $p = 0.404$; Table 5.5). Specifically,
2218 the general negative effect of increasing fertilization on nodule biomass ($p < 0.001$;
2219 Table 5.5) was stronger under elevated CO₂ than ambient CO₂ (Tukey: $p <$
2220 0.001; Fig. 5.5a), which reduced the stimulation in nodule biomass under elevated
2221 CO₂ with increasing fertilization. A strong interaction between fertilization and
2222 inoculation (fertilization-by-inoculation interaction: $p < 0.001$; Table 5.5) was
2223 driven by a stronger negative effect of increasing fertilization in inoculated pots
2224 (Tukey: $p < 0.001$; Fig. 5.5a).

2225 There was no effect of CO₂ on nodule: root biomass ($p = 0.767$; Table
2226 5.5), although an interaction between CO₂ and inoculation (CO₂-by-inoculation
2227 interaction: $p < 0.001$; Table 5.5) indicated that the general positive effect of in-
2228 oculation on nodule: root biomass ($p < 0.001$; Table 5.5) was stronger under am-
2229 bient CO₂ (3129% increase; Tukey: $p < 0.001$) than elevated CO₂ (379% increase;
2230 Tukey: $p < 0.001$; Fig. 5.5b). The null effect of CO₂ on nodule: root biomass
2231 was consistently observed across the fertilization gradient ($p = 0.183$; Table 5.5;
2232 Fig. 5.5b). An interaction between fertilization and inoculation (fertilization-by-
2233 inoculation interaction: $p < 0.001$; Table 5.5) indicated that the general negative
2234 effect of increasing fertilization on nodule: root biomass ($p < 0.001$; Table 5.5)
2235 was stronger in inoculated pots (Tukey: $p < 0.001$; Fig. 5.5b).

2236 There was no effect of CO₂ on %N_{dfa} ($p = 0.472$; Table 5.5), a pattern

2237 that was not modified by inoculation (CO_2 -by-inoculation interaction: $p = 0.156$;
2238 Table 5.5) or fertilization (CO_2 -by-fertilization interaction: $p = 0.099$; Table 5.5).
2239 An interaction between fertilization and inoculation (fertilization-by-inoculation
2240 interaction: $p < 0.001$; Table 5.5) indicated that the general negative effect of
2241 increasing fertilization on $\%N_{dfa}$ ($p < 0.001$; Table 5.5) was only observed in
2242 inoculated pots (Tukey: $p < 0.001$), with no apparent effect of fertilization on
2243 $\%N_{dfa}$ in uninoculated pots (Tukey: $p = 0.651$; Table 5.5; Fig. 5.5c).

Table 5.5. Effects of soil N availability, soil pH, species, and N_{area} on root nodule biomass and plant investments in symbiotic nitrogen fixation

	Root nodule biomass ^b			Root nodule: root biomass ^b			% N_{dfa}^b			
	df	Coefficient	χ^2	p	Coefficient	χ^2	p	Coefficient	χ^2	p
(Intercept)	-	9.41E-03	-	-	1.33E-02	-	-	7.48E-01	-	-
CO ₂	1	1.20E-01	19.258	<0.001	9.94E-02	0.087	0.768	-1.00E-01	0.518	0.472
Inoculation (I)	1	5.74E-01	755.020	<0.001	5.40E-01	903.691	<0.001	9.01E+00	955.570	<0.001
Fertilization (N)	1	7.71E-06	84.376	<0.001	-5.99E-06	258.099	<0.001	3.64E-04	292.938	<0.001
CO ₂ *I	1	-4.68E-02	0.950	0.330	-1.38E-01	20.614	<0.001	-1.44E-01	2.010	0.156
CO ₂ *N	1	-1.59E-04	2.106	0.147	-1.73E-04	1.773	0.183	-6.21E-05	2.716	0.099
I*N	1	-5.82E-04	44.622	<0.001	-7.45E-04	133.918	<0.001	-1.58E-02	231.290	<0.001
CO ₂ *I*N	1	7.26E-05	0.196	0.658	1.76E-04	2.359	0.125	2.77E-03	2.119	0.145

2244 *Significance determined using Type II Wald χ^2 tests ($\alpha = 0.05$). P-values < 0.05 are in bold, while p-values between
2245 0.05 and 0.1 are italicized. Superscript letters indicate model coefficients fit to square-root (^b) transformed data.
2246 Key: df = degrees of freedom % N_{dfa} = percent nitrogen fixed from the atmosphere.

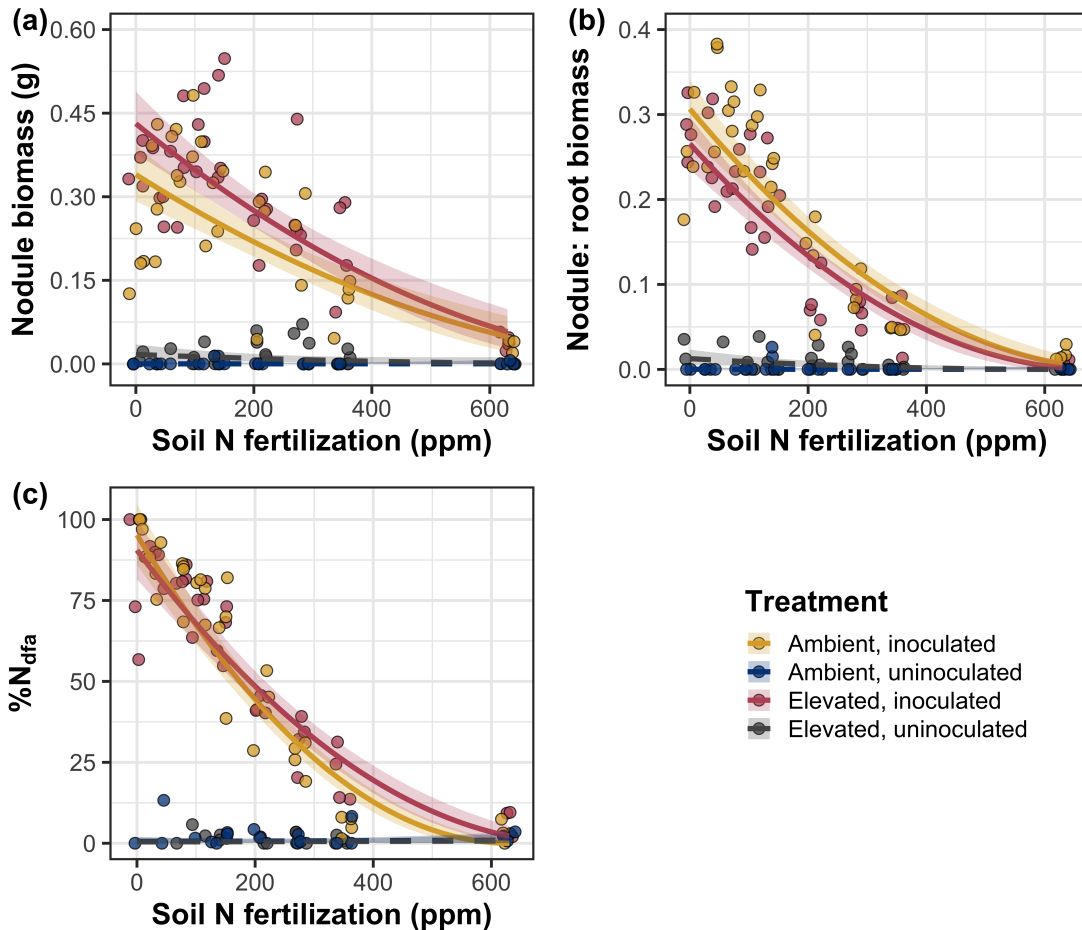


Figure 5.5. Effects of CO_2 , fertilization, and inoculation on nodule biomass (a), nodule: root biomass (b), and percent nitrogen fixed from the atmosphere (c). Soil nitrogen fertilization is represented on the x-axis. Yellow points and trendlines indicate inoculated individuals grown under ambient CO_2 , blue points and trendlines indicate uninoculated individuals grown under ambient CO_2 , red points and trendlines indicate inoculated individuals grown under elevated CO_2 , and grey points indicate uninoculated individuals grown under elevated CO_2 . Solid trendlines indicate slopes that are different from zero ($p < 0.05$), while dashed trendlines indicate slopes that are not different from zero ($p > 0.05$). Curvilinear trendlines occur as a result of back-transforming models where response variables received either a natural log or square root transformation prior to fitting.

2247 5.4 Discussion

2248 In this study, I determined leaf and whole plant acclimation responses of
2249 7-week *G. max* seedlings grown under two CO₂ concentrations, two inoculation
2250 treatments, and nine soil nitrogen fertilization treatments in a full-factorial growth
2251 chamber experiment. In support of my hypotheses and patterns expected from
2252 theory, elevated CO₂ reduced N_{area} , V_{cmax25} , and J_{max25} . The relatively stronger
2253 downregulation in V_{cmax25} than J_{max25} under elevated CO₂ resulted in a stimulation
2254 in $J_{\text{max25}}:V_{\text{cmax25}}$ under elevated CO₂. The downregulation of V_{cmax25} and J_{max25}
2255 under elevated CO₂ was similar across fertilization and inoculation treatments,
2256 indicating that the CO₂ responses were not due to nitrogen limitation. Interest-
2257 ingly, results indicate that elevated CO₂ increased the fraction of leaf nitrogen
2258 allocated to photosynthesis and structure, leading to a stimulation in nitrogen
2259 use efficiency under elevated CO₂ despite the apparent downregulation in N_{area} ,
2260 V_{cmax25} , and J_{max25} . The downregulation in leaf photosynthetic processes under
2261 elevated CO₂ also corresponded with a strong stimulation in total leaf area and to-
2262 tal biomass. Strong stimulations in whole plant growth due to elevated CO₂ were
2263 generally enhanced with increasing fertilization and were negatively related to
2264 structural carbon costs to acquire nitrogen. Inoculation generally did not modify
2265 whole plant responses to elevated CO₂ across the fertilization gradient, likely due
2266 to a strong reduction in root nodulation with increasing fertilization. However,
2267 strong positive effects of inoculation on whole plant growth were observed under
2268 low fertilization, consistent with our hypothesis. Overall, observed leaf and whole
2269 plant acclimation responses to CO₂ support hypotheses and patterns expected
2270 from photosynthetic least-cost theory, showing that leaf acclimation responses to

2271 CO₂ were decoupled from soil nitrogen availability and ability to acquire nitro-
2272 gen via symbiotic nitrogen fixation. Instead, leaf and whole plant acclimation
2273 responses to CO₂ were driven by optimal resource investment to photosynthetic
2274 capacity, where optimal resource investment at the leaf level maximized nitrogen
2275 allocation to structures that support whole plant growth.

2276 5.4.1 *Soil nitrogen fertilization has divergent effects on leaf and whole plant*
2277 *acclimation responses to CO₂*

2278 Elevated CO₂ reduced N_{area} , V_{cmax25} , J_{max25} , and stomatal conductance by
2279 29%, 16%, 10%, and 20%, respectively (Table 5.2). The larger downregulation in
2280 V_{cmax25} than J_{max25} led to an 8% stimulation in $J_{\text{max25}}:V_{\text{cmax25}}$ (Table 5.2), while
2281 the larger downregulation in N_{area} than V_{cmax25} resulted in a 21% stimulation
2282 in the fraction of leaf nitrogen allocated to photosynthesis under elevated CO₂.
2283 These acclimation responses are directionally consistent with previous studies that
2284 have investigated or reviewed leaf acclimation responses to CO₂ (Drake et al.
2285 1997; Makino et al. 1997; Ainsworth et al. 2002; Ainsworth and Long 2005;
2286 Ainsworth and Rogers 2007; Smith and Dukes 2013; Smith and Keenan 2020;
2287 Poorter et al. 2022), and follow patterns expected from photosynthetic least-cost
2288 theory (Wright et al. 2003; Prentice et al. 2014; Smith et al. 2019; Smith and
2289 Keenan 2020). Together, the stimulation in $J_{\text{max25}}:V_{\text{cmax25}}$ and the fraction of leaf
2290 nitrogen allocated to photosynthesis, and nitrogen use efficiency under elevated
2291 CO₂ provide strong support for the idea that leaves were downregulating V_{cmax25}
2292 in response to elevated CO₂ in order to optimally coordinate photosynthesis such
2293 that net photosynthesis rates approached becoming equally co-limited by Rubisco

2294 carboxylation and RuBP regeneration (Chen et al. 1993; Maire et al. 2012).

2295 Increasing fertilization and inoculation induced strong positive effects on
2296 N_{area} (Fig. 1a), $V_{\text{cmax}25}$ (Fig. 5.2a), $J_{\text{max}25}$ (Fig. 5.2b). The general positive
2297 response of N_{area} to increasing fertilization and in inoculated pots was enhanced
2298 under ambient CO_2 , which, paired with the general downregulation in N_{area} un-
2299 der elevated CO_2 , resulted in a stronger downregulation of N_{area} under elevated
2300 CO_2 with increasing fertilization and in inoculated pots (Fig. 5.1a). These pat-
2301 terns suggest that N_{area} responses to CO_2 were at least partially dependent on
2302 soil nitrogen fertilization and nitrogen acquisition strategy. However, the general
2303 stimulation in the fraction of leaf nitrogen allocated to Rubisco, bioenergetics,
2304 or photosynthesis under elevated CO_2 was not modified across the fertilization
2305 gradient and was only marginally enhanced in inoculated pots. These patterns
2306 suggest that the increased downregulation of N_{area} under elevated CO_2 with in-
2307 creasing fertilization was not associated with a change in relative investment to
2308 photosynthetic tissue. Instead, a stronger downregulation in the fraction of leaf
2309 nitrogen allocated to structure under ambient CO_2 resulted in a stronger stim-
2310 ulation in $\rho_{\text{structure}}$ under elevated CO_2 with increasing fertilization (Fig. 5.3b),
2311 indicating that fertilization shifted relative investment in leaf structural tissue un-
2312 der elevated CO_2 . These results, combined with a stimulation in PNUE (Fig. SX)
2313 and iWUE (Fig. SX) under elevated CO_2 that was independent of fertilization
2314 or inoculation treatment, provide additional support for the hypothesis that leaf
2315 acclimation photosynthetic responses to CO_2 were independent of fertilization;
2316 though fertilization may contribute to changes in leaf morphology under elevated
2317 CO_2 through shifts in M_{area} (Onoda et al. 2017; Wang et al. 2017; Dong et al.

2318 2022).

2319 The downregulation in N_{area} , $V_{\text{cmax}25}$, and $J_{\text{max}25}$ under elevated CO₂ cor-
2320 responded with a respective 62% and 100% stimulation in total leaf area (Fig.
2321 5.4a) and total biomass (Fig. 5.4b). The stimulation in total leaf area and total
2322 biomass under elevated CO₂ also corresponded with generally higher structural
2323 carbon costs to acquire nitrogen (Fig. 5.4c), a pattern driven by a stimulation
2324 in belowground carbon biomass and reduction in whole plant nitrogen biomass.
2325 Alone, this result suggests that elevated CO₂ reduces plant nitrogen uptake effi-
2326 ciency, which does not explain why plants grown under elevated CO₂ generally had
2327 higher biomass and total leaf area. However, a strong negative effect of increasing
2328 fertilization on structural carbon costs to acquire nitrogen, which were generally
2329 similar between CO₂ concentrations, was driven by a stronger increase in whole
2330 plant nitrogen biomass than belowground carbon biomass. Thus, increases in the
2331 positive response of whole plant growth and total leaf area under elevated CO₂
2332 with increasing fertilization were likely driven by an increase in nitrogen uptake
2333 efficiency, allowing plants to satisfy any increase in whole plant nitrogen demand
2334 associated with increased CO₂.

2335 Interestingly, these results indicate that the general stimulation in total
2336 leaf area and whole plant growth under elevated CO₂ was not modified by inoc-
2337 ulation despite an apparent general negative effect of inoculation on N_{cost} . This
2338 response could have been due to strong negative effect of increasing fertilization on
2339 nodulation (Fig. 5.5), which may have caused the strong increase in the positive
2340 effect of elevated CO₂ on whole plant growth with increasing fertilization to mask
2341 any increase in the positive effect of elevated CO₂ on whole plant growth due to

2342 inoculation. Reductions in nodulation with increasing fertilization are commonly
2343 observed patterns that have been inferred to be a response that allows species
2344 optimize nitrogen uptake efficiency as costs to acquire nitrogen via direct uptake
2345 become more similar (Fig. 5.4c) (Gibson and Harper 1985; Rastetter et al. 2001).
2346 In this study, pairwise comparisons indicated strong positive effects of inocula-
2347 tion on total leaf area and total biomass (158% increase in total leaf area, 119%
2348 increase in total biomass) under elevated CO₂ at 0 ppm N, but no observable
2349 inoculation effect on total leaf area or total biomass under elevated CO₂ at 350
2350 ppm N or 630 ppm N. While these responses did not generally differ from those
2351 observed under ambient CO₂, they do confirm the hypothesis that positive effects
2352 of inoculation on whole plant growth responses to elevated CO₂ would decrease
2353 with increasing fertilization.

2354 Combined, results reported here suggest that soil nitrogen availability has
2355 a divergent role in modifying leaf and whole plant acclimation responses to CO₂.
2356 Leaf acclimation responses were generally decoupled from fertilization, while whole
2357 plant acclimation responses relied heavily on an increase in nitrogen uptake ef-
2358 ficiency and consequent reduction in costs of acquiring nitrogen associated with
2359 increasing fertilization. However, whole plant responses to CO₂ indicated that
2360 fertilization may play a more important role in determining whole plant acclima-
2361 tion responses to CO₂ than nitrogen acquisition strategy, although these patterns
2362 were likely driven by reductions in nodulation with increasing fertilization. These
2363 results suggest that plants acclimate to CO₂ in nitrogen-limited systems by mini-
2364 mizing the number of optimally coordinated leaves, and that the downregulation
2365 in leaf nitrogen content under elevated CO₂ is not a direct response to changes in

2366 soil nitrogen availability as previously implied.

2367 5.4.2 *Implications for future model development*

2368 Many terrestrial biosphere models predict photosynthetic capacity through
2369 plant functional group-specific linear regressions between N_{area} and V_{cmax} (Rogers
2370 2014; Rogers et al. 2017), which assumes that leaf nitrogen-photosynthesis rela-
2371 tionships are constant across growing environments. Our results build on previ-
2372 ous work suggesting that leaf nitrogen-photosynthesis relationships dynamically
2373 change across growing environments (Luo et al. 2021; Dong et al. 2022). Specif-
2374 ically, results from this experiment indicate that CO_2 concentration increased
2375 the fraction of leaf nitrogen content allocated to photosynthesis, while a general
2376 negative effect of increasing fertilization on the fraction of leaf nitrogen content
2377 allocated to photosynthesis was dependent on inoculation treatment. Similar in-
2378 creases in N_{area} , $V_{\text{cmax}25}$, and $J_{\text{max}25}$ with increasing fertilization resulted in no
2379 change in the fraction of leaf nitrogen allocated to photosynthesis in uninoculated
2380 pots, while larger increases in N_{area} than $V_{\text{cmax}25}$ and $J_{\text{max}25}$ with increasing fertil-
2381 ization decreased the fraction of leaf nitrogen allocated to photosynthesis in inoc-
2382 ulated pots (Fig. 5.3a). As inoculated pots were able to access less finite supply of
2383 nitrogen across the fertilization gradient, these patterns suggest that constant leaf
2384 nitrogen-photosynthesis relationships may only apply in environments where ni-
2385 trogen is limiting and will likely change with increasing CO_2 concentrations. Thus,
2386 terrestrial biosphere models that parameterize photosynthetic capacity through
2387 linear relationships between N_{area} and V_{cmax} (Rogers 2014; Rogers et al. 2017)
2388 may be overestimating photosynthetic capacity in systems where nitrogen is not

2389 as limiting and may contribute to erroneous model simulations under future CO₂
2390 concentrations.

2391 These results also demonstrate that optimal resource investment to photo-
2392 synthetic capacity defines leaf acclimation responses to elevated CO₂, and that
2393 these responses were independent of fertilization or inoculation treatment. Cur-
2394 rent approaches for simulating photosynthetic responses to CO₂ generally invoke
2395 patterns expected from progressive nitrogen limitation, where the downregulation
2396 in N_{area} , and therefore photosynthetic capacity, due to elevated CO₂ are com-
2397 monly a function of progressive reductions in soil nitrogen availability. Results
2398 reported here contradict this formulation, suggesting that the leaf acclimation re-
2399 sponse is driven by optimal resource investment to photosynthetic capacity and
2400 is independent of soil resource supply. Optimality models that leverage prin-
2401 ciples from optimal coordination and photosynthetic least-cost theories (Wang
2402 et al. 2017; Stocker et al. 2020; Scott and Smith 2022) are capable of capturing
2403 such acclimation responses to CO₂ (Smith and Keenan 2020), suggesting that the
2404 implementation of these models may improve the simulation of photosynthetic
2405 processes in terrestrial biosphere models under increasing CO₂ concentrations.

2406 5.4.3 *Study limitations and future directions*

2407 There are two study limitations that must be addressed to contextualize
2408 patterns observed in this study. First, restricting the volume of belowground
2409 substrate via a potted experiment does not adequately replicate belowground en-
2410 vironments of natural systems, and therefore may modify effects of soil resource
2411 availability and inoculation on plant nitrogen uptake, particularly if pot size limits

2412 whole plant growth (Poorter et al. 2012). I attempted to minimize the extent of
2413 pot size limitation experienced in the first experimental chapters while account-
2414 ing for the expected stimulation in whole plant growth under elevated CO₂ by
2415 using 6-liter pots. Despite attempts to minimize growth limitation imposed by
2416 pot volume, fertilization and CO₂ treatments increased the biomass: pot volume
2417 ratio such that all treatment combinations to exceed 1 g L⁻¹ biomass: pot volume
2418 under high fertilization. The 1 g L⁻¹ biomass: pot volume recommendation from
2419 Poorter et al. (2012) was designated to avoid growth limitation imposed by pot
2420 volume. However, if pot size limitation indeed limited whole plant growth, then
2421 structural carbon costs to acquire nitrogen, belowground carbon biomass, whole
2422 plant nitrogen biomass, and whole plant biomass should each exhibit strong sat-
2423 uration points with increasing fertilization, which was not observed here. Addi-
2424 tionally, a second set of photosynthetic measurements from one week prior to the
2425 harvest (6 weeks post-germination) revealed ... As pot limitation is expected
2426 to decrease net photosynthesis, and focal leaves were of similar ages between the
2427 sixth and seventh week, one might expect growth limitation induced by constricted
2428 pot volume to result in a dampened effect of inoculation and fertilization on net
2429 photosynthesis, V_{cmax} , and J_{max25} . Analyses from the sixth week of development
2430 revealed ... Additionally, analyses revealed a stronger/weaker downregulation in
2431 V_{cmax25} and J_{max25} on week 7, though disentangling the causality of this response
2432 (i.e. whether due to pot size limitation or simply a stronger acclimation response)
2433 would be difficult.

2434 Second, this study evaluated leaf and whole plant responses to CO₂ in 7-
2435 week seedlings. Given the long-term scale of the progressive nitrogen limitation

2436 hypothesis, patterns observed here should be validated in longer-term nitrogen
2437 manipulation experiments. Previous work in free air CO₂ enrichment experiments
2438 show some support for patterns expected from the progressive nitrogen limitation
2439 hypothesis (Reich et al. 2006; Norby et al. 2010), although results are not consis-
2440 tent across experimental sites (Finzi et al. 2006; Moore et al. 2006; Liang et al.
2441 2016). We found some support for patterns expected by the progressive nitrogen
2442 limitation hypothesis, namely an increase in plant nitrogen uptake under elevated
2443 CO₂ (Luo et al. 2004), though leaf acclimation responses to CO₂ were strongly
2444 indicative of optimal resource investment to photosynthetic capacity as expected
2445 from photosynthetic least-cost theory (Prentice et al. 2014; Smith et al. 2019;
2446 Smith and Keenan 2020).

2447 5.4.4 *Conclusions*

2448 This study provides strong evidence suggesting that leaf acclimation re-
2449 sponds to elevated CO₂ did not vary with soil nitrogen fertilization or ability
2450 to acquire nitrogen through symbiotic nitrogen fixation. However, whole plant
2451 acclimation responses to CO₂ were dependent on fertilization, where increasing
2452 fertilization increased the positive effect of whole plant growth under elevated
2453 CO₂. Results also indicate that fertilization played a relatively more important
2454 role in modifying whole plant responses to CO₂, perhaps due to a reduction in
2455 nodulation across the fertilization gradient. These patterns strongly support the
2456 hypothesis that leaf and whole plant acclimation responses are driven by opti-
2457 mal resource investment to photosynthetic capacity, and that leaf acclimation
2458 responses to CO₂ were not modified by changes in soil nitrogen availability. Ad-

2459 ditionally, strong interactions between fertilization and inoculation on leaf and
2460 whole plant traits indicated positive effects of fertilization on leaf and whole plant
2461 traits in uninoculated pots, but null effects of fertilization on leaf and whole plant
2462 traits in inoculated pots. These results build on previous work suggesting that
2463 constant leaf nitrogen-photosynthesis relationships are dynamic and change across
2464 growing environments, calling the use of constant relationships by terrestrial bio-
2465 sphere models into question.

2466

Chapter 6

2467

Conclusions

2468 Experiments included in this dissertation leverage patterns expected from
2469 photosynthetic least-cost theory to investigate effects of soil resource availability
2470 and aboveground climate on costs of nitrogen acquisition, leaf nitrogen-water use
2471 tradeoffs, and plant acclimation responses to elevated CO₂. Photosynthetic least-
2472 cost theory provides a contemporary framework for understanding impacts of
2473 climatic and edaphic characteristics on plant ecophysiological processes, namely
2474 leaf nitrogen allocation and photosynthetic capacity. When I began planning
2475 experiments for this dissertation in August 2018,, empirical tests of the theory
2476 were sparse and model development was just beginning with a goal of eventually
2477 implementing the theory in terrestrial biosphere models. At the time, it was
2478 critical that experimentation be done to test underlying assumptions of the theory
2479 and validate its suitability for implementing in terrestrial biosphere models.

2480 Early iterations of model development held the unit cost of acquiring ni-
2481 trogen relative to water constant (Wang et al. 2017), in part because limited data
2482 existed to evaluate how this parameter changes across spatiotemporal scales and
2483 different environmental gradients. However, the Fixation and Uptake of Nitrogen
2484 model (Fisher et al. 2010; Brzostek et al. 2014) indicates that costs of nitro-
2485 gen acquisition decreased with increasing soil nitrogen availability and varies in
2486 species with different nitrogen acquisition strategies, suggesting that the unit cost
2487 of acquiring nitrogen relative to water should change across nitrogen availability
2488 gradients. Additionally,

2489 All experimental chapters in this dissertation provide strong and consist-
2490 ent support for patterns expected from the theory across different experimental
2491 approaches, spatiotemporal scales, and different plant functional groups. In this
2492 chapter, I first summarize experimental approaches and primary findings of each
2493 experimental chapter. Then, I use findings from the four experimental chapters
2494 to synthesize recommendations for future photosynthetic least-cost theory model
2495 development, and propose experiments that will allow for further understanding
2496 of mechanisms that drive patterns expected from photosynthetic least-cost theory
2497 across environmental gradients.

2498

References

- 2499 Abrams, M. D. and S. A. Mostoller (1995). Gas exchange, leaf structure and
2500 nitrogen in contrasting successional tree species growing in open and under-
2501 story sites during a drought. *Tree Physiology* 15(6), 361–370.
- 2502 Adams, M. A., T. L. Turnbull, J. I. Sprent, and N. Buchmann (2016). Legumes
2503 are different: Leaf nitrogen, photosynthesis, and water use efficiency. *Pro-
2504 ceedings of the National Academy of Sciences of the United States of Amer-
2505 ica* 113(15), 4098–4103.
- 2506 Ainsworth, E. A., P. A. Davey, C. J. Bernacchi, O. C. Dermody, E. A. Heaton,
2507 D. J. Moore, P. B. Morgan, S. L. Naidu, H. S. Y. Ra, X. G. Zhu, P. S. Curtis,
2508 and S. P. Long (2002). A meta-analysis of elevated [CO₂] effects on soybean
2509 (*Glycine max*) physiology, growth and yield. *Global Change Biology* 8(8),
2510 695–709.
- 2511 Ainsworth, E. A. and S. P. Long (2005). What have we learned from 15 years of
2512 free-air CO₂ enrichment (FACE)? A meta-analytic review of the responses
2513 of photosynthesis, canopy properties and plant production to rising CO₂.
2514 *New Phytologist* 165(2), 351–372.
- 2515 Ainsworth, E. A. and A. Rogers (2007). The response of photosynthesis and
2516 stomatal conductance to rising [CO₂]: mechanisms and environmental in-
2517 teractions. *Plant, Cell and Environment* 30(3), 258–270.
- 2518 Allen, K., J. B. Fisher, R. P. Phillips, J. S. Powers, and E. R. Brzostek (2020).
2519 Modeling the carbon cost of plant nitrogen and phosphorus uptake across
2520 temperate and tropical forests. *Frontiers in Forests and Global Change* 3,

- 2521 1–12.
- 2522 Allison, S. D., C. I. Czimczik, and K. K. Treseder (2008). Microbial activity
2523 and soil respiration under nitrogen addition in Alaskan boreal forest. *Global
2524 Change Biology* 14(5), 1156–1168.
- 2525 Andersen, M. K., H. Hauggaard-Nielsen, P. Ambus, and E. S. Jensen (2005).
2526 Biomass production, symbiotic nitrogen fixation and inorganic N use in dual
2527 and tri-component annual intercrops. *Plant and Soil* 266(1-2), 273–287.
- 2528 Andrews, M., E. K. James, J. I. Sprent, R. M. Boddey, E. Gross, and F. B. dos
2529 Reis (2011). Nitrogen fixation in legumes and actinorhizal plants in natural
2530 ecosystems: Values obtained using ^{15}N natural abundance. *Plant Ecology
2531 and Diversity* 4(2-3), 117–130.
- 2532 Arndal, M. F., A. Tolver, K. S. Larsen, C. Beier, and I. K. Schmidt (2018). Fine
2533 root growth and vertical distribution in response to elevated CO₂, warming
2534 and drought in a mixed heathland–grassland. *Ecosystems* 21(1), 15–30.
- 2535 Arnone, J. A. (1997). Indices of plant N availability in an alpine grassland under
2536 elevated atmospheric CO₂. *Plant and Soil* 190(1), 61–66.
- 2537 Arora, V. K., A. Katavouta, R. G. Williams, C. D. Jones, V. Brovkin,
2538 P. Friedlingstein, J. Schwinger, L. Bopp, O. Boucher, P. Cadule, M. A.
2539 Chamberlain, J. R. Christian, C. Delire, R. A. Fisher, T. Hajima, T. Ilyina,
2540 E. Joetzjer, M. Kawamiya, C. D. Koven, J. P. Krasting, R. M. Law, D. M.
2541 Lawrence, A. Lenton, K. Lindsay, J. Pongratz, T. Raddatz, R. Séférian,
2542 K. Tachiiri, J. F. Tjiputra, A. Wiltshire, T. Wu, and T. Ziehn (2020).
2543 Carbon-concentration and carbon-climate feedbacks in CMIP6 models and
2544 their comparison to CMIP5 models. *Biogeosciences* 17(16), 4173–4222.

- 2545 Bae, K., T. J. Fahey, R. D. Yanai, and M. Fisk (2015). Soil nitrogen availability affects belowground carbon allocation and soil respiration in northern
2546 hardwood forests of New Hampshire. *Ecosystems* 18(7), 1179–1191.
- 2547
- 2548 Barber, S. A. (1962). A diffusion and mass-flow concept of soil nutrient availability. *Soil Science* 93(1), 39–49.
- 2549
- 2550 Barnes, J. D., L. Balaguer, E. Manrique, S. Elvira, and A. W. Davison (1992).
2551 A reappraisal of the use of DMSO for the extraction and determination
2552 of chlorophylls a and b in lichens and higher plants. *Environmental and
2553 Experimental Botany* 32(2), 85–100.
- 2554 Bates, D., M. Mächler, B. Bolker, and S. Walker (2015). Fitting linear mixed-
2555 effects models using lme4. *Journal of Statistical Software* 67(1), 1–48.
- 2556 Beaudette, D., J. Skovlin, S. Roeker, and A. Brown (2022). soilDB: Soil
2557 Database Interface.
- 2558 Bengtson, P., J. Barker, and S. J. Grayston (2012). Evidence of a strong cou-
2559 pling between root exudation, C and N availability, and stimulated SOM
2560 decomposition caused by rhizosphere priming effects. *Ecology and Evolu-
2561 tion* 2(8), 1843–1852.
- 2562 Bernacchi, C. J., E. L. Singsaas, C. Pimentel, A. R. Portis, and S. P. Long
2563 (2001). Improved temperature response functions for models of Rubisco-
2564 limited photosynthesis. *Plant, Cell and Environment* 24(2), 253–259.
- 2565 Bialic-Murphy, L., N. G. Smith, P. Voothuluru, R. M. McElderry, M. D.
2566 Roche, S. T. Cassidy, S. N. Kivlin, and S. Kalisz (2021). Invasion-induced
2567 root–fungal disruptions alter plant water and nitrogen economies. *Ecology*

- 2568 *Letters* 24(6), 1145–1156.
- 2569 Bloom, A. J., F. S. Chapin, and H. A. Mooney (1985). Resource limitation
2570 in plants - an economic analogy. *Annual Review of Ecology and Systemat-*
2571 *ics* 16(1), 363–392.
- 2572 Bloomfield, K. J., B. D. Stocker, T. F. Keenan, and I. C. Prentice (2023).
2573 Environmental controls on the light use efficiency of terrestrial gross primary
2574 production. *Global Change Biology* 29(4), 0–2.
- 2575 Bonan, G. B., M. D. Hartman, W. J. Parton, and W. R. Wieder (2013). Eval-
2576 uating litter decomposition in earth system models with long-term litter
2577 bag experiments: an example using the Community Land Model version 4
2578 (CLM4). *Global Change Biology* 19(3), 957–974.
- 2579 Bonan, G. B., P. J. Lawrence, K. W. Oleson, S. Levis, M. Jung, M. Reich-
2580 stein, D. M. Lawrence, and S. C. Swenson (2011). Improving canopy pro-
2581 cesses in the Community Land Model version 4 (CLM4) using global flux
2582 fields empirically inferred from FLUXNET data. *Journal of Geophysical Re-*
2583 *search* 116(G2), G02014.
- 2584 Booth, B. B. B., C. D. Jones, M. Collins, I. J. Totterdell, P. M. Cox, S. Sitch,
2585 C. Huntingford, R. A. Betts, G. R. Harris, and J. Lloyd (2012). High sen-
2586 sitivity of future global warming to land carbon cycle processes. *Environ-*
2587 *mental Research Letters* 7(2), 024002.
- 2588 Borer, E. T., W. S. Harpole, P. B. Adler, E. M. Lind, J. L. Orrock, E. W.
2589 Seabloom, and M. D. Smith (2014). Finding generality in ecology: A model
2590 for globally distributed experiments. *Methods in Ecology and Evolution* 5(1),
2591 65–73.

- 2592** Braghieri, R. K., J. B. Fisher, K. Allen, E. Brzostek, M. Shi, X. Yang, D. M.
2593 Ricciuto, R. A. Fisher, Q. Zhu, and R. P. Phillips (2022). Modeling global
2594 carbon costs of plant nitrogen and phosphorus acquisition. *Journal of Ad-*
2595 *vances in Modeling Earth Systems* 14(8), 1–23.
- 2596** Brix, H. (1971). Effects of nitrogen fertilization on photosynthesis and respi-
2597 ration in Douglas-fir. *Forest Science* 17(4), 407–414.
- 2598** Brzostek, E. R., J. B. Fisher, and R. P. Phillips (2014). Modeling the carbon
2599 cost of plant nitrogen acquisition: Mycorrhizal trade-offs and multipath
2600 resistance uptake improve predictions of retranslocation. *Journal of Geo-*
2601 *physical Research: Biogeosciences* 119, 1684–1697.
- 2602** Bubier, J. L., R. Smith, S. Juutinen, T. R. Moore, R. Minocha, S. Long, and
2603 S. Minocha (2011). Effects of nutrient addition on leaf chemistry, morphol-
2604 ogy, and photosynthetic capacity of three bog shrubs. *Oecologia* 167(2),
2605 355–368.
- 2606** Cernusak, L. A., N. Ubierna, K. Winter, J. A. M. Holtum, J. D. Marshall, and
2607 G. D. Farquhar (2013). Environmental and physiological determinants of
2608 carbon isotope discrimination in terrestrial plants. *New Phytologist* 200(4),
2609 950–965.
- 2610** Chen, J.-L., J. F. Reynolds, P. C. Harley, and J. D. Tenhunen (1993). Coor-
2611 dination theory of leaf nitrogen distribution in a canopy. *Oecologia* 93(1),
2612 63–69.
- 2613** Clark, D. B., L. M. Mercado, S. Sitch, C. D. Jones, N. Gedney, M. J. Best,
2614 M. Pryor, G. G. Rooney, R. L. H. Essery, E. Blyth, O. Boucher, R. J.
2615 Harding, C. Huntingford, and P. M. Cox (2011). The Joint UK Land Envi-

- 2616** ronment Simulator (JULES), model description. Part 2: Carbon fluxes and
2617 vegetation dynamics. *Geoscientific Model Development* 4(3), 701–722.
- 2618** Cornwell, W. K., J. H. C. Cornelissen, K. Amatangelo, E. Dorrepaal, V. T.
2619 Eviner, O. Godoy, S. E. Hobbie, B. Hoorens, H. Kurokawa, N. Pérez-
2620 Harguindeguy, H. M. Quested, L. S. Santiago, D. A. Wardle, I. J. Wright,
2621 R. Aerts, S. D. Allison, P. van Bodegom, V. Brovkin, A. Chatain, T. V.
2622 Callaghan, S. Díaz, E. Garnier, D. E. Gurvich, E. Kazakou, J. A. Klein,
2623 J. Read, P. B. Reich, N. A. Soudzilovskaia, M. V. Vaieretti, and M. Westoby
2624 (2008). Plant species traits are the predominant control on litter decompo-
2625 sition rates within biomes worldwide. *Ecology Letters* 11(10), 1065–1071.
- 2626** Cornwell, W. K., I. J. Wright, J. Turner, V. Maire, M. M. Barbour, L. A.
2627 Cernusak, T. E. Dawson, D. S. Ellsworth, G. D. Farquhar, H. Griffiths,
2628 C. Keitel, A. Knohl, P. B. Reich, D. G. Williams, R. Bhaskar, J. H. C. Cor-
2629 nelissen, A. Richards, S. Schmidt, F. Valladares, C. Körner, E.-D. Schulze,
2630 N. Buchmann, and L. S. Santiago (2018). Climate and soils together regulate
2631 photosynthetic carbon isotope discrimination within C₃ plants worldwide.
2632 *Global Ecology and Biogeography* 27(9), 1056–1067.
- 2633** Cramer, W. and I. C. Prentice (1988). Simulation of regional soil moisture
2634 deficits on a European scale. *Norsk Geografisk Tidsskrift - Norwegian Jour-
2635 nal of Geography* 42(2-3), 149–151.
- 2636** Curtis, P. S. (1996). A meta-analysis of leaf gas exchange and nitrogen in trees
2637 grown under elevated carbon dioxide. *Plant, Cell and Environment* 19(2),
2638 127–137.
- 2639** Daly, C., M. Halbleib, J. I. Smith, W. P. Gibson, M. K. Doggett, G. H. Taylor,

- 2640** J. Curtis, and P. P. Pasteris (2008). Physiographically sensitive mapping
2641 of climatological temperature and precipitation across the conterminous
2642 United States. *International Journal of Climatology* 28(15), 2031–2064.
- 2643** Davies-Barnard, T., J. Meyerholt, S. Zaehle, P. Friedlingstein, V. Brovkin,
2644 Y. Fan, R. A. Fisher, C. D. Jones, H. Lee, D. Peano, B. Smith, D. Wårlind,
2645 and A. J. Wiltshire (2020). Nitrogen cycling in CMIP6 land surface models:
2646 progress and limitations. *Biogeosciences* 17(20), 5129–5148.
- 2647** Davis, T. W., I. C. Prentice, B. D. Stocker, R. T. Thomas, R. J. Whitley,
2648 H. Wang, B. J. Evans, A. V. Gallego-Sala, M. T. Sykes, and W. Cramer
2649 (2017). Simple process-led algorithms for simulating habitats (SPLASH
2650 v.1.0): robust indices of radiation, evapotranspiration and plant-available
2651 moisture. *Geoscientific Model Development* 10, 689–708.
- 2652** Delaire, M., E. Frak, M. Sigogne, B. Adam, F. Beaujard, and X. Le Roux
2653 (2005). Sudden increase in atmospheric CO₂ concentration reveals strong
2654 coupling between shoot carbon uptake and root nutrient uptake in young
2655 walnut trees. *Tree Physiology* 25(2), 229–235.
- 2656** Doane, T. A. and W. R. Horwáth (2003). Spectrophotometric determination of
2657 nitrate with a single reagent. *Analytical Letters* 36(12), 2713–2722.
- 2658** Dong, N., I. C. Prentice, B. J. Evans, S. Caddy-Retalic, A. J. Lowe, and I. J.
2659 Wright (2017). Leaf nitrogen from first principles: field evidence for adaptive
2660 variation with climate. *Biogeosciences* 14(2), 481–495.
- 2661** Dong, N., I. C. Prentice, I. J. Wright, B. J. Evans, H. F. Togashi, S. Caddy-
2662 Retalic, F. A. McInerney, B. Sparrow, E. Leitch, and A. J. Lowe (2020).
2663 Components of leaf-trait variation along environmental gradients. *New Phy-*

- 2664** *tologist* 228(1), 82–94.
- 2665** Dong, N., I. C. Prentice, I. J. Wright, H. Wang, O. K. Atkin, K. J. Bloomfield,
- 2666** T. F. Domingues, S. M. Gleason, V. Maire, Y. Onoda, H. Poorter, and N. G.
- 2667** Smith (2022). Leaf nitrogen from the perspective of optimal plant function.
- 2668** *Journal of Ecology* 110(11), 2585–2602.
- 2669** Dong, N., I. J. Wright, J. M. Chen, X. Luo, H. Wang, T. F. Keenan, N. G.
- 2670** Smith, and I. C. Prentice (2022). Rising CO₂ and warming reduce global
- 2671** canopy demand for nitrogen. *New Phytologist* 235(5), 1692–1700.
- 2672** Dovrat, G., H. Bakhshian, T. Masci, and E. Sheffer (2020). The nitrogen eco-
- 2673** nomic spectrum of legume stoichiometry and fixation strategy. *New Phytol-*
- 2674** *ogist* 227(2), 365–375.
- 2675** Dovrat, G., T. Masci, H. Bakhshian, E. Mayzlish Gati, S. Golan, and E. Shef-
- 2676** fer (2018). Drought-adapted plants dramatically downregulate dinitrogen
- 2677** fixation: Evidences from Mediterranean legume shrubs. *Journal of Ecol-*
- 2678** *ogy* 106(4), 1534–1544.
- 2679** Drake, B. G., M. A. Gonzàlez-Meler, and S. P. Long (1997). More efficient
- 2680** plants: a consequence of rising atmospheric CO₂? *Annual Review of Plant*
- 2681** *Biology* 48, 609–639.
- 2682** Duursma, R. A. (2015). Plantecophys - An R Package for Analyzing and Mod-
- 2683** elling Leaf Gas Exchange Data. *PLOS ONE* 10(11), e0143346.
- 2684** Eastman, B. A., M. B. Adams, E. R. Brzostek, M. B. Burnham, J. E. Carrara,
- 2685** C. Kelly, B. E. McNeil, C. A. Walter, and W. T. Peterjohn (2021). Altered
- 2686** plant carbon partitioning enhanced forest ecosystem carbon storage after 25

- 2687 years of nitrogen additions. *New Phytologist* 230(4), 1435–1448.
- 2688 Ellsworth, D. S. and P. B. Reich (1996). Photosynthesis and leaf nitrogen in five
- 2689 Amazonian tree species during early secondary succession. *Ecology* 77(2),
- 2690 581–594.
- 2691 Espelta, J. M., P. Cortés, M. Mangirón, and J. Retana (2005). Differences in
- 2692 biomass partitioning, leaf nitrogen content, and water use efficiency $\delta^{13}\text{C}$
- 2693 result in similar performance of seedlings of two Mediterranean oaks with
- 2694 contrasting leaf habit. *Ecoscience* 12(4), 447–454.
- 2695 Evans, J. R. (1989). Photosynthesis and nitrogen relationships in leaves of C_3
- 2696 plants. *Oecologia* 78(1), 9–19.
- 2697 Evans, J. R. and V. C. Clarke (2019). The nitrogen cost of photosynthesis.
- 2698 *Journal of Experimental Botany* 70(1), 7–15.
- 2699 Evans, J. R. and H. Poorter (2001). Photosynthetic acclimation of plants to
- 2700 growth irradiance: the relative importance of specific leaf area and nitrogen
- 2701 partitioning in maximizing carbon gain. *Plant, Cell and Environment* 24(8),
- 2702 755–767.
- 2703 Evans, J. R. and J. R. Seemann (1989). The allocation of protein nitrogen in
- 2704 the photosynthetic apparatus: costs, consequences, and control. *Photosyn-*
- 2705 *thesis* 8, 183–205.
- 2706 Exbrayat, J.-F., A. A. Bloom, P. Falloon, A. Ito, T. L. Smallman, and
- 2707 M. Williams (2018). Reliability ensemble averaging of 21st century projec-
- 2708 tions of terrestrial net primary productivity reduces global and regional
- 2709 uncertainties. *Earth System Dynamics* 9(1), 153–165.

- 2710 Farquhar, G. D., J. R. Ehleringer, and K. T. Hubick (1989). Carbon Isotope
2711 Discrimination and Photosynthesis. *Annual Review of Plant Physiology and*
2712 *Plant Molecular Biology* 40(1), 503–537.
- 2713 Farquhar, G. D. and T. D. Sharkey (1982). Stomatal conductance and photo-
2714 synthesis. *Annual Review of Plant Physiology* 33(1), 317–345.
- 2715 Farquhar, G. D., S. von Caemmerer, and J. A. Berry (1980). A biochemical
2716 model of photosynthetic CO₂ assimilation in leaves of C₃ species.
2717 *Planta* 149(1), 78–90.
- 2718 Fay, P. A., S. M. Prober, W. S. Harpole, J. M. H. Knops, J. D. Bakker, E. T.
2719 Borer, E. M. Lind, A. S. MacDougall, E. W. Seabloom, P. D. Wragg, P. B.
2720 Adler, D. M. Blumenthal, Y. M. Buckley, C. Chu, E. E. Cleland, S. L.
2721 Collins, K. F. Davies, G. Du, X. Feng, J. Firn, D. S. Gruner, N. Hagenah,
2722 Y. Hautier, R. W. Heckman, V. L. Jin, K. P. Kirkman, J. A. Klein, L. M.
2723 Ladwig, Q. Li, R. L. McCulley, B. A. Melbourne, C. E. Mitchell, J. L. Moore,
2724 J. W. Morgan, A. C. Risch, M. Schütz, C. J. Stevens, D. A. Wedin, and
2725 L. H. Yang (2015). Grassland productivity limited by multiple nutrients.
2726 *Nature Plants* 1(7), 15080.
- 2727 Feng, X. (1999). Trends in intrinsic water-use efficiency of natural trees for the
2728 past 100-200 years: A response to atmospheric CO₂ concentration. *Geochim-
2729 ica et Cosmochimica Acta* 63(13-14), 1891–1903.
- 2730 Field, C. B. and H. A. Mooney (1986). The photosynthesis-nitrogen relationship
2731 in wild plants. In T. J. Givnish (Ed.), *On the Economy of Plant Form and*
2732 *Function*, pp. 25–55. Cambridge: Cambridge University Press.
- 2733 Finzi, A. C., D. J. P. Moore, E. H. DeLucia, J. Lichter, K. S. Hofmockel, R. B.

- 2734** Jackson, H. S. Kim, R. Matamala, H. R. McCarthy, R. Oren, J. S. Pippen,
2735 and W. H. Schlesinger (2006). Progressive nitrogen limitation of ecosystem
2736 processes under elevated CO₂ in a warm-temperate forest. *Ecology* 87(1),
2737 15–25.
- 2738** Firn, J., J. M. McGree, E. Harvey, H. Flores Moreno, M. Schutz, Y. M. Buckley,
2739 E. T. Borer, E. W. Seabloom, K. J. La Pierre, A. M. MacDougall, S. M.
2740 Prober, C. J. Stevens, L. L. Sullivan, E. Porter, E. Ladouceur, C. Allen,
2741 K. H. Moromizato, J. W. Morgan, W. S. Harpole, Y. Hautier, N. Eisen-
2742 hauer, J. P. Wright, P. B. Adler, C. A. Arnillas, J. D. Bakker, L. Biederman,
2743 A. A. D. Broadbent, C. S. Brown, M. N. Bugalho, M. C. Caldeira, E. E. Cle-
2744 land, A. Ebeling, P. A. Fay, N. Hagenah, A. R. Kleinhesselink, R. Mitchell,
2745 J. L. Moore, C. Nogueira, P. L. Peri, C. Roscher, M. D. Smith, P. D. Wragg,
2746 and A. C. Risch (2019). Leaf nutrients, not specific leaf area, are consistent
2747 indicators of elevated nutrient inputs. *Nature Ecology and Evolution* 3(3),
2748 400–406.
- 2749** Fisher, J. B., S. Sitch, Y. Malhi, R. A. Fisher, C. Huntingford, and S.-Y. Tan
2750 (2010). Carbon cost of plant nitrogen acquisition: A mechanistic, globally
2751 applicable model of plant nitrogen uptake, retranslocation, and fixation.
2752 *Global Biogeochemical Cycles* 24(1), 1–17.
- 2753** Fox, J. and S. Weisberg (2019). *An R companion to applied regression* (Third
2754 edit ed.). Thousand Oaks, California: Sage.
- 2755** Franklin, O., R. E. McMurtrie, C. M. Iversen, K. Y. Crous, A. C. Finzi, D. Tis-
2756 sue, D. S. Ellsworth, R. Oren, and R. J. Norby (2009). Forest fine-root
2757 production and nitrogen use under elevated CO₂: contrasting responses

- 2758 in evergreen and deciduous trees explained by a common principle. *Global*
2759 *Change Biology* 15(1), 132–144.
- 2760 Friedlingstein, P., M. Meinshausen, V. K. Arora, C. D. Jones, A. Anav, S. K.
2761 Liddicoat, and R. Knutti (2014). Uncertainties in CMIP5 climate projections
2762 due to carbon cycle feedbacks. *Journal of Climate* 27(2), 511–526.
- 2763 Friel, C. A. and M. L. Friesen (2019). Legumes modulate allocation to rhizobial
2764 nitrogen fixation in response to factorial light and nitrogen manipulation.
2765 *Frontiers in Plant Science* 10, 1316.
- 2766 Fujikake, H., A. Yamazaki, N. Ohtake, K. Sueoshi, S. Matsuhashi, T. Ito,
2767 C. Mizuniwa, T. Kume, S. Hoshimoto, N.-S. Ishioka, S. Watanabe, A. Osa,
2768 T. Sekine, H. Uchida, A. Tsuji, and T. Ohyama (2003). Quick and reversible
2769 inhibition of soybean root nodule growth by nitrate involves a decrease in
2770 sucrose supply to nodules. *Journal of Experimental Botany* 54(386), 1379–
2771 1388.
- 2772 Ghimire, B., W. J. Riley, C. D. Koven, J. Kattge, A. Rogers, P. B. Reich, and
2773 I. J. Wright (2017). A global trait-based approach to estimate leaf nitro-
2774 gen functional allocation from observations:. *Ecological Applications* 27(5),
2775 1421–1434.
- 2776 Giardina, C. P., M. D. Coleman, J. E. Hancock, J. S. King, E. A. Lilleskov,
2777 W. M. Loya, K. S. Pregitzer, M. G. Ryan, and C. C. Trettin (2005). The
2778 response of belowground carbon allocation in forests to global change. In
2779 D. Binkley and O. Manyailo (Eds.), *Tree Species Effects on Soils: Implica-*
2780 *tions for Global Change* (Volume 55 ed.), Chapter Chapter 7, pp. 119–154.
2781 Berlin/Heidelberg: Springer-Verlag.

- 2782 Gibson, A. H. and J. E. Harper (1985). Nitrate effect on nodulation of soybean
2783 by *Bradyrhizobium japonicum*. *Crop Science* 25(3), 497–501.
- 2784 Gill, A. L. and A. C. Finzi (2016). Belowground carbon flux links biogeochemical
2785 cycles and resource-use efficiency at the global scale. *Ecology Letters* 19(12),
2786 1419–1428.
- 2787 Goll, D. S., V. Brovkin, B. R. Parida, C. H. Reick, J. Kattge, P. B. Reich, P. M.
2788 van Bodegom, and Ü. Niinemets (2012). Nutrient limitation reduces land
2789 carbon uptake in simulations with a model of combined carbon, nitrogen
2790 and phosphorus cycling. *Biogeosciences Discussions* 9(3), 3173–3232.
- 2791 Gregory, L. M., A. M. McClain, D. M. Kramer, J. D. Pardo, K. E. Smith, O. L.
2792 Tessmer, B. J. Walker, L. G. Ziccardi, and T. D. Sharkey (2021, oct). The
2793 triose phosphate utilization limitation of photosynthetic rate: Out of global
2794 models but important for leaf models. *Plant, Cell and Environment* 44(10),
2795 3223–3226.
- 2796 Grossiord, C., T. N. Buckley, L. A. Cernusak, K. A. Novick, B. Poulter, R. T. W.
2797 Siegwolf, J. S. Sperry, and N. G. McDowell (2020). Plant responses to rising
2798 vapor pressure deficit. *New Phytologist* 226(6), 1550–1566.
- 2799 Guerrieri, R., M. Mencuccini, L. J. Sheppard, M. Saurer, M. P. Perks, P. Levy,
2800 M. A. Sutton, M. Borghetti, and J. Grace (2011). The legacy of enhanced
2801 N and S deposition as revealed by the combined analysis of $\delta^{13}\text{C}$, $\delta^{18}\text{O}$ and
2802 $\delta^{15}\text{N}$ in tree rings. *Global Change Biology* 17(5), 1946–1962.
- 2803 Gulmon, S. L. and C. C. Chu (1981). The effects of light and nitrogen on pho-
2804 tosynthesis, leaf characteristics, and dry matter allocation in the chaparral
2805 shrub, <i>Diplacus aurantiacus</i>. *Oecologia* 49(2), 207–212.

- 2806 Gutschick, V. P. (1981). Evolved strategies in nitrogen acquisition by plants.
- 2807 *The American Naturalist* 118(5), 607–637.
- 2808 Hallik, L., Ü. Niinemets, and I. J. Wright (2009). Are species shade and drought
- 2809 tolerance reflected in leaf-level structural and functional differentiation in
- 2810 Northern Hemisphere temperate woody flora? *New Phytologist* 184(1), 257–
- 2811 274.
- 2812 Harrison, M. T., E. J. Edwards, G. D. Farquhar, A. B. Nicotra, and J. R.
- 2813 Evans (2009). Nitrogen in cell walls of sclerophyllous leaves accounts for
- 2814 little of the variation in photosynthetic nitrogen-use efficiency. *Plant, Cell*
- 2815 and *Environment* 32(3), 259–270.
- 2816 Harrison, S. P., W. Cramer, O. Franklin, I. C. Prentice, H. Wang,
- 2817 Å. Bränström, H. de Boer, U. Dieckmann, J. Joshi, T. F. Keenan,
- 2818 A. Lavergne, S. Manzoni, G. Mengoli, C. Morfopoulos, J. Peñuelas,
- 2819 S. Pietsch, K. T. Rebel, Y. Ryu, N. G. Smith, B. D. Stocker, and I. J.
- 2820 Wright (2021). Eco-evolutionary optimality as a means to improve vegeta-
- 2821 tion and land-surface models. *New Phytologist* 231(6), 2125–2141.
- 2822 Henneron, L., P. Kardol, D. A. Wardle, C. Cros, and S. Fontaine (2020). Rhizo-
- 2823 sphere control of soil nitrogen cycling: a key component of plant economic
- 2824 strategies. *New Phytologist* 228(4), 1269–1282.
- 2825 Hijmans, R. J. (2022). terra: Spatial Data Analysis.
- 2826 Hikosaka, K. and A. Shigeno (2009). The role of Rubisco and cell walls in the
- 2827 interspecific variation in photosynthetic capacity. *Oecologia* 160(3), 443–
- 2828 451.

- 2829 Hoagland, D. R. and D. I. Arnon (1950). The water culture method for growing
2830 plants without soil. *California Agricultural Experiment Station: 347* 347(2),
2831 1–32.
- 2832 Hobbie, E. A. (2006). Carbon allocation to ectomycorrhizal fungi correlates
2833 with belowground allocation in culture studies. *Ecology* 87(3), 563–569.
- 2834 Hobbie, E. A. and J. E. Hobbie (2008). Natural abundance of ^{15}N in nitrogen-
2835 limited forests and tundra can estimate nitrogen cycling through mycorrhizal
2836 fungi: a review. *Ecosystems* 11(5), 815–830.
- 2837 Hoek, T. A., K. Axelrod, T. Biancalani, E. A. Yurtsev, J. Liu, and J. Gore
2838 (2016). Resource availability modulates the cooperative and competitive na-
2839 ture of a microbial cross-feeding mutualism. *PLOS Biology* 14(8), e1002540.
- 2840 Höglberg, M. N., M. J. I. Briones, S. G. Keel, D. B. Metcalfe, C. Campbell, A. J.
2841 Midwood, B. Thornton, V. Hurry, S. Linder, T. Näsholm, and P. Höglberg
2842 (2010). Quantification of effects of season and nitrogen supply on tree below-
2843 ground carbon transfer to ectomycorrhizal fungi and other soil organisms in
2844 a boreal pine forest. *New Phytologist* 187(2), 485–493.
- 2845 Höglberg, P., M. N. Höglberg, S. G. Göttlicher, N. R. Betson, S. G. Keel, D. B.
2846 Metcalfe, C. Campbell, A. Schindlbacher, V. Hurry, T. Lundmark, S. Linder,
2847 and T. Näsholm (2008). High temporal resolution tracing of photosynthate
2848 carbon from the tree canopy to forest soil microorganisms. *New Phytolo-*
2849 *gist* 177(1), 220–228.
- 2850 Houlton, B. Z., Y.-P. Wang, P. M. Vitousek, and C. B. Field (2008). A uni-
2851 fying framework for dinitrogen fixation in the terrestrial biosphere. *Na-*
2852 *ture* 454(7202), 327–330.

- 2853 Huber, M. L., R. A. Perkins, A. Laesecke, D. G. Friend, J. V. Sengers, M. J.
- 2854 Assael, I. N. Metaxa, E. Vogel, R. Mareš, and K. Miyagawa (2009). New
- 2855 international formulation for the viscosity of H₂O. *Journal of Physical and*
- 2856 *Chemical Reference Data* 38(2), 101–125.
- 2857 Hungate, B. A., J. S. Dukes, M. R. Shaw, Y. Luo, and C. B. Field (2003).
- 2858 Nitrogen and climate change. *Science* 302(5650), 1512–1513.
- 2859 IPCC (2021). *Climate Change 2021: The Physical Science Basis. Contribution*
- 2860 *of Working Group I to the Sixth Assessment Report of the Intergovernmental*
- 2861 *Panel on Climate Change*, Volume In Press. Cambridge, United Kingdom
- 2862 and New York, NY, USA: Cambridge University Press.
- 2863 Johnson, N. C., J. H. Graham, and F. A. Smith (1997). Functioning of mycor-
- 2864 rhizal associations along the mutualism-parasitism continuum. *New Phytol-*
- 2865 *ogist* 135(4), 575–585.
- 2866 Kachurina, O. M., H. Zhang, W. R. Raun, and E. G. Krenzer (2000). Simul-
- 2867 taneous determination of soil aluminum, ammonium- and nitrate- nitrogen
- 2868 using 1 M potassium chloride. *Communications in Soil Science and Plant*
- 2869 *Analysis* 31(7-8), 893–903.
- 2870 Kaiser, C., M. R. Kilburn, P. L. Clode, L. Fuchslueger, M. Koranda, J. B. Cliff,
- 2871 Z. M. Solaiman, and D. V. Murphy (2015). Exploring the transfer of recent
- 2872 plant photosynthates to soil microbes: mycorrhizal pathway vs direct root
- 2873 exudation. *New Phytologist* 205(4), 1537–1551.
- 2874 Katabuchi, M. (2015). LeafArea: An R package for rapid digital analysis of leaf
- 2875 area. *Ecological Research* 30(6), 1073–1077.

- 2876** Kattge, J. and W. Knorr (2007). Temperature acclimation in a biochemical
2877 model of photosynthesis: a reanalysis of data from 36 species. *Plant, Cell*
2878 and *Environment* 30(9), 1176–1190.
- 2879** Kattge, J., W. Knorr, T. Raddatz, and C. Wirth (2009). Quantifying photosyn-
2880 thetic capacity and its relationship to leaf nitrogen content for global-scale
2881 terrestrial biosphere models. *Global Change Biology* 15(4), 976–991.
- 2882** Kayler, Z., A. Gessler, and N. Buchmann (2010). What is the speed of link
2883 between aboveground and belowground processes? *New Phytologist* 187(4),
2884 885–888.
- 2885** Kayler, Z., C. Keitel, K. Jansen, and A. Gessler (2017). Experimental evi-
2886 dence of two mechanisms coupling leaf-level C assimilation to rhizosphere
2887 CO₂ release. *Environmental and Experimental Botany* 135,
2888 21–26.
- 2889** Keeling, C. D., W. G. Mook, and P. P. Tans (1979, jan). Recent trends in the
2890 ¹³C/¹²C ratio of atmospheric carbon dioxide.
2891 *Nature* 277(5692), 121–123.
- 2892** Kenward, M. G. and J. H. Roger (1997). Small sample inference for fixed effects
2893 from restricted maximum likelihood. *Biometrics* 53(3), 983.
- 2894** Knapp, A. K., M. L. Avolio, C. Beier, C. J. W. Carroll, S. L. Collins, J. S.
2895 Dukes, L. H. Fraser, R. J. Griffin-Nolan, D. L. Hoover, A. Jentsch, M. E.
2896 Loik, R. P. Phillips, A. K. Post, O. E. Sala, I. J. Slette, L. Yahdjian, and
2897 M. D. Smith (2017). Pushing precipitation to the extremes in distributed
2898 experiments: recommendations for simulating wet and dry years. *Global*
2899 *Change Biology* 23(5), 1774–1782.

- 2900 Knorr, W. (2000). Annual and interannual CO₂ exchanges of the
2901 terrestrial biosphere: process-based simulations and uncertainties. *Global*
2902 *Ecology and Biogeography* 9(3), 225–252.
- 2903 Knorr, W. and M. Heimann (2001). Uncertainties in global terrestrial biosphere
2904 modeling: 1. A comprehensive sensitivity analysis with a new photosynthesis
2905 and energy balance scheme. *Global Biogeochemical Cycles* 15(1), 207–225.
- 2906 Kulmatiski, A., P. B. Adler, J. M. Stark, and A. T. Tredennick (2017). Water
2907 and nitrogen uptake are better associated with resource availability than
2908 root biomass. *Ecosphere* 8(3), e01738.
- 2909 Lavergne, A., D. Sandoval, V. J. Hare, H. Graven, and I. C. Prentice (2020).
2910 Impacts of soil water stress on the acclimated stomatal limitation of pho-
2911 tosynthesis: Insights from stable carbon isotope data. *Global Change Biol-*
2912 *ogy* 26(12), 7158–7172.
- 2913 Lawrence, D. M., R. A. Fisher, C. D. Koven, K. W. Oleson, S. C. Swen-
2914 son, G. B. Bonan, N. Collier, B. Ghimire, L. Kampenhout, D. Kennedy,
2915 E. Kluzek, P. J. Lawrence, F. Li, H. Li, D. L. Lombardozzi, W. J. Riley,
2916 W. J. Sacks, M. Shi, M. Vertenstein, W. R. Wieder, C. Xu, A. A. Ali,
2917 A. M. Badger, G. Bisht, M. Broeke, M. A. Brunke, S. P. Burns, J. Buzan,
2918 M. Clark, A. Craig, K. M. Dahlin, B. Drewniak, J. B. Fisher, M. Flanner,
2919 A. M. Fox, P. Gentine, F. M. Hoffman, G. Keppel-Aleks, R. Knox, S. Ku-
2920 mar, J. Lenaerts, L. R. Leung, W. H. Lipscomb, Y. Lu, A. Pandey, J. D.
2921 Pelletier, J. Perket, J. T. Randerson, D. M. Ricciuto, B. M. Sanderson,
2922 A. Slater, Z. M. Subin, J. Tang, R. Q. Thomas, M. Val Martin, and X. Zeng
2923 (2019). The Community Land Model Version 5: description of new features,

- 2924 benchmarking, and impact of forcing uncertainty. *Journal of Advances in*
2925 *Modeling Earth Systems* 11(12), 4245–4287.
- 2926 LeBauer, D. S. and K. K. Treseder (2008). Nitrogen limitation of net primary
2927 productivity. *Ecology* 89(2), 371–379.
- 2928 Lefcheck, J. S. (2016). piecewiseSEM: Piecewise structural equation modelling
2929 in r for ecology, evolution, and systematics. *Methods in Ecology and Evolu-*
2930 *tion* 7(5), 573–579.
- 2931 Lenth, R. (2019). emmeans: estimated marginal means, aka least-squares
2932 means.
- 2933 Li, W., H. Zhang, G. Huang, R. Liu, H. Wu, C. Zhao, and N. G. McDowell
2934 (2020). Effects of nitrogen enrichment on tree carbon allocation: A global
2935 synthesis. *Global Ecology and Biogeography* 29(3), 573–589.
- 2936 Liang, J., X. Qi, L. Souza, and Y. Luo (2016). Processes regulating progressive
2937 nitrogen limitation under elevated carbon dioxide: a meta-analysis. *Biogeo-*
2938 *sciences* 13(9), 2689–2699.
- 2939 Liang, X., T. Zhang, X. Lu, D. S. Ellsworth, H. BassiriRad, C. You, D. Wang,
2940 P. He, Q. Deng, H. Liu, J. Mo, and Q. Ye (2020). Global response patterns of
2941 plant photosynthesis to nitrogen addition: A meta-analysis. *Global Change*
2942 *Biology* 26(6), 3585–3600.
- 2943 Lu, J., J. Yang, C. Keitel, L. Yin, P. Wang, W. Cheng, and F. A. Dijkstra
2944 (2022). Belowground Carbon Efficiency for Nitrogen and Phosphorus Ac-
2945 quisition Varies Between *Lolium perenne* and *Trifolium repens* and Depends
2946 on Phosphorus Fertilization. *Frontiers in Plant Science* 13, 1–9.

- 2947** Luo, X., T. F. Keenan, J. M. Chen, H. Croft, I. C. Prentice, N. G. Smith,
2948 A. P. Walker, H. Wang, R. Wang, C. Xu, and Y. Zhang (2021). Global
2949 variation in the fraction of leaf nitrogen allocated to photosynthesis. *Nature*
2950 *Communications* 12(1), 4866.
- 2951** Luo, Y., W. S. Currie, J. S. Dukes, A. C. Finzi, U. A. Hartwig, B. A. Hungate,
2952 R. E. McMurtrie, R. Oren, W. J. Parton, D. E. Pataki, R. M. Shaw, D. R.
2953 Zak, and C. B. Field (2004). Progressive nitrogen limitation of ecosystem
2954 responses to rising atmospheric carbon dioxide. *BioScience* 54(8), 731–739.
- 2955** Maire, V., P. Martre, J. Kattge, F. Gastal, G. Esser, S. Fontaine, and J.-F.
2956 Soussana (2012). The coordination of leaf photosynthesis links C and N
2957 fluxes in C₃ plant species. *PLoS ONE* 7(6), e38345.
- 2958** Makino, A. (2003). Rubisco and nitrogen relationships in rice: leaf photosyn-
2959 thesis and plant growth. *Soil Science and Plant Nutrition* 49(3), 319–327.
- 2960** Makino, A., M. Harada, T. Sato, H. Nakano, and T. Mae (1997). Growth and N
2961 Allocation in Rice Plants under CO₂ Enrichment. *Plant Physiology* 115(1),
2962 199–203.
- 2963** Markham, J. H. and C. Zekveld (2007). Nitrogen fixation makes biomass al-
2964 location to roots independent of soil nitrogen supply. *Canadian Journal of*
2965 *Botany* (9), 787–793.
- 2966** Marschner, H. and B. Dell (1994). Nutrient uptake in mycorrhizal symbiosis.
2967 *Plant and Soil* 159(1), 89–102.
- 2968** Matamala, R. and W. H. Schlesinger (2000). Effects of elevated atmospheric
2969 CO₂ on fine root production and activity in an intact tem-

- 2970** perate forest ecosystem. *Global Change Biology* 6(8), 967–979.
- 2971** Medlyn, B. E., E. Dreyer, D. S. Ellsworth, M. Forstreuter, P. C. Harley,
- 2972** M. U. F. Kirschbaum, X. Le Roux, P. Montpied, J. Strassmeyer, A. Wal-
- 2973** croft, K. Wang, and D. Loustau (2002). Temperature response of parameters
- 2974** of a biochemically based model of photosynthesis. II. A review of experimen-
- 2975** tal data. *Plant, Cell and Environment* 25(9), 1167–1179.
- 2976** Menge, D. N. L., S. A. Levin, and L. O. Hedin (2008). Evolutionary tradeoffs can
- 2977** select against nitrogen fixation and thereby maintain nitrogen limitation.
- 2978** *Proceedings of the National Academy of Sciences* 105(5), 1573–1578.
- 2979** Menne, M. J., I. Durre, R. S. Vose, B. E. Gleason, and T. G. Houston (2012).
- 2980** An overview of the global historical climatology network-daily database.
- 2981** *Journal of Atmospheric and Oceanic Technology* 29(7), 897–910.
- 2982** Meyerholt, J., K. Sickel, and S. Zaehle (2020). Ensemble projections elucidate
- 2983** effects of uncertainty in terrestrial nitrogen limitation on future carbon up-
- 2984** take. *Global Change Biology* 26(7), 3978–3996.
- 2985** Meyerholt, J., S. Zaehle, and M. J. Smith (2016). Variability of pro-
- 2986** jected terrestrial biosphere responses to elevated levels of atmospheric
- 2987** CO₂ due to uncertainty in biological nitrogen fixation. *Bio-*
- 2988** *geosciences* 13(5), 1491–1518.
- 2989** Minochka, R., S. Long, A. H. Magill, J. D. Aber, and W. H. McDowell (2000).
- 2990** Foliar free polyamine and inorganic ion content in relation to soil and soil
- 2991** solution chemistry in two fertilized forest stands at the Harvard Forest,
- 2992** Massachusetts. *Plant and Soil* 222(1-2), 119–137.

- 2993** Moore, D. J., S. Aref, R. M. Ho, J. S. Pippen, J. G. Hamilton, and E. H. De Lucia (2006). Annual basal area increment and growth duration of *Pinus taeda* in response to eight years of free-air carbon dioxide enrichment. *Global Change Biology* 12(8), 1367–1377.
- 2997** Morgan, J. A., D. E. Pataki, C. Körner, H. Clark, S. J. Del Grosso, J. M. Grünzweig, A. K. Knapp, A. R. Mosier, P. C. D. Newton, P. A. Niklaus, J. B. Nippert, R. S. Nowak, W. J. Parton, H. W. Polley, and M. R. Shaw (2004). Water relations in grassland and desert ecosystems exposed to elevated atmospheric CO₂. *Oecologia* 140(1), 11–25.
- 3002** Muñoz, N., X. Qi, M. W. Li, M. Xie, Y. Gao, M. Y. Cheung, F. L. Wong, and H.-M. Lam (2016). Improvement in nitrogen fixation capacity could be part of the domestication process in soybean. *Heredity* 117(2), 84–93.
- 3005** Nadelhoffer, K. J. and J. W. Raich (1992). Fine root production estimates and belowground carbon allocation in forest ecosystems. *Ecology* 73(4), 1139–1147.
- 3008** Niinemets, Ü. and J. D. Tenhunen (1997). A model separating leaf structural and physiological effects on carbon gain along light gradients for the shade-tolerant species <i>Acer saccharum</i>. *Plant, Cell and Environment* 20(7), 845–866.
- 3012** Norby, R. J., J. Ledford, C. D. Reilly, N. E. Miller, and E. G. O'Neill (2004). Fine-root production dominates response of a deciduous forest to atmospheric CO₂ enrichment. *Proceedings of the National Academy of Sciences* 101(26), 9689–9693.
- 3016** Norby, R. J., J. M. Warren, C. M. Iversen, B. E. Medlyn, and R. E. Mc-

- 3017** Murtrie (2010). CO₂ enhancement of forest productivity constrained by
3018 limited nitrogen availability. *Proceedings of the National Academy of Sci-
3019 ences* 107(45), 19368–19373.
- 3020** Novick, K. A., D. L. Ficklin, P. C. Stoy, C. A. Williams, G. Bohrer, A. C.
3021 Oishi, S. A. Papuga, P. D. Blanken, A. Noormets, B. N. Sulman, R. L.
3022 Scott, L. Wang, and R. P. Phillips (2016). The increasing importance of
3023 atmospheric demand for ecosystem water and carbon fluxes. *Nature Climate
Change* 6(11), 1023–1027.
- 3025** Noyce, G. L., M. L. Kirwan, R. L. Rich, and J. P. Megonigal (2019). Asyn-
3026 chronous nitrogen supply and demand produce nonlinear plant allocation
3027 responses to warming and elevated CO₂. *Proceedings of the
National Academy of Sciences* 116(43), 21623–21628.
- 3029** Onoda, Y., K. Hikosaka, and T. Hirose (2004). Allocation of nitrogen to
3030 cell walls decreases photosynthetic nitrogen-use efficiency. *Functional Ecol-
ogy* 18(3), 419–425.
- 3032** Onoda, Y., I. J. Wright, J. R. Evans, K. Hikosaka, K. Kitajima, Ü. Niinemets,
3033 H. Poorter, T. Tosens, and M. Westoby (2017). Physiological and structural
3034 trade-offs underlying the leaf economics spectrum. *New Phytologist* 214(4),
3035 1447–1463.
- 3036** Oreskes, N., K. Shrader-Frechette, and K. Belitz (1994). Verification, vali-
3037 dation, and confirmation of numerical models in the Earth sciences. *Sci-
ence* 263(5147), 641–646.
- 3039** Paillassa, J., I. J. Wright, I. C. Prentice, S. Pepin, N. G. Smith, G. Ethier,
3040 A. C. Westerband, L. J. Lamarque, H. Wang, W. K. Cornwell, and V. Maire

- 3041 (2020). When and where soil is important to modify the carbon and water
3042 economy of leaves. *New Phytologist* 228(1), 121–135.
- 3043 Parvin, S., S. Uddin, S. Tausz Posch, R. Armstrong, and M. Tausz (2020). Car-
3044 bon sink strength of nodules but not other organs modulates photosynthesis
3045 of faba bean (*i>Vicia faba</i>)) grown under elevated [CO₂] and different
3046 water supply. *New Phytologist* 227(1), 132–145.*
- 3047 Peng, Y., K. J. Bloomfield, L. A. Cernusak, T. F. Domingues, and I. C. Pren-
3048 tice (2021). Global climate and nutrient controls of photosynthetic capacity.
3049 *Communications Biology* 4(1), 462.
- 3050 Perkowski, E. A., E. F. Waring, and N. G. Smith (2021). Root mass carbon
3051 costs to acquire nitrogen are determined by nitrogen and light availabil-
3052 ity in two species with different nitrogen acquisition strategies. *Journal of*
3053 *Experimental Botany* 72(15), 5766–5776.
- 3054 Phillips, R. P., E. R. Brzostek, and M. G. Midgley (2013). The mycorrhizal-
3055 associated nutrient economy: a new framework for predicting carbon-
3056 nutrient couplings in temperate forests. *New Phytologist* 199(1), 41–51.
- 3057 Phillips, R. P., A. C. Finzi, and E. S. Bernhardt (2011). Enhanced root ex-
3058 udation induces microbial feedbacks to N cycling in a pine forest under
3059 long-term CO₂ fumigation. *Ecology Letters* 14(2), 187–194.
- 3060 Pinheiro, J. and D. Bates (2022). nlme: linear and nonlinear mixed effects
3061 models.
- 3062 Poggio, L., L. M. De Sousa, N. H. Batjes, G. B. M. Heuvelink, B. Kempen,
3063 E. Ribeiro, and D. Rossiter (2021). SoilGrids 2.0: Producing soil information

- 3064 for the globe with quantified spatial uncertainty. *Soil* 7(1), 217–240.
- 3065 Pons, T. L. and R. W. Pearcy (1994). Nitrogen reallocation and photosynthetic
- 3066 acclimation in response to partial shading in soybean plants. *Physiologia*
- 3067 *Plantarum* 92(4), 636–644.
- 3068 Poorter, H., J. Bühler, D. Van Dusschoten, J. Climent, and J. A. Postma (2012).
- 3069 Pot size matters: A meta-analysis of the effects of rooting volume on plant
- 3070 growth. *Functional Plant Biology* 39(11), 839–850.
- 3071 Poorter, H., O. Knopf, I. J. Wright, A. A. Temme, S. W. Hogewoning, A. Graf,
- 3072 L. A. Cernusak, and T. L. Pons (2022). A meta-analysis of responses of C₃
- 3073 plants to atmospheric CO₂: dose–response curves for 85 traits ranging from
- 3074 the molecular to the whole-plant level. *New Phytologist* 233(4), 1560–1596.
- 3075 Prentice, I. C., N. Dong, S. M. Gleason, V. Maire, and I. J. Wright (2014).
- 3076 Balancing the costs of carbon gain and water transport: testing a new theo-
- 3077 retical framework for plant functional ecology. *Ecology Letters* 17(1), 82–91.
- 3078 Prentice, I. C., X. Liang, B. E. Medlyn, and Y.-P. Wang (2015). Reliable, ro-
- 3079 bust and realistic: The three R's of next-generation land-surface modelling.
- 3080 *Atmospheric Chemistry and Physics* 15, 5987–6005.
- 3081 Priestley, C. H. B. and R. J. Taylor (1972). On the Assessment of Surface
- 3082 Heat Flux and Evaporation Using Large-Scale Parameters. *Monthly Weather*
- 3083 *Review* 100(2), 81–92.
- 3084 Querejeta, J. I., I. Prieto, C. Armas, F. Casanoves, J. S. Diémé, M. Diouf,
- 3085 H. Yossi, B. Kaya, F. I. Pugnaire, and G. M. Rusch (2022). Higher leaf
- 3086 nitrogen content is linked to tighter stomatal regulation of transpiration

- 3087 and more efficient water use across dryland trees. *New Phytologist* 235(4),
3088 1351–1364.
- 3089 R Core Team (2021). R: A language and environment for statistical computing.
- 3090 Raich, J. W., D. A. Clark, L. Schwendenmann, and T. E. Wood (2014). Above-
3091 ground tree growth varies with belowground carbon allocation in a tropical
3092 rainforest environment. *PLoS ONE* 9(6), e100275.
- 3093 Rastetter, E. B., P. M. Vitousek, C. B. Field, G. R. Shaver, D. Herbert, and
3094 G. I. Ågren (2001). Resource optimization and symbiotic nitrogen fixation.
3095 *Ecosystems* 4(4), 369–388.
- 3096 Reich, P. B. (2014). The world-wide 'fast-slow' plant economics spectrum: a
3097 traits manifesto. *Journal of Ecology* 102(2), 275–301.
- 3098 Reich, P. B., S. E. Hobbie, T. Lee, D. S. Ellsworth, J. B. West, D. Tilman,
3099 J. M. H. Knops, S. Naeem, and J. Trost (2006). Nitrogen limitation con-
3100 strains sustainability of ecosystem response to CO₂. *Nature* 440(7086), 922–925.
- 3101
- 3102 Rhine, E. D., R. L. Mulvaney, E. J. Pratt, and G. K. Sims (1998). Improving
3103 the Berthelot reaction for determining ammonium in soil extracts and water.
3104 *Soil Science Society of America Journal* 62(2), 473.
- 3105 Rogers, A. (2014). The use and misuse of $V_{c\max}$ in Earth System Models. *Pho-*
3106 *tosynthesis Research* 119(1-2), 15–29.
- 3107 Rogers, A., B. E. Medlyn, J. S. Dukes, G. B. Bonan, S. Caemmerer, M. C.
3108 Dietze, J. Kattge, A. D. B. Leakey, L. M. Mercado, Ü. Niinemets, I. C.
3109 Prentice, S. P. Serbin, S. Sitch, D. A. Way, and S. Zaehle (2017). A roadmap

- 3110 for improving the representation of photosynthesis in Earth system models.
- 3111 *New Phytologist* 213(1), 22–42.
- 3112 Saathoff, A. J. and J. Welles (2021). Gas exchange measurements in the un-
- 3113 steady state. *Plant Cell and Environment* 44(11), 3509–3523.
- 3114 Saleh, A. M., M. Abdel-Mawgoud, A. R. Hassan, T. H. Habeeb, R. S. Yehia,
- 3115 and H. AbdElgawad (2020). Global metabolic changes induced by arbuscular
- 3116 mycorrhizal fungi in oregano plants grown under ambient and elevated levels
- 3117 of atmospheric CO₂. *Plant Physiology and Biochemistry* 151, 255–263.
- 3118 Saxton, K. E. and W. J. Rawls (2006). Soil water characteristic estimates by
- 3119 texture and organic matter for hydrologic solutions. *Soil Science Society of*
- 3120 *America Journal* 70(5), 1569–1578.
- 3121 Schaefer, K., C. R. Schwalm, C. Williams, M. A. Arain, A. Barr, J. M. Chen,
- 3122 K. J. Davis, D. Dimitrov, T. W. Hilton, D. Y. Hollinger, E. Humphreys,
- 3123 B. Poulter, B. M. Racza, A. D. Richardson, A. Sahoo, P. Thornton, R. Var-
- 3124 gas, H. Verbeeck, R. Anderson, I. Baker, T. A. Black, P. Bolstad, J. Chen,
- 3125 P. S. Curtis, A. R. Desai, M. C. Dietze, D. Dragoni, C. M. Gough, R. F.
- 3126 Grant, L. Gu, A. K. Jain, C. Kucharik, B. E. Law, S. Liu, E. Lokipitiya,
- 3127 H. A. Margolis, R. Matamala, J. H. McCaughey, R. Monson, J. W. Munger,
- 3128 W. Oechel, C. Peng, D. T. Price, D. Ricciuto, W. J. Riley, N. Roulet,
- 3129 H. Tian, C. Tonitto, M. Torn, E. Weng, and X. Zhou (2012). A model-
- 3130 data comparison of gross primary productivity: Results from the North
- 3131 American Carbon Program site synthesis. *Journal of Geophysical Research:*
- 3132 *Biogeosciences* 117(G3), G03010.
- 3133 Schneider, C. A., W. S. Rasband, and K. W. Eliceiri (2012). NIH Image to

- 3134** ImageJ: 25 years of image analysis. *Nature Methods* 9(7), 671–675.
- 3135** Scott, H. G. and N. G. Smith (2022). A Model of C4 Photosynthetic Acclimation
- 3136** Based on Least-Cost Optimality Theory Suitable for Earth System Model
- 3137** Incorporation. *Journal of Advances in Modeling Earth Systems* 14(3), 1–16.
- 3138** Shi, M., J. B. Fisher, E. R. Brzostek, and R. P. Phillips (2016). Carbon cost
- 3139** of plant nitrogen acquisition: Global carbon cycle impact from an improved
- 3140** plant nitrogen cycle in the Community Land Model. *Global Change Biology*
- 3141** 22(3), 1299–1314.
- 3142** Shi, M., J. B. Fisher, R. P. Phillips, and E. R. Brzostek (2019). Neglecting
- 3143** plant–microbe symbioses leads to underestimation of modeled climate im-
- 3144** pacts. *Biogeosciences* 16(2), 457–465.
- 3145** Smith, B., D. Wärldin, A. Arneth, T. Hickler, P. Leadley, J. Siltberg, and
- 3146** S. Zaehle (2014). Implications of incorporating N cycling and N limitations
- 3147** on primary production in an individual-based dynamic vegetation model.
- 3148** *Biogeosciences* 11(7), 2027–2054.
- 3149** Smith, N. G. and J. S. Dukes (2013). Plant respiration and photosynthesis in
- 3150** global-scale models: incorporating acclimation to temperature and CO₂.
- 3151** *Global Change Biology* 19(1), 45–63.
- 3152** Smith, N. G. and T. F. Keenan (2020). Mechanisms underlying leaf photosyn-
- 3153** thetic acclimation to warming and elevated CO₂ as inferred from least-cost
- 3154** optimality theory. *Global Change Biology* 26(9), 5202–5216.
- 3155** Smith, N. G., T. F. Keenan, I. C. Prentice, H. Wang, I. J. Wright, Ü. Niinemets,
- 3156** K. Y. Crous, T. F. Domingues, R. Guerrieri, F. oko Ishida, J. Kattge, E. L.

- 3157** Kruger, V. Maire, A. Rogers, S. P. Serbin, L. Tarvainen, H. F. Togashi,
3158 P. A. Townsend, M. Wang, L. K. Weerasinghe, and S.-X. Zhou (2019).
3159 Global photosynthetic capacity is optimized to the environment. *Ecology*
3160 *Letters* 22(3), 506–517.
- 3161** Smith, N. G., D. L. Lombardozzi, A. Tawfik, G. B. Bonan, and J. S. Dukes
3162 (2017). Biophysical consequences of photosynthetic temperature acclimation
3163 for climate. *Journal of Advances in Modeling Earth Systems* 9(1), 536–547.
- 3164** Smith, N. G., S. L. Malyshev, E. Shevliakova, J. Kattge, and J. S. Dukes
3165 (2016). Foliar temperature acclimation reduces simulated carbon sensitivity
3166 to climate. *Nature Climate Change* 6(4), 407–411.
- 3167** Smith, S. E. and D. J. Read (2008). *Mycorrhizal Symbiosis*. Academic Press.
- 3168** Soil Survey Staff (2022). Web Soil Survey.
- 3169** Soudzilovskaia, N. A., J. C. Douma, A. A. Akhmetzhanova, P. M. van Bode-
3170 gom, W. K. Cornwell, E. J. Moens, K. K. Treseder, and J. H. C. Cornelissen
3171 (2015). Global patterns of plant root colonization intensity by mycorrhizal
3172 fungi explained by climate and soil chemistry. *Global Ecology and Biogeogra-*
3173 *phy* 24(3), 371–382.
- 3174** Stocker, B. D., H. Wang, N. G. Smith, S. P. Harrison, T. F. Keenan, D. San-
3175 doval, T. Davis, and I. C. Prentice (2020). P-model v1.0: An optimality-
3176 based light use efficiency model for simulating ecosystem gross primary pro-
3177 duction. *Geoscientific Model Development* 13(3), 1545–1581.
- 3178** Stocker, B. D., J. Zscheischler, T. F. Keenan, I. C. Prentice, J. Peñuelas, and
3179 S. I. Seneviratne (2018). Quantifying soil moisture impacts on light use

- 3180 efficiency across biomes. *New Phytologist* 218(4), 1430–1449.
- 3181 Sulman, B. N., D. T. Roman, K. Yi, L. Wang, R. P. Phillips, and K. A.
3182 Novick (2016). High atmospheric demand for water can limit forest car-
3183 bon uptake and transpiration as severely as dry soil. *Geophysical Research
3184 Letters* 43(18), 9686–9695.
- 3185 Sulman, B. N., E. Shevliakova, E. R. Brzostek, S. N. Kivlin, S. L. Malyshev,
3186 D. N. L. Menge, and X. Zhang (2019). Diverse mycorrhizal associations
3187 enhance terrestrial C storage in a global model. *Global Biogeochemical Cy-
3188 cles* 33(4), 501–523.
- 3189 Sweet, S. K., D. W. Wolfe, A. DeGaetano, and R. Benner (2017). Anatomy
3190 of the 2016 drought in the Northeastern United States: Implications for
3191 agriculture and water resources in humid climates. *Agricultural and Forest
3192 Meteorology* 247, 571–581.
- 3193 Taylor, B. N. and D. N. L. Menge (2018). Light regulates tropical symbiotic
3194 nitrogen fixation more strongly than soil nitrogen. *Nature Plants* 4(9), 655–
3195 661.
- 3196 Terrer, C., S. Vicca, B. A. Hungate, R. P. Phillips, and I. C. Prentice (2016).
3197 Mycorrhizal association as a primary control of the CO₂ fertilization effect.
3198 *Science* 353(6294), 72–74.
- 3199 Terrer, C., S. Vicca, B. D. Stocker, B. A. Hungate, R. P. Phillips, P. B. Reich,
3200 A. C. Finzi, and I. C. Prentice (2018). Ecosystem responses to elevated CO₂
3201 governed by plant–soil interactions and the cost of nitrogen acquisition. *New
3202 Phytologist* 217(2), 507–522.

- 3203** Thieurmel, B. and A. Elmarhraoui (2019). suncalc: Compute sun position,
- 3204** sunlight phases, moon position, and lunar phase.
- 3205** Thomas, R. Q., E. N. J. Brookshire, and S. Gerber (2015). Nitrogen limita-
- 3206** tion on land: how can it occur in Earth system models? *Global Change*
- 3207** *Biology* 21(5), 1777–1793.
- 3208** Thomas, R. Q., S. Zaehle, P. H. Templer, and C. L. Goodale (2013). Global pat-
- 3209** terns of nitrogen limitation: confronting two global biogeochemical models
- 3210** with observations. *Global Change Biology* 19(10), 2986–2998.
- 3211** Thornton, P. E., J.-F. Lamarque, N. A. Rosenbloom, and N. M. Mahowald
- 3212** (2007). Influence of carbon-nitrogen cycle coupling on land model response
- 3213** to CO₂ fertilization and climate variability. *Global Bioge-*
- 3214** *chemical Cycles* 21(4), GB4018.
- 3215** Tingey, D. T., D. L. Phillips, and M. G. Johnson (2000). Elevated CO₂ and
- 3216** conifer roots: effects on growth, life span and turnover. *New Phytolo-*
- 3217** *gist* 147(1), 87–103.
- 3218** Udvardi, M. and P. S. Poole (2013). Transport and metabolism in legume-
- 3219** rhizobia symbioses. *Annual Review of Plant Biology* 64, 781–805.
- 3220** USDA NRCS (2022). The PLANTS Database.
- 3221** Uselman, S. M., R. G. Qualls, and R. B. Thomas (2000). Effects of increased
- 3222** atmospheric CO₂, temperature, and soil N availability on root exudation
- 3223** of dissolved organic carbon by an N-fixing tree (*Robinia pseudoacacia* L.).
- 3224** *Plant and Soil* 222, 191–202.
- 3225** van Diepen, L. T. A., E. A. Lilleskov, K. S. Pregitzer, and R. M. Miller (2007).

- 3226** Decline of arbuscular mycorrhizal fungi in northern hardwood forests exposed to chronic nitrogen additions. *New Phytologist* 176(1), 175–183.
- 3227**
- 3228** Vance, C. P. and G. H. Heichel (1991). Carbon in N₂ fixation: Limitation or
- 3229** exquisite adaptation. *Annual Review of Plant Physiology and Plant Molecular Biology* 42(1), 373–392.
- 3230**
- 3231** Viet, H. D., J.-H. Kwak, K.-S. Lee, S.-S. Lim, M. Matsushima, S. X. Chang,
- 3232** K.-H. Lee, and W.-J. Choi (2013). Foliar chemistry and tree ring δ¹³C of
- 3233** *Pinus densiflora* in relation to tree growth along a soil pH gradient. *Plant*
- 3234** *and Soil* 363(1-2), 101–112.
- 3235** Vitousek, P. M., K. Cassman, C. C. Cleveland, T. Crews, C. B. Field, N. B.
- 3236** Grimm, R. W. Howarth, R. Marino, L. Martinelli, E. B. Rastetter, and
- 3237** J. I. Sprent (2002). Towards an ecological understanding of biological nitrogen fixation. In *The Nitrogen Cycle at Regional to Global Scales*, pp. 1–45.
- 3238** Springer Netherlands.
- 3239**
- 3240** Vitousek, P. M. and R. W. Howarth (1991). Nitrogen limitation on land and in
- 3241** the sea: How can it occur? *Biogeochemistry* 13(2), 87–115.
- 3242** Vitousek, P. M., S. Porder, B. Z. Houlton, and O. A. Chadwick (2010).
- 3243** Terrestrial phosphorus limitation: mechanisms, implications, and nitro-
- 3244** gen–phosphorus interactions. *Ecological Applications* 20(1), 5–15.
- 3245** Walker, A. P., A. P. Beckerman, L. Gu, J. Kattge, L. A. Cernusak, T. F.
- 3246** Domingues, J. C. Scales, G. Wohlfahrt, S. D. Wullschleger, and F. I. Woodward (2014). The relationship of leaf photosynthetic traits - V_{cmax} and J_{max} - to leaf nitrogen, leaf phosphorus, and specific leaf area: a meta-analysis
- 3247** and modeling study. *Ecology and Evolution* 4(16), 3218–3235.
- 3248**
- 3249**

- 3250 Wang, H., I. C. Prentice, T. F. Keenan, T. W. Davis, I. J. Wright, W. K.
3251 Cornwell, B. J. Evans, and C. Peng (2017). Towards a universal model for
3252 carbon dioxide uptake by plants. *Nature Plants* 3(9), 734–741.
- 3253 Wang, W., Y. Wang, G. Hoch, Z. Wang, and J. Gu (2018). Linkage of root mor-
3254 phology to anatomy with increasing nitrogen availability in six temperate
3255 tree species. *Plant and Soil* 425(1-2), 189–200.
- 3256 Weatherburn, M. W. (1967). Phenol-hypochlorite reaction for determination of
3257 ammonia. *Analytical Chemistry* 39(8), 971–974.
- 3258 Wellburn, A. R. (1994). The spectral determination of chlorophylls a and b, as
3259 well as total carotenoids, using various solvents with spectrophotometers of
3260 different resolution. *Journal of Plant Physiology* 144(3), 307–313.
- 3261 Wen, Z., P. J. White, J. Shen, and H. Lambers (2022). Linking root exuda-
3262 tion to belowground economic traits for resource acquisition. *New Phytolo-*
3263 *gist* 233(4), 1620–1635.
- 3264 Westerband, A. C., I. J. Wright, V. Maire, J. Paillassa, I. C. Prentice, O. K.
3265 Atkin, K. J. Bloomfield, L. A. Cernusak, N. Dong, S. M. Gleason, C. Guil-
3266 herme Pereira, H. Lambers, M. R. Leishman, Y. Malhi, and R. H. Nolan
3267 (2023). Coordination of photosynthetic traits across soil and climate gradi-
3268 ents. *Global Change Biology* 29(3), 1–29.
- 3269 Wieder, W. R., C. C. Cleveland, W. K. Smith, and K. Todd-Brown (2015).
3270 Future productivity and carbon storage limited by terrestrial nutrient avail-
3271 ability. *Nature Geoscience* 8(6), 441–444.
- 3272 Wieder, W. R., D. M. Lawrence, R. A. Fisher, G. B. Bonan, S. J. Cheng, C. L.

- 3273** Goodale, A. S. Grandy, C. D. Koven, D. L. Lombardozzi, K. W. Oleson,
3274 and R. Q. Thomas (2019). Beyond static benchmarking: using experimental
3275 manipulations to evaluate land model assumptions. *Global Biogeochemical*
3276 *Cycles* 33(10), 1289–1309.
- 3277** Wright, I. J., P. B. Reich, and M. Westoby (2003). Least-cost input mixtures
3278 of water and nitrogen for photosynthesis. *The American Naturalist* 161(1),
3279 98–111.
- 3280** Wright, I. J., P. B. Reich, M. Westoby, D. D. Ackerly, Z. Baruch, F. Bongers,
3281 J. Cavender-Bares, T. Chapin, J. H. C. Cornelissen, M. Diemer, J. Flexas,
3282 E. Garnier, P. K. Groom, J. Gulias, K. Hikosaka, B. B. Lamont, T. Lee,
3283 W. Lee, C. Lusk, J. J. Midgley, M.-L. Navas, Ü. Niinemets, J. Oleksyn,
3284 N. Osada, H. Poorter, P. Poot, L. Prior, V. I. Pyankov, C. Roumet, S. C.
3285 Thomas, M. G. Tjoelker, E. J. Veneklaas, and R. Villar (2004). The world-
3286 wide leaf economics spectrum. *Nature* 428(6985), 821–827.
- 3287** Xu-Ri and I. C. Prentice (2017). Modelling the demand for new nitrogen fixation
3288 by terrestrial ecosystems. *Biogeosciences* 14(7), 2003–2017.
- 3289** Zaehle, S., B. E. Medlyn, M. G. De Kauwe, A. P. Walker, M. C. Dietze, T. Hick-
3290 ler, Y. Luo, Y. P. Wang, B. El-Masri, P. Thornton, A. Jain, S. Wang,
3291 D. Warlind, E. Weng, W. Parton, C. M. Iversen, A. Gallet-Budynek, H. Mc-
3292 carthy, A. C. Finzi, P. J. Hanson, I. C. Prentice, R. Oren, and R. J. Norby
3293 (2014). Evaluation of 11 terrestrial carbon-nitrogen cycle models against
3294 observations from two temperate Free-Air CO₂ Enrichment studies. *New*
3295 *Phytologist* 202(3), 803–822.
- 3296** Zaehle, S., S. Sitch, B. Smith, and F. Hatterman (2005). Effects of parame-

- 3297** ter uncertainties on the modeling of terrestrial biosphere dynamics. *Global
3298 Biogeochemical Cycles* 19(3), GB3020.
- 3299** Zhu, Q., W. J. Riley, J. Tang, N. Collier, F. M. Hoffman, X. Yang, and G. Bisht
3300 (2019). Representing nitrogen, phosphorus, and carbon interactions in the
3301 E3SM land model: development and global benchmarking. *Journal of Ad-
3302 vances in Modeling Earth Systems* 11(7), 2238–2258.
- 3303** Ziegler, C., M. E. Dusenge, B. Nyirambangutse, E. Zibera, G. Wallin, and
3304 J. Uddling (2020). Contrasting Dependencies of Photosynthetic Capacity
3305 on Leaf Nitrogen in Early- and Late-Successional Tropical Montane Tree
3306 Species. *Frontiers in Plant Science* 11, 1–12.
- 3307** Ziehn, T., J. Kattge, W. Knorr, and M. Scholze (2011). Improving the pre-
3308 dictability of global CO₂ assimilation rates under climate change. *Geophys-
3309 ical Research Letters* 38(10), L10404.